Università degli Studi di Padova

DIPARTIMENTO DI MATEMATICA
Laurea Magistrale in Matematica

Master Thesis

Spectral filtering for the resolution of the Gibbs phenomenon in MPI applications by Lissajous sampling

Candidate:
Francesco Marchetti
1109320

Supervisor:
Prof. Stefano De Marchi

Co-Supervisor:
Dr. Wolfgang Erb

October 14, 2016

Contents

Introduction

The Magnetic Particle Imaging (MPI) is an emerging medical imaging technology which attracted the interest of different research groups in the last years [14]. The technique of the MPI is based on the detection of a tracer which consists of superparamagnetic iron oxide nanoparticles through the superimposition of different magnetic fields.
When the particles are excited by oscillating magnetic fields, an electromagnetic induction phenomenon is induced and measured. The acquisition of the signal which comes from the particles is performed moving a field free point along suitable sampling trajectories, using appropriate magnetic gradient fields.
A possible choice is to move along Lissajous curves [13], but the problem of selecting the set of sampling points to take along the curve is not trivial. The first time in which the Lissajous curves have been considered in polynomial interpolation and approximation topic is the debut of the Padua points.

Let n be a positive integer. The *Padua points* are the set of points $(x_m, y_k) \in [-1,1]^2$ defined as

$$x_m = \cos\left(\frac{(m-1)\pi}{n}\right) \quad , \quad y_k = \begin{cases} \cos\left(\dfrac{(2k-2)\pi}{n+1}\right) & \text{if } m \text{ is odd} \ , \\ \cos\left(\dfrac{(2k-1)\pi}{n+1}\right) & \text{if } m \text{ is even} \ , \end{cases} \tag{1}$$

where $1 \leq m \leq n+1$ and $1 \leq k \leq n/2+1$.
They can be seen as a modified version of *Morrow-Patterson points* and they are equispaced with respect to the *Dubiner metric* [8].
They were first presented in 2005 in [7] and they turned out to be the best nodes for polynomial interpolation on the square. Indeed, if Λ_{PD_n} is the *Lebesgue constant* in $[-1,1]^2$ related to the set of Padua points, then we have the very good result $\Lambda_{PD_n} = \mathcal{O}(\log^2(n))$ and it is well known that the Lebesgue constant gives information about how suitable a set is for global polynomial interpolation on a certain domain.

In the light of these considerations, efforts have been made in order to understand more about this particular set of points and different definitions for this set were presented.
First of all, the Padua points PD_n are related to the *Chebyshev-Lobatto points* given by

$$C_n := \left\{ z_k^n := \cos\left(\frac{k\pi}{n}\right) \ , \ n \in \mathbb{N} \ , \ k = 0, ..., n \right\} . \tag{2}$$

We can decompose C_n in the disjoint union

$$\begin{aligned} C_n^e &= \{ z_k^n \ , \ k = 0, ..., n \ , \ j \text{ even} \} \ , \\ C_n^o &= \{ z_k^n \ , \ k = 0, ..., n \ , \ j \text{ odd} \} \ , \end{aligned} \tag{3}$$

getting

$$PD_n = (C_n^e \times C_{n+1}^e) \cup (C_n^o \times C_{n+1}^o) \ . \tag{4}$$

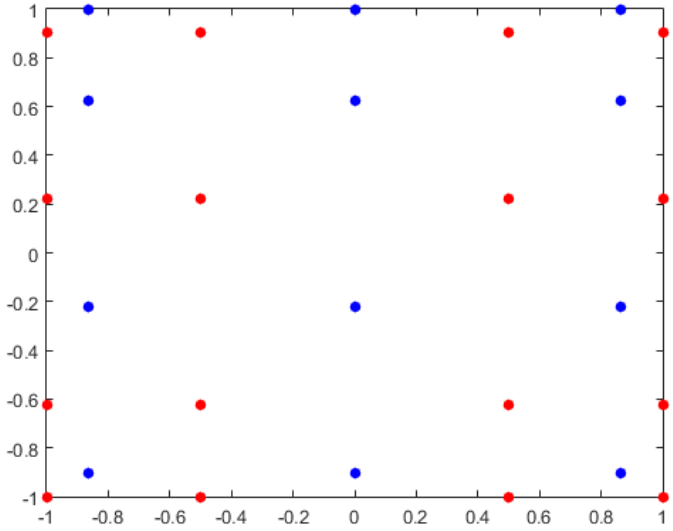

Figure 1: Padua points with $n = 6$. They are the union of an even grid (red) and an odd one (blue)

We observe that $\#PD_n = \frac{(n+1)(n+2)}{2}$ which is the cardinality of the space of bivariate polynomials of degree $\leq n$.
For the next fundamental definition for the Padua points we consider the following parametric curves:

$$\begin{aligned} \gamma_n^1(t) &= (-\cos(n+1)t, -\cos nt) \ , \\ \gamma_n^2(t) &= (-\cos nt, -\cos(n+1)t) \ , \\ \gamma_n^3(t) &= (\cos(n+1)t, \cos nt) \ , \\ \gamma_n^4(t) &= (\cos nt, \cos(n+1)t) \ , \end{aligned} \tag{5}$$

where $0 \leq t \leq \pi$, $n \geq 1$.

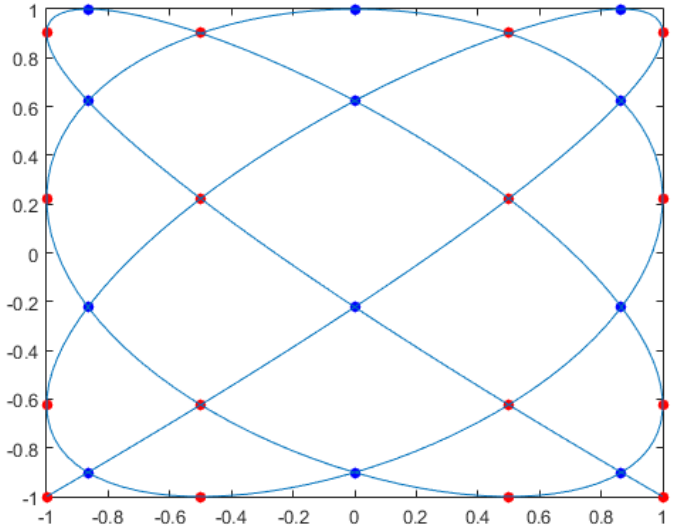

Figure 2: Padua points in Figure 1 are generated by the curve $\gamma_6^1(t)$ and they belong to the first family

The curves are contained in the square $[-1,1]^2$ and they are particular *Lissajous curves*. We can define four different families of Padua points writing, for $i = 1, ..., 4$,

$$PD_n^i = \left\{ \gamma_n^i \left(\frac{k}{n(n+1)} \pi \right) \ , \ k = 0, ..., n(n+1) \right\} . \tag{6}$$

Hence, each family of Padua points is the union of the self-intersection points of γ_n^i and the points where the curve touches the boundary of the square [8].
The four families have the same properties and they differ just for a rotation with respect to the center of the axis. Moreover, exactly two points of the set are always lying in two consecutive vertices of the square.
This relation between Lissajous curves and Padua points stimulated interest in such a class of curves for polynomial interpolation issues.

In the first chapter we introduce a more general setting, which allows us to define the Lissajous node points. Lissajous nodes are provided with the similar excellent properties of Padua points about stability and can be divided in two classes: nodes given by degenerated Lissajous curves and nodes extracted from non-degenerated Lissajous curves. We see that Padua points are Lissajous nodes given by a particular degenerated Lissajous curve. After a general introduction, we focus our attention on the non-degenerate case. The main reason for this choice is that non-degenerate curves are more suitable for applications in MPI, since it's preferable to take the centre of the square as Lissajous node in order to calibrate the scanner.

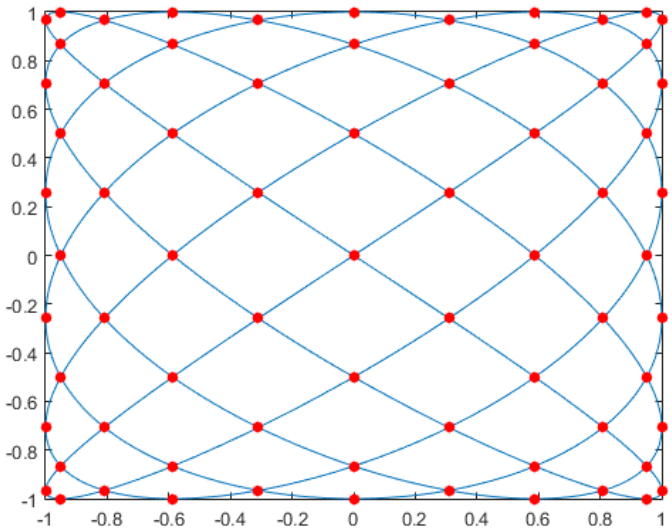

Figure 3: A non-degenerate Lissajous curve.

We state some important results about interpolation on Lissajous nodes, using peculiar quadrature rules for such a set of nodes. Almost every result which we state for the non-degenerate case is valid, fixing some parameters, for the degenerate case also.
For this chapter we mainly refer to [10], where both cases are discussed.

In the second chapter we move to the cube $[-1,1]^3$, considering three-dimensional degenerate Lissajous curves [3] [4].
Recent results have been reached in this topic, providing algebraic cubature formulas on particular sets of points lying on these curves. Using conjectured optimal parameters, we can perform the hyperinterpolation polynomial approximation, which considers a discretized expansion of a function in series of chosen orthogonal polynomial up to a fixed

total-degree.
The hyperinterpolation coefficients can be computed by a single one-dimensional discrete Chebyshev transform. Moreover, the hyperinterpolation operator norm has the minimal growth property.

In applications, we typically deal with objects represented by underlying discontinuous functions. This causes the arise of the Gibbs phenomenon and as a consequence a distortion in the image reconstruction given by the Lissajous sampling. The connection between Chebyshev and Fourier series let us to consider the polynomial (hyper)interpolant as a Fourier series.
In Chapter 3 we recall some well known facts about Fourier theory and we define a proper set of functions for our applications, showing that the Gibbs phenomenon is caused by the slow decreasing of the Fourier coefficients related to discontinuous functions. We present the topic first in one dimension and then in a general multidimensional case.

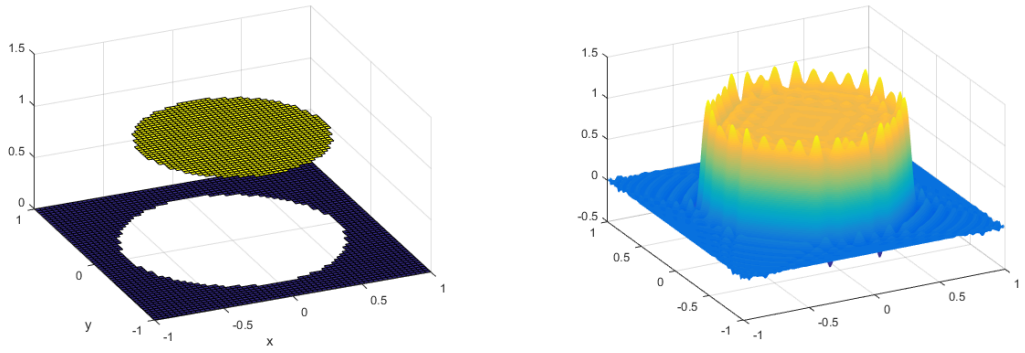

Figure 4: An example of the appearance of the Gibbs phenomenon.

In the fourth chapter we start to discuss about how we can dimish this distortion phenomenon and recover precision, looking for a fast and as efficient as possible solution.
A classic method is the application of Fourier spectral filters on the coefficients of the polynomial (hyper)interpolant (see [12] [15] for possible applications). We define what we mean with filter functions and we present some common used one-dimensional filters. Then, we extend the filtering process to a multidimensional setting through a tensor product structure.
The spectral filtering dimishes the Gibbs phenomenon but it also causes a general smoothing in the image with a loss of definition and precision. In order to get a better result, we introduce the concept of adaptivity, considering a filter function whose level parameter depends on the physical position of every point in the domain. In particular, considering an adaptive parameter which changes with respect to the distance between each point and its correspondent closest discontinuity we prove that we can get an asymptotic exponential reduction of the error away from the discontinuities, assuming some hypothesis about the regularity of the underlying function.

In Chapter 5 we do some numerical experiments applying the results of the previous chapters. First we introduce the reconstruction problem and the parameter which we use to evaluate the images, the SSIM, justifying this choice among other possible solutions. After that, we describe the setting of our two-dimensional experiments and we describe all the steps needed to reach the final results. The complete Matlab codes are avaiable in the inclosed CD.
Applying the adaptive filtering process, we notice that the tensor product structure combined with the separation of the distances in one-dimensional ones causes the appearance of a distortion phenomenon which affects the final result. In order to get rid of such a prob-

lem, we conjecture an efficient solution modifying the definition of the adaptive parameter of the filter.

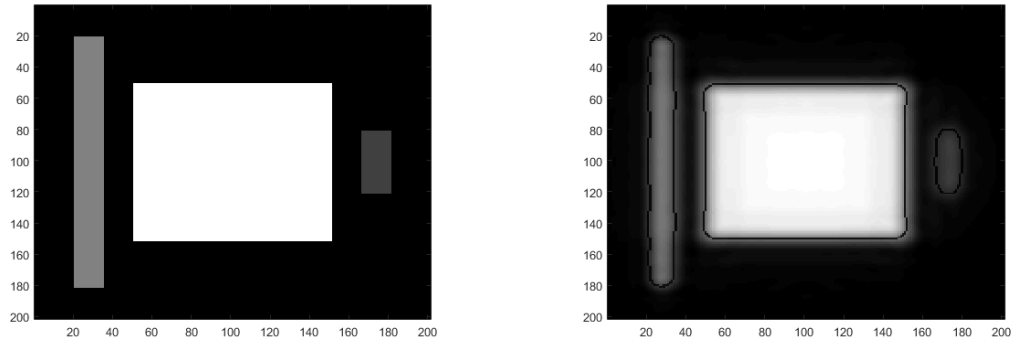

Figure 5: A reconstruction (right) of a test function (left) using the modified adaptive parameter.

We extend the procedure doing some experiments in three dimensions also.

In the last chapter we write some conclusions and considerations about this work and about the obtained results.

Chapter 1

Lissajous node points in the square

1.1 Lissajous curves and nodes

Let $\boldsymbol{n} = (n_1, n_2) \in \mathbb{N}^2$, $\boldsymbol{s} = (s_1, s_2) \in \mathbb{R}^2$ and $\boldsymbol{u} = (u_1, u_2) \in \{-1, 1\}^2$.
We call a two-dimensional *Lissajous curve* the closed curve $\gamma^{\boldsymbol{n}}_{\boldsymbol{s},\boldsymbol{u}}$ defined as

$$\gamma^{\boldsymbol{n}}_{\boldsymbol{s},\boldsymbol{u}} : [0, 2\pi] \to [-1, 1]^2 \ , \ \gamma^{\boldsymbol{n}}_{\boldsymbol{s},\boldsymbol{u}}(t) \coloneqq \begin{pmatrix} u_1 \cos(n_2 t - s_1\pi/(2n_1)) \\ u_2 \cos(n_1 t - s_2\pi/(2n_2)) \end{pmatrix}. \tag{1.1}$$

From now on we assume that the numbers n_1 and n_2 are relative prime. This condition implies that 2π is the minimal period of $\gamma^{\boldsymbol{n}}_{\boldsymbol{s},\boldsymbol{u}}$.
The Lissajous curve $\gamma^{\boldsymbol{n}}_{\boldsymbol{s},\boldsymbol{u}}$ is called *degenerate* if $s_2 - s_1 \in 2\mathbb{Z}$ and *non-degenerate* otherwise.
With some manipulations of the parameters we get a very useful rewrite of the definition of Lissajous curve.

Proposition 1. *There exist $t' \in \mathbb{R}$, $\eta \in [0, 2)$ and $\boldsymbol{u}' \in \{-1, 1\}^2$ such that*

$$\gamma^{\boldsymbol{n}}_{\boldsymbol{s},\boldsymbol{u}}(t - t') = \gamma^{\boldsymbol{n}}_{(0,\eta),\boldsymbol{u}'}(t) \ . \tag{1.2}$$

where $t \in [0, 2\pi]$.
Moreover, $\gamma^{\boldsymbol{n}}_{\boldsymbol{s},\boldsymbol{u}}$ is degenerate if and only if $\eta = 0$. Finally, if $\boldsymbol{s} \in \mathbb{Z}^2$ then $\eta \in \{0, 1\}$.

Proof. Surely we can find a t'' such that $\gamma^{\boldsymbol{n}}_{\boldsymbol{s},\boldsymbol{u}}(t - t'') = \gamma^{\boldsymbol{n}}_{\boldsymbol{s}',\boldsymbol{u}}(t)$ with $s'_1 = 0$.
Let $a \in \mathbb{Z}$ be the unique integer such that $0 \leq a + s'_2/2 < 1$. As n_1 and n_2 are relatively prime we can find $i, j \in \mathbb{Z}$ such that $a = in_1 + jn_2$. Let $t' = t'' + i\pi/n_2$ and $\eta = 2a + s'_2$. Then

$$n_1(t - t') - s_2\pi/(2n_2) = s_1(t - i\pi/n_2) - s'_2\pi/(2n_2) = n_1 t - \eta\pi/(2n_2) + j\pi$$

$$n_2(t - t') - s_1\pi/(2n_1) = n_2 t - i\pi$$

and we obtain (1.2) for $u'_1 = (-1)^i u_1$, $u'_2 = (-1)^j u_2$.
The curve $\gamma^{\boldsymbol{n}}_{\boldsymbol{s},\boldsymbol{u}}$ is degenerate if and only if $\gamma^{\boldsymbol{n}}_{(0,\eta),\boldsymbol{u}'}$ is degenerate. By definition $\eta \in 2\mathbb{Z}$ if and only if $\eta = 0$. In order to complete the proof, we note that $\boldsymbol{s} \in \mathbb{Z}^2$ implies $s'_2 \in \mathbb{Z}$ and then $\eta \in \{0, 1\}$. □

From now on $\boldsymbol{s} \in \mathbb{Z}^2$, as many Lissajous curves which are important in applications have this property.
This allows us to restrict our considerations to the curves

$$\gamma^{\boldsymbol{n}}_{\epsilon} : [0, 2\pi] \to [-1, 1]^2 \ , \ \gamma^{\boldsymbol{n}}_{\epsilon}(t) \coloneqq \gamma^{\boldsymbol{n}}_{(0,\epsilon-1),\mathbf{1}}(t) = \begin{pmatrix} \cos(n_2 t) \\ \cos(n_1 t - (\epsilon - 1)\pi/(2n_2)) \end{pmatrix} \tag{1.3}$$

with $\epsilon \in \{1, 2\}$ and where we fix the reflection parameter $\mathbf{1} = (1, 1)$.
Up to a shift t' and up to a reflection with respect to the coordinate axis, all degenerate curves can be written in the form $\gamma^{\boldsymbol{n}}_1$ and all non-degenerate curves can be written as $\gamma^{\boldsymbol{n}}_2$.

Observation 1. *The Lissajous curve generating the Padua points (see [5]) can be written in the form* $\gamma_1^{(n,n+1)}$ *or* $\gamma_1^{(n+1,n)}$ *up to a reflection.*

We are interested in the sets of points generated by Lissajous curves, in the sense given by the following definition.

Definition 1. *Let* $\gamma_\epsilon^{\boldsymbol{n}}$ *be a Lissajous curve with* $\epsilon \in \{1,2\}$ *and let*

$$t_k^{\epsilon\boldsymbol{n}} := \frac{\pi k}{\epsilon n_1 n_2} \quad , \quad k = 0, ..., 2\epsilon n_1 n_2 - 1 \, . \tag{1.4}$$

The set

$$LS_\epsilon^{\boldsymbol{n}} := \{\gamma_\epsilon^{\boldsymbol{n}}(t_k^{\epsilon\boldsymbol{n}}) : k = 0, ..., 2\epsilon n_1 n_2 - 1\} \tag{1.5}$$

is the set of Lissajous node points related to $\gamma_\epsilon^{\boldsymbol{n}}$.

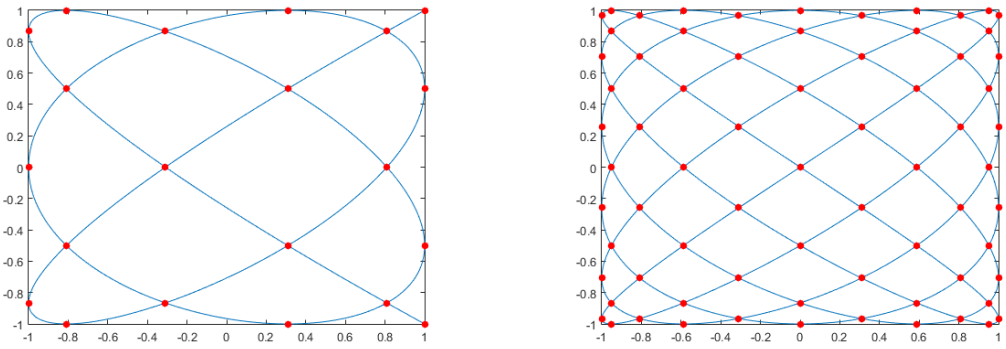

(a) The degenerate curve $\gamma_1^{(5,6)}$ (b) The non-degenerate curve $\gamma_2^{(5,6)}$

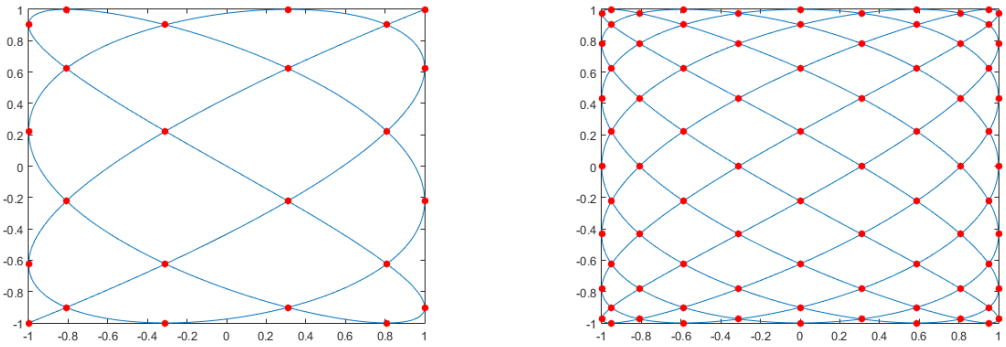

(c) The degenerate curve $\gamma_1^{(5,7)}$ (d) The non-degenerate curve $\gamma_2^{(5,7)}$

Figure 1.1: Some examples of Lissajous curves and nodes. Notice that (a) is the same as in Figure 3 in the Introduction and in (b) the center of the square is a node.

We define also for $\epsilon \in \{1,2\}$ the following index set associated to Lissajous nodes

$$\Gamma^{\epsilon\boldsymbol{n}} := \left\{(i,j) \in \mathbb{N}_0^2 \ : \ \frac{i}{\epsilon n_1} + \frac{j}{\epsilon n_2} < 1\right\} \cup \{(0, \epsilon n_2)\} \, . \tag{1.6}$$

The set $\Gamma^{\epsilon\boldsymbol{n}}$ plays an important role for bivariate interpolation.

1.1.1 The non-degenerate case

Let $\gamma_2^{\boldsymbol{n}}$ be a non-degenerate Lissajous curve. The set $LS_2^{\boldsymbol{n}}$ contains all self-intersection points $LS_{int,2}^{\boldsymbol{n}}$ of $\gamma_2^{\boldsymbol{n}}$. Indeed, a necessary condition for $\gamma_2^{\boldsymbol{n}}(t) = \gamma_2^{\boldsymbol{n}}(t')$ with $t \neq t'$ is

(see [2])

$$t=\left(\frac{i}{n_1}+\frac{j}{n_2}\right)\pi\ ,\ t'=\left(-\frac{i}{n_1}+\frac{j}{n_2}\right)\pi\ ,\quad i,j\in\mathbb{Z}\ , \tag{1.7}$$

or

$$t=\left(\frac{i}{n_1}+\frac{j}{n_2}-\frac{1}{2n_1n_2}\right)\pi\ ,\ t'=\left(\frac{i}{n_1}-\frac{j}{n_2}-\frac{1}{2n_1n_2}\right)\pi\ ,\quad i,j\in\mathbb{Z}\ . \tag{1.8}$$

We only show that if t is as in (1.7) then $\gamma_2^{\boldsymbol{n}}(t)\in LS_2^{\boldsymbol{n}}$, the other cases can be investigated with similar calculations.
If we expand the definition of $LS_2^{\boldsymbol{n}}$, we get

$$\gamma_2^{\boldsymbol{n}}\left(\frac{\pi k}{2n_1n_2}\right)=\begin{pmatrix}\cos(\pi k/(2n_1))\\ \cos(\pi(k-1)/(2n_2))\end{pmatrix}\ ,\quad k=0,...,4n_1n_2-1\ . \tag{1.9}$$

On the other hand,

$$\gamma_2^{\boldsymbol{n}}\left(\left(\frac{i}{n_1}+\frac{j}{n_2}\right)\pi\right)=\begin{pmatrix}\cos(\pi[2(in_2+jn_1)]/(2n_1))\\ \cos(\pi[2(in_2+jn_1)-1]/(2n_2))\end{pmatrix}\ ,\quad i,j\in\mathbb{Z}\ . \tag{1.10}$$

The previous equations gives us

$$k=2(in_2+jn_1)\ ,\quad i,j\in\mathbb{Z}\ , \tag{1.11}$$

which allows us to conclude the proof observing that the condition (1.11) holds, since n_1 and n_2 are relative prime (see [1] for further details).

We can decompose the set $LS_2^{\boldsymbol{n}}$ in the two disjoint sets

$$LS_{e,2}^{\boldsymbol{n}}\coloneqq\{\gamma_2^{\boldsymbol{n}}(t_{2k}^{2\boldsymbol{n}}):k=0,...,2n_1n_2-1\}\ ,\ LS_{o,2}^{\boldsymbol{n}}\coloneqq\{\gamma_2^{\boldsymbol{n}}(t_{2k-1}^{2\boldsymbol{n}}):k=1,...,2n_1n_2\}\ . \tag{1.12}$$

In view of (1.7), t generates a self-intersection point in $LS_{e,2}^{\boldsymbol{n}}$ if and only if $i\notin n_1\mathbb{Z}$, therefore we have $2n_2$ elements in $LS_{e,2}^{\boldsymbol{n}}$ that are not in $LS_{int,2}^{\boldsymbol{n}}$ and that lie on the boundary of $[-1,1]^2$. The same reasoning tells us that $2n_1$ elements of $LS_{o,2}^{\boldsymbol{n}}$ are on the boundary of $[-1,1]^2$. It is then natural to define the subset $LS_{out,2}^{\boldsymbol{n}}$ consisting in the $2n_1+2n_2$ elements of $LS_2^{\boldsymbol{n}}$ which lie on the boundary of $[-1,1]^2$. Hence we can write

$$\#LS_{int,2}^{\boldsymbol{n}}=\frac{4n_1n_2-2n_1-2n_2}{2}=2n_1n_2-n_1-n_2\ . \tag{1.13}$$

In particular,

$$\#LS_2^{\boldsymbol{n}}=\#LS_{int,2}^{\boldsymbol{n}}+\#LS_{out,2}^{\boldsymbol{n}}=2n_1n_2+n_1+n_2\ . \tag{1.14}$$

Lissajous node points are related to the *Chebyshev-Lobatto points* defined on the interval $[-1,1]$. We recall the definition:

$$z_k^n\coloneqq\cos\left(\frac{k\pi}{n}\right)\ ,\quad n\in\mathbb{N}\ ,\ k=0,...,n\ . \tag{1.15}$$

Using this notation, we can write

$$LS_2^{\boldsymbol{n}}=\{(z_r^{2n_1},z_s^{2n_2})\ :\ r=0,...,2n_1\ ,\ s=0,...,2n_2\ ,\ r+s=1\mod 2\}\ . \tag{1.16}$$

Further, we can see $LS_2^{\boldsymbol{n}}$ as disjoint union of two rectangular grids given as

$$LS_{e,2}^{\boldsymbol{n}}=\{(z_r^{2n_1},z_s^{2n_2})\ :\ r=0,...,2n_1\ ,\ s=0,...,2n_2\ ,\ r=0\mod 2\ ,\ s=1\mod 2\}\ ,$$

$$LS_{o,2}^{\boldsymbol{n}}=\{(z_r^{2n_1},z_s^{2n_2})\ :\ r=0,...,2n_1\ ,\ s=0,...,2n_2\ ,\ r=1\mod 2\ ,\ s=0\mod 2\}\ .$$

We point out that

$$\#\Gamma^{2\boldsymbol{n}}=\frac{(2n_1+1)(2n_2+1)-1}{2}=\#LS_2^{\boldsymbol{n}}\ . \tag{1.17}$$

We end this section with the following geometric observation.

Observation 2. *The set $LS_2^{\boldsymbol{n}}$ is symmetric with respect to reflections at the coordinate axis. Moreover, there are no points of $LS_2^{\boldsymbol{n}}$ on the vertices of the square $[-1,1]^2$.*

1.2 Quadrature formulae

We state some results about quadrature rules for Lissajous nodes. We will not enter in details, since we are more interested in interpolation issues. Nevertheless, interpolation results are consequences of quadrature formulas.
Let

$$\Pi^N \coloneqq \operatorname{span}\{T_i(x)T_j(y) \,:\, i+j \leq N\} \tag{1.18}$$

be a polynomial space in $[-1,1]^2$, where

$$T_i(x) = \cos(i \arccos(x)) \tag{1.19}$$

is the *i-th Chebyshev polynomial of the first kind.*
It is well-known that $\{T_i(x)T_j(y) \,:\, i+j \leq N\}$ forms an orthogonal basis of the space Π^N with respect to the inner product

$$\langle f, g\rangle \coloneqq \frac{1}{\pi^2}\int_{-1}^{1}\int_{-1}^{1} f(x,y)g(x,y)\omega(x,y)\mathrm{d}x\mathrm{d}y \tag{1.20}$$

with the weight function ω defined as

$$\omega(x,y) \coloneqq \frac{1}{\sqrt{1-x^2}}\frac{1}{\sqrt{1-y^2}}\,. \tag{1.21}$$

We can also formulate the corresponding normalized basis as $\{\hat{T}_i(x)\hat{T}_j(y) \,:\, i+j \leq N\}$ where

$$\hat{T}_i(x) = \begin{cases} 1 & \text{if } i = 0, \\ \sqrt{2}T_i(x) & \text{if } i \neq 0. \end{cases} \tag{1.22}$$

Our purpose is to find an appropriate polynomial space for interpolation and quadrature related to Lissajous nodes given by a non-degenerate curve. The following results can be easily extended to the degenerate case [10] [1].
We recall the set $\Gamma^{2\boldsymbol{n}}$ defined in (1.6) and we define the following polynomial space

$$\Pi^{2\boldsymbol{n}} \coloneqq \operatorname{span}\{T_i(x)T_j(y) \,:\, (i,j) \in \Gamma^{2\boldsymbol{n}}\}\,. \tag{1.23}$$

We state this fundamental lemma.

Lemma 1. *For all bivariate polynomials P satisfying $\langle P, T_{2kn_1}T_{2kn_2}\rangle = 0$, $k \in \mathbb{N}$, the following holds:*

$$\frac{1}{\pi^2}\int_{-1}^{1}\int_{-1}^{1} P(x,y)\omega(x,y)\mathrm{d}x\mathrm{d}y = \frac{1}{2\pi}\int_{0}^{2\pi} P(\gamma_2^{\boldsymbol{n}}(t))\mathrm{d}t \tag{1.24}$$

Proof. See [10]. □

From now on, we use the notation $\mathcal{A} = (x_{\mathcal{A}}, y_{\mathcal{A}})$ for points in $LS_2^{\boldsymbol{n}}$.
We introduce then the following weights for $\mathcal{A} \in LS_2^{\boldsymbol{n}}$:

$$w_{\mathcal{A}} \coloneqq \frac{1}{4n_1n_2}\cdot\begin{cases} 2 & \text{if } \mathcal{A} \in LS_{int,2}^{\boldsymbol{n}}, \\ 1 & \text{if } \mathcal{A} \in LS_{out,2}^{\boldsymbol{n}}. \end{cases} \tag{1.25}$$

We get the following quadrature rule.

Theorem 3. *For all polynomials $P \in \Pi^{4\boldsymbol{n}}$ with $\langle P, T_{4n_2}(y)\rangle = 0$ the quadrature formula*

$$\frac{1}{\pi^2}\int_{-1}^{1}\int_{-1}^{1} P(x,y)\omega(x,y)\mathrm{d}x\mathrm{d}y = \sum_{\mathcal{A}\in LS_2^{\boldsymbol{n}}} w_{\mathcal{A}}P(\mathcal{A}) \tag{1.26}$$

is exact. Moreover, for the polynomial $P(x,y) = (\hat{T}_{2n_2}(y))^2$ we have

$$\frac{1}{\pi^2}\int_{-1}^{1}\int_{-1}^{1} |\hat{T}_{2n_2}(y)|^2\omega(x,y)\mathrm{d}x\mathrm{d}y = \frac{1}{2}\sum_{\mathcal{A}\in LS_2^{\boldsymbol{n}}} w_{\mathcal{A}}|\hat{T}_{2n_2}(y_{\mathcal{A}})|^2 = 1\,. \tag{1.27}$$

Proof. The proof is mainly based on the previous lemma and on the fact that for all trigonometric 2π-perodic polynomials q of degree less than $4n_1n_2$ the following quadrature rule is exact:

$$\frac{1}{2\pi}\int_0^{2\pi} q(t)\mathrm{d}t = \frac{1}{4n_1n_2}\sum_{k=1}^{4n_1n_2} q(t_k^{2\boldsymbol{n}}).$$

See again [10] for further details. □

1.3 Interpolation on Lissajous nodes

In this section we consider the bivariate interpolation problem on Lissajous node points in the non-degenerate case.
Taking then $\mathcal{A} \in LS_2^{\boldsymbol{n}}$ as node points with given data values $f(\mathcal{A}) \in \mathbb{R}$, our aim is to find an unique interpolating polynomial $\mathcal{L}^{\boldsymbol{n}} f$ in $[-1,1]^2$ which satisfies

$$\mathcal{L}^{\boldsymbol{n}} f(\mathcal{A}) = f(\mathcal{A}) \text{ for all } \mathcal{A} \in LS_2^{\boldsymbol{n}} . \tag{1.28}$$

In the bivariate case it is a priori not clear which polynomial space we should consider to obtain a solution for this problem.
We observe that from(1.17)-(1.23) we got

$$\dim \Pi^{2\boldsymbol{n}} = \#\Gamma^{2\boldsymbol{n}} = \#LS_2^{\boldsymbol{n}} . \tag{1.29}$$

Hence, the space $\Pi^{2\boldsymbol{n}}$ is a natural candidate as interpolation space for the set $LS_2^{\boldsymbol{n}}$.

We introduce the reproducing kernel $\mathcal{K}^{2\boldsymbol{n}} : \mathbb{R}^2 \times \mathbb{R}^2 \to \mathbb{R}$ related to the space $\Pi^{2\boldsymbol{n}}$ as

$$\mathcal{K}^{2\boldsymbol{n}}(x,y;x',y') \coloneqq \sum_{(i,j)\in\Gamma^{2\boldsymbol{n}}} \hat{T}_i(x)\hat{T}_j(y)\hat{T}_i(x')\hat{T}_j(y') . \tag{1.30}$$

Let $\mathcal{A} = (x_{\mathcal{A}}, y_{\mathcal{A}}) \in LS_2^{\boldsymbol{n}}$, we define the polynomial $L_{\mathcal{A}} \in \Pi^{2\boldsymbol{n}}$ as

$$L_{\mathcal{A}}(x,y) \coloneqq w_{\mathcal{A}}\left(\mathcal{K}^{2\boldsymbol{n}}(x,y;x_{\mathcal{A}},y_{\mathcal{A}}) - \frac{1}{2}\hat{T}_{2n_2}(y)\hat{T}_{2n_2}(y_{\mathcal{A}})\right) . \tag{1.31}$$

We are ready for the following theorem.

Theorem 4. *The interpolation problem* (1.28) *has the unique solution*

$$\mathcal{L}^{\boldsymbol{n}} f(x,y) = \sum_{\mathcal{A}\in LS_2^{\boldsymbol{n}}} f(\mathcal{A}) L_{\mathcal{A}}(x,y) \tag{1.32}$$

in the polynomial space $\Pi^{2\boldsymbol{n}}$.
Moreover, the coefficients $c_{ij} = \langle \mathcal{L}^{\boldsymbol{n}} f, \hat{T}_i(x)\hat{T}_j(y)\rangle$ *of* $\mathcal{L}^{\boldsymbol{n}}$ *with respect to the orthonormal basis* $\{\hat{T}_i(x)\hat{T}_j(y) : (i,j) \in \Gamma^{2\boldsymbol{n}}\}$ *of* $\Pi^{2\boldsymbol{n}}$ *can be computed as*

$$c_{ij} = \begin{cases} \displaystyle\sum_{\mathcal{A}\in LS_2^{\boldsymbol{n}}} w_{\mathcal{A}} f(\mathcal{A})\hat{T}_i(x_{\mathcal{A}})\hat{T}_j(y_{\mathcal{A}}) & \text{if } (i,j) \in \Gamma^{2\boldsymbol{n}} \setminus (0,2n_2) , \\ \displaystyle\frac{1}{2}\sum_{\mathcal{A}\in LS_2^{\boldsymbol{n}}} w_{\mathcal{A}} f(\mathcal{A})\hat{T}_i(x_{\mathcal{A}})\hat{T}_{2n_2}(y_{\mathcal{A}}) & \text{if } (i,j) = (0,2n_2) . \end{cases} \tag{1.33}$$

Proof. Let $\mathbb{R}^{LS_2^{\boldsymbol{n}}}$ be the vector space of real functions on the set $LS_2^{\boldsymbol{n}}$. We can define the inner product

$$\langle g,h\rangle_w = \sum_{\mathcal{A}\in LS_2^{\boldsymbol{n}}} w_{\mathcal{A}} g(\mathcal{A})h(\mathcal{A}) , \quad g,h \in \mathbb{R}^{LS_2^{\boldsymbol{n}}} , \tag{1.34}$$

then we consider the functions $e^{(i,j)} \in \mathbb{R}^{LS_2^{\boldsymbol{n}}}$ given by $e^{(i,j)}(\mathcal{A}) = \hat{T}_i(x_{\mathcal{A}})\hat{T}_j(y_{\mathcal{A}})$.
We want to show that the set $\mathcal{E} = \{e^{(i,j)} : (i,j) \in \Gamma^{2\boldsymbol{n}}\}$ is an orthogonal basis of the vector space $\mathbb{R}^{LS_2^{\boldsymbol{n}}}$ with respect to the discrete inner product $\langle \cdot, \cdot \rangle_w$.
First of all we recall that $\#\Gamma^{2\boldsymbol{n}} = \#LS_2^{\boldsymbol{n}}$.
For the basis polynomials $e^{(i,j)}(x,y)e^{(i',j')}(x,y) = \hat{T}_i(x)\hat{T}_j(y)\hat{T}_{i'}(x)\hat{T}_{j'}(y) \in \Pi^{2\boldsymbol{n}}$ with $(i,j) \neq (i',j')$ we have the inequality $i/n_1 + j/n_2 + i'/n_1 + j'/n_2 < 4$ (see (1.6)), that implies $e^{(i,j)}(x,y)e^{(i',j')}(x,y) \in \Pi^{4\boldsymbol{n}}$. Then we can apply the quadrature formula of Theorem 3 and we get for $(i,j) \neq (i',j')$

$$\langle e^{(i,j)}, e^{(i',j')} \rangle_w = \sum_{\mathcal{A} \in LS_2^{\boldsymbol{n}}} w_{\mathcal{A}} \hat{T}_i(x_{\mathcal{A}})\hat{T}_j(y_{\mathcal{A}})\hat{T}_{i'}(x_{\mathcal{A}})\hat{T}_{j'}(y_{\mathcal{A}}) = \langle \hat{T}_i(x)\hat{T}_j(y), \hat{T}_{i'}(x)\hat{T}_{j'}(y) \rangle = 0 \, .$$

Moreover, if $(i,j) = (i',j')$ then

$$\|e^{(i,j)}\|_w^2 = \langle e^{(i,j)}, e^{(i,j)} \rangle_w = \sum_{\mathcal{A} \in LS_2^{\boldsymbol{n}}} w_{\mathcal{A}} (\hat{T}_i(x_{\mathcal{A}})\hat{T}_j(y_{\mathcal{A}}))^2 = \begin{cases} 1 & \text{if } (i,j) \in \Gamma^{2\boldsymbol{n}} \setminus (0, 2n_2) \, , \\ 2 & \text{if } (i,j) = (0, 2n_2) \, . \end{cases}$$

Hence we proved that $\mathcal{E}$ is an orthogonal basis of the vector space $\mathbb{R}^{LS_2^{\boldsymbol{n}}}$ with respect to the discrete inner product $\langle \cdot, \cdot \rangle_w$.
For all $\mathcal{A}, \mathcal{A}' \in \Gamma^{2\boldsymbol{n}}$ we have

$$L_{\mathcal{A}'}(\mathcal{A}) = w_{\mathcal{A}'} \sum_{(i,j) \in \Gamma^{2\boldsymbol{n}}} \frac{1}{\|e^{(i,j)}\|_w^2} e^{(i,j)}(\mathcal{A}')e^{(i,j)}(\mathcal{A}) \tag{1.35}$$

Then, for all $(i,j) \in \Gamma^{2\boldsymbol{n}}$ we can write

$$\langle L_{\mathcal{A}'}, e^{(i,j)} \rangle_w = w_{\mathcal{A}'} e^{(i,j)}(\mathcal{A}') = \langle \delta_{\mathcal{A}'}, e^{(i,j)} \rangle_w \, , \tag{1.36}$$

where $\delta_{\mathcal{A}'}$ denotes the Kronecker delta function on $LS_2^{\boldsymbol{n}}$ corresponding to $\mathcal{A}'$. Therefore, since $\mathcal{E}$ is a basis of $\mathbb{R}^{LS_2^{\boldsymbol{n}}}$ we have $L_{\mathcal{A}'}(\mathcal{A}) = \delta_{\mathcal{A}'}(\mathcal{A})$ for all $\mathcal{A}, \mathcal{A}' \in \Gamma^{2\boldsymbol{n}}$, that implies (1.28). The vector space homomorphism $f \to \mathcal{L}^{\boldsymbol{n}} f$ from $\mathbb{R}^{LS_2^{\boldsymbol{n}}}$ to $\Pi^{2\boldsymbol{n}}$ is not only injective but also bijective, because the dimensions of the spaces agree. Hence, $\mathcal{L}^{\boldsymbol{n}} f \in \Pi^{2\boldsymbol{n}}$ is also uniquely determined.
Finally, the definition of $L_{\mathcal{A}}(x,y)$ implies $\mathcal{L}^{\boldsymbol{n}} f(x,y) = \sum_{(i,j) \in \Gamma^{2\boldsymbol{n}}} c_{ij} \hat{T}_i(x)\hat{T}_j(y)$ for the values in (1.33). □

1.3.1 Fast computation for the coefficients of the interpolant

We can derive a fast scheme for the computation of the coefficients c_{ij} defined in (1.33), using the characterization (1.16) of the points $LS_2^{\boldsymbol{n}}$.
The first step is to store all relevant information in data matrices. We define a matrix $\boldsymbol{C}^{2\boldsymbol{n}} = (c_{ij}) \in \mathbb{R}^{(2n_1+1)\times(2n_2+1)}$ as

$$c_{ij} = \begin{cases} \langle \mathcal{L}^{\boldsymbol{n}} f, \hat{T}_i(x)\hat{T}_j(y) \rangle & \text{if } (i,j) \in \Gamma^{2\boldsymbol{n}} \, , \\ 0 & \text{otherwise} \, , \end{cases} \tag{1.37}$$

with $i \in \{0, ..., 2n_1\}$ and $j \in \{0, ..., 2n_2\}$.
The weights $w_{\mathcal{A}}$ and the data values $f(\mathcal{A})$ are stored in a matrix $\boldsymbol{G}_f = (g_{ij}) \in \mathbb{R}^{(2n_1+1)\times(2n_2+1)}$ defined as

$$g_{ij} \coloneqq \begin{cases} w_{\mathcal{A}} f(\mathcal{A}) & \text{if } \mathcal{A} = (z_i^{2n_1}, z_j^{2n_2}) \in LS_2^{\boldsymbol{n}} \, , \\ 0 & \text{if } \mathcal{A} \notin LS_2^{\boldsymbol{n}} \, . \end{cases} \tag{1.38}$$

For a general finite set of points $\chi = \{x_0, ..., x_m\} \subset [-1, 1]$ we define

$$\boldsymbol{T}_n(\chi) \coloneqq (\hat{T}_i(x_j)) \in \mathbb{R}^{(n+1)\times(m+1)} \tag{1.39}$$

with $i \in \{0, ..., n\}$ and $j \in \{0, ..., m\}$.
Finally, we define a mask $\boldsymbol{M}^{2\boldsymbol{n}} = (m_{ij}) \in \mathbb{R}^{(2n_1+1)\times(2n_2+1)}$ as

$$m_{ij} \coloneqq \begin{cases} 1 & \text{if } (i,j) \in \Gamma^{2\boldsymbol{n}} \setminus (0, 2n_2) \ , \\ 1/2 & \text{if } (i,j) = (0, 2n_2) \ , \\ 0 & \text{if } (i,j) \notin \Gamma^{2\boldsymbol{n}} \ . \end{cases} \tag{1.40}$$

Then, the coefficient matrix $\boldsymbol{C}^{2\boldsymbol{n}}$ of the interpolating polynomial $\mathcal{L}^{\boldsymbol{n}} f$ can be computed as

$$\boldsymbol{C}^{2\boldsymbol{n}} = (\boldsymbol{T}_{2n_1}(Z_{2n_1}) \boldsymbol{G}_f \boldsymbol{T}_{2n_2}(Z_{2n_2})^T) \odot \boldsymbol{M}^{2\boldsymbol{n}} \ , \tag{1.41}$$

where $\odot$ denotes the pointwise multiplication and $Z_{2n_i} = \{z_0^{2n_i}, ..., z_{2n_i}^{2n_i}\}$, $i = 1, 2$.
For an arbitrary point $(x, y) \in [-1, 1]^2$, we get

$$\mathcal{L}^{\boldsymbol{n}} f(x, y) = \boldsymbol{T}_{2n_1}(x)^T \boldsymbol{C}^{2\boldsymbol{n}} \boldsymbol{T}_{2n_2}(y) \ . \tag{1.42}$$

The matrices $\boldsymbol{T}_{2n_1}(Z_{2n_1}), \boldsymbol{T}_{2n_2}(Z_{2n_2})$ have a particular structure and describe discrete cosine transforms. Hence it is possible to evaluate the matrix-matrix product in (1.41) using fast Fourier methods. We obtain indeed

$$c_{ij} = m_{ij}\alpha_{ij} \sum_{l=0}^{2n_2} \left(\sum_{k=0}^{2n_1} g_{kl} \cos \frac{ik\pi}{2n_1} \right) \cos \frac{jl\pi}{2n_2} \tag{1.43}$$

where $\alpha_{ij} = \sqrt{2 - \delta_{0,i}}\sqrt{2 - \delta_{0,j}}$. Then the use of fast Fourier methods is justified by the following fact,

$$\sum_{k=0}^{2n_1} g_{kl} \cos \frac{ik\pi}{2n_1} = \mathrm{Re} \sum_{k=0}^{2n_1} g_{kl} e^{-i\frac{2\pi ik}{4n_1}} \ , \tag{1.44}$$

with $l = 0, ..., 2n_2$.
An implementation formula in Matlab code can be found in [1].

1.4 Lebesgue constant related to Lissajous nodes

In this section we state and summarize the good stability properties of Lissajous nodes, which justify the choice of such a set of points for bivariate Lagrange interpolation.
We consider the absolute condition number for the interpolation problem (1.28) given as the *Lebesgue constant*

$$\Lambda^{\boldsymbol{n}} \coloneqq \max_{(x,y)\in[-1,1]^2} \sum_{\mathcal{A}\in LS_2^{\boldsymbol{n}}} |L_{\mathcal{A}}(x, y)| \ . \tag{1.45}$$

We have the following results.

Theorem 5. *Let* $n_{\min} = \min\{n_1, n_2\}$ *and* $n_{\max} = \max\{n_1, n_2\}$. *Then*

$$D_\Lambda \log^2(n_{\min}) \le \Lambda^{\boldsymbol{n}} \le C_\Lambda \log^2(n_{\max}) \ , \tag{1.46}$$

where the positive constants C_Λ *and* D_Λ *do not dipend on* n_1, n_2.

Corollary 1. *For any continuous function* $f \in C([-1, 1]^2)$, *we have*

$$\|f - \mathcal{L}^{\boldsymbol{n}} f\|_\infty \le (C_\Lambda \log^2(n_{\max}) + 2) E_{n_{\min}}(f) \ , \tag{1.47}$$

where $E_{n_{\min}}(f)$ *denotes the best approximation error of* f *in the polynomial space* $\Pi^{n_{\min}}$. *Moreover, if* $f \in C^s([-1, 1]^2)$ *is* s*-times continuously differentiable and* ω_f^s *denotes the modulus of continuity of* $f^{(s)}$, *then*

$$\|f - \mathcal{L}^{\boldsymbol{n}} f\|_\infty \le C \frac{\log^2(n_{\max})}{n_{\min}^s} \omega_f^s \left(\frac{1}{n_{\min}} \right) \ . \tag{1.48}$$

For further details about this section see [10].

Chapter 2

Three-dimensional Lissajous curves

2.1 Admissible and optimal tuples

Given $\boldsymbol{a} = (a_1, a_2, a_3) \in \mathbb{N}^3$, we consider the curve in the cube $[-1, 1]^3$ defined as

$$\gamma_{\boldsymbol{a}}(t) = (\cos(a_1 t), \cos(a_2 t), \cos(a_3 t)) \ , \tag{2.1}$$

where $t \in [0, \pi]$.
In the view of (1.3), we can say that $\gamma_{\boldsymbol{a}}$ is a degenerate tridimensional Lissajous curve.
This setting brings new problems with respect to the bidimensional case. First of all, $\gamma_{\boldsymbol{a}}$ is not self-intersecting and thus we have to use a different approach in order to find a set of points interesting for approximation issues.
The first important step is to find an extension of Lemma 1, providing a formula whose nodes lie on $\gamma_{\boldsymbol{a}}$.
Fortunately this is possible, but we have to pay more attention as we will see.

Definition 2. *Let $V = \mathbb{P}_m^3$ be the space of trivariate polynomials of total degree at most m and let $\boldsymbol{a} = (a_1, a_2, a_3) \in \mathbb{N}^3$.*
We say that $\boldsymbol{a}$ is V-admissible (of order m) if

$$\nexists\, \mathbf{0} \neq \boldsymbol{b} \in \mathbb{Z}^3 \ , \ |\boldsymbol{b}| = |b_1| + |b_2| + |b_3| \leq m \ , \tag{2.2}$$

such that

$$a_1 b_1 + a_2 b_2 + a_3 b_3 = 0 \ . \tag{2.3}$$

We call $\mathcal{A}(V)$ the set of such admissible tuples.

The set $\mathcal{A}(V)$ is important for our purposes, as we are able to obtain a quadrature formula just for tuples belonging to this set. Indeed, we have the following.

Theorem 6. *Let V and $\boldsymbol{a}$ be as in Definition 2 and let $\boldsymbol{x} = (x_1, x_2, x_3)$, $w(\boldsymbol{x}) = \frac{1}{\sqrt{(1-x_1^2)(1-x_2^2)(1-x_3^2)}}$. Then*

$$\int_{[-1,1]^3} P(\boldsymbol{x}) w(\boldsymbol{x}) \mathrm{d}\boldsymbol{x} = \pi^2 \int_0^\pi P(\gamma_{\boldsymbol{a}}(t)) \mathrm{d}t \tag{2.4}$$

for all polynomials $P \in V$ if and only if $\boldsymbol{a} \in \mathcal{A}(V)$.

Proof. See [4]. □

Restricting a polynomial $P(\boldsymbol{x})$ to the curve $\gamma_{\boldsymbol{a}}(t)$ we can write

$$\deg(P(\gamma_{\boldsymbol{a}}(t)) \leq m \cdot \max_{i=1,2,3} a_i \ . \tag{2.5}$$

We are interested in determining the admissible tuple $\boldsymbol{a}_\star \in \mathcal{A}(V)$ which minimizes $\deg(P(\gamma_{\boldsymbol{a}}(t))$, i.e.

$$\boldsymbol{a}_\star = \min_{\boldsymbol{a}\in\mathcal{A}(V)} \max_{i=1,2,3} a_i \ . \tag{2.6}$$

In [3] it has been proved that the growth of $\boldsymbol{a}_\star$ is at least of $\mathcal{O}(m^2)$.
Through a computer search and calculations the following conjecture has been provided in [4].

Conjecture 7. *Let $\boldsymbol{a}_\star$ be an admissible and optimal tuple. Then:*

1. *For $m \equiv 0(4)$*

$$a_1 = \frac{3m^2+4m}{16} \ , \ a_2 = \frac{3m^2+8m}{16} \ , \ a_3 = \frac{3m^2+12m+16}{16} \ .$$

2. *For $m \equiv 1(4)$*

$$a_1 = \frac{3m^2+6m+7}{16} \ , \ a_2 = \frac{3m^2+10m+19}{16} \ , \ a_3 = \frac{3m^2+14m+15}{16} \ .$$

3. *For $m \equiv 2(4)$*

$$a_1 = \frac{3m^2+4}{16} \ , \ a_2 = \frac{3m^2+12m-4}{16} \ , \ a_3 = \frac{3m^2+12m+12}{16} \ .$$

4. *For $m \equiv 3(4)$*

$$a_1 = \begin{cases} \dfrac{3m^2+2m-1}{16} & m \equiv 3(8) \\ \dfrac{3m^2+6m+19}{16} & m \equiv 7(8) \end{cases} \ , \ a_2 = \begin{cases} \dfrac{3m^2+14m+11}{16} & m \equiv 3(8) \\ \dfrac{3m^2+10m+7}{16} & m \equiv 7(8) \end{cases} \ ,$$

$$a_3 = \frac{3m^2+14m+27}{16} \ .$$

2.2 Quadrature formula and hyperinterpolation

Similarly to the two-dimensional case, we can obtain a quadrature formula which is a consequence of Theorem 6.

Corollary 2. *Let $P \in V$ and $\gamma_{\boldsymbol{a}}$ as in (2.1). Let*

$$\nu = m \cdot \max\{a_1, a_2, a_3\} \ . \tag{2.7}$$

Then

$$\int_{[-1,1]^3} P(\boldsymbol{x}) w(\boldsymbol{x}) \mathrm{d}\boldsymbol{x} = \sum_{s=0}^{\mu} w_s P(\gamma_{\boldsymbol{a}}(\theta_s)) \ , \tag{2.8}$$

where for

$$w_s = \pi^2 \omega_s \ , \quad s = 0, ..., \mu \ , \tag{2.9}$$

and

$$\begin{gathered} \mu = \nu + 1 \ , \ , \theta_s = \tfrac{s\pi}{\mu} \ , \quad s = 0, ..., \mu \ , \\ \omega_0 = \omega_\mu = \tfrac{\pi}{2\mu} \ , \ \omega_s = \tfrac{\pi}{\mu} \ , \quad s = 1, ..., \mu - 1 \ . \end{gathered} \tag{2.10}$$

Proof. The proof follows the idea of the one given for Corollary 1 in [3].
We observe that with the change of variables $\tau = \cos t$ we have

$$\int_{[-1,1]^3} P(\boldsymbol{x})w(\boldsymbol{x})\mathrm{d}\boldsymbol{x} = \pi^2 \int_0^\pi P(\gamma_{\boldsymbol{a}}(t))\mathrm{d}t = \pi^2 \int_{-1}^1 P(T_{a_1}(\tau), T_{a_2}(\tau), T_{a_3}(\tau))\frac{\mathrm{d}\tau}{\sqrt{1-\tau^2}} \ . \tag{2.11}$$

Observing that $P(T_{a_1}(\tau), T_{a_2}(\tau), T_{a_3}(\tau))$ is a polynomial of degree not exceeding 2ν, the conclusion follows by using the Gauss-Chebyshev-Lobatto univariate quadrature rules, exact up to degree $2\nu + 1$. □

We consider the total-degree orthonormal basis of $\mathbb{P}^3_m$ with respect to the Chebyshev product measure writing

$$\hat{\phi}_{ijk}(\boldsymbol{x}) = \hat{T}_i(x_1)\hat{T}_j(x_2)\hat{T}_k(x_3) \quad , \quad i,j,k \geq 0 \ , \ i+j+k \leq m \ , \tag{2.12}$$

where $\hat{T}_n(\cdot)$ is the normalized Chebyshev polynomial of degree n

$$\hat{T}_n(\cdot) = \varsigma_n \cos(n \arccos(\cdot)) \ , \tag{2.13}$$

with

$$\varsigma_n = \sqrt{\frac{1+\mathrm{sign}(n)}{\pi}} \tag{2.14}$$

defining $\mathrm{sign}(0) = 0$.
Using the quadrature formula introduced in Corollary 2, we can approximate a function $f : [-1,1]^3 \to \mathbb{R}$ through a series of orthogonal polynomials up to total-degree m,

$$\mathcal{H}_m f(\boldsymbol{x}) = \sum_{0 \leq i+j+k \leq m} c_{ijk}\hat{\phi}_{ijk}(\boldsymbol{x}) \ , \tag{2.15}$$

where the Fourier-like coefficients are

$$c_{ijk} = \sum_{s=0}^{\mu} w_s f(\gamma_{\boldsymbol{a}}(\theta_s))\hat{\phi}_{ijk}(\gamma_{\boldsymbol{a}}(\theta_s)) \ . \tag{2.16}$$

The hyperinterpolation coefficients can be computed as follows.

Proposition 2. *Let $f : [-1,1]^3 \to \mathbb{R}$, $\gamma_{\boldsymbol{a}}, \nu, \mu, \theta_s, w_s, \omega_s$ as in Corollary 2. Then we have*

$$c_{ijk} = \frac{\pi^2}{4}\varsigma_{ia_1}\varsigma_{ja_2}\varsigma_{ka_3}\left(\frac{\psi_{\alpha_1}}{\varsigma_{\alpha_1}} + \frac{\psi_{\alpha_2}}{\varsigma_{\alpha_2}} + \frac{\psi_{\alpha_3}}{\varsigma_{\alpha_3}} + \frac{\psi_{\alpha_4}}{\varsigma_{\alpha_4}}\right) , \tag{2.17}$$

where

$$\begin{gathered} \alpha_1 = ia_1 + ja_2 + ka_3 \ , \ \alpha_2 = |ia_1 + ja_2 - ka_3| \ , \\ \alpha_3 = |ia_1 - ja_2| + ka_3 \ , \ \alpha_4 = ||ia_1 - ja_2| - ka_3| \ , \\ \psi_{\alpha_i} = \textstyle\sum_{s=0}^{\mu} \omega_s \hat{T}_{\alpha_i}(\tau_s) f(T_{a_1}(\tau_s), T_{a_2}(\tau_s), T_{a_3}(\tau_s)) \ , \end{gathered} \tag{2.18}$$

with $\tau_s = \cos(\theta_s)$.

Proof. See [3]. □

$\mathcal{H}_m$ is a projection operator, since $\mathcal{H}_m P = P$ for every $P \in \mathbb{P}^3_m$.
For our purposes, a fundamental property of the $\mathcal{H}_m$ operator is

$$\|\mathcal{H}_m\| = \sup_{f \neq 0} \frac{\|\mathcal{H}_m f\|_\infty}{\|f\|_\infty} = \mathcal{O}((\log m)^3) \ , \tag{2.19}$$

since this implies

$$\|\mathcal{H}_m f - f\|_\infty = \mathcal{O}((\log m)^3 E_m(f)) \ , \tag{2.20}$$

where $E_m(f)$ denote the best approximation error of f in $\mathbb{P}^3_m$.

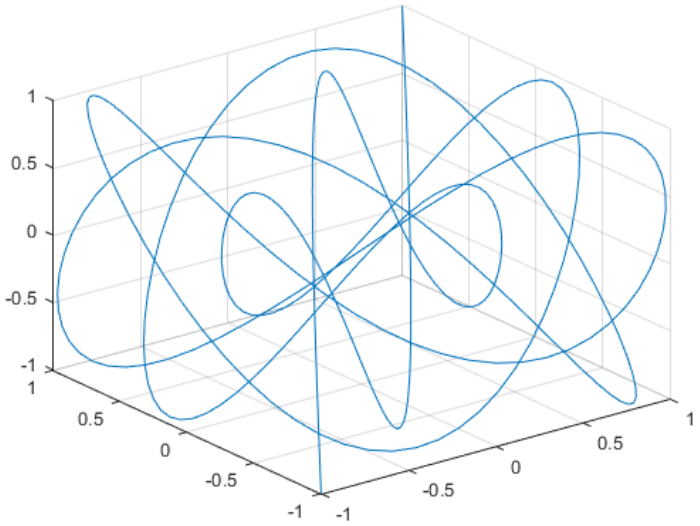

Figure 2.1: The curve $t \to (\cos(9t), \cos(11t), \cos(17t))$.

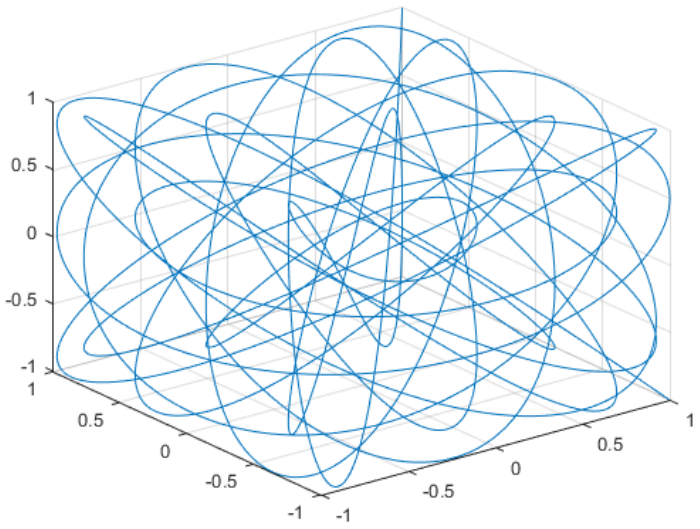

Figure 2.2: The curve $t \to (\cos(30t), \cos(33t), \cos(37t))$.

Chapter 3

Fourier series and Gibbs phenomenon

3.1 Trigonometric series for function approximation

Definition 3. *A 2π-periodic trigonometric series in complex form*

$$\sum_{n\in\mathbb{Z}} c_n e^{inx} \quad , \quad x \in \mathbb{R}\,, \tag{3.1}$$

is a two-sided series of functions defined in $\mathbb{R}$, where $c_n \in \mathbb{C}$ are the complex coefficients of the series.
If we fix $m \in \mathbb{N}$, the m-reduction of the series (3.1) is the series

$$\sum_{k=-m}^{k=m} c_k e^{ikx} \quad , \quad x \in \mathbb{R}\,. \tag{3.2}$$

From now on we use the simplifying notation $e_k(x) = e^{ikx}$.
Let $L^1_{2\pi}(\mathbb{R})$ be the set of functions defined as

$$L^1_{2\pi}(\mathbb{R}) = \left\{ f \ : \ f : \mathbb{R} \to \mathbb{R} \text{ is } 2\pi\text{-periodic and } \frac{1}{2\pi}\int_{-\pi}^{\pi} |f(x)|\mathrm{d}x < \infty \right\}, \tag{3.3}$$

equipped with the (semi)-norm

$$\|f\|_1 \coloneqq \frac{1}{2\pi}\int_{-\pi}^{\pi} |f(x)|\mathrm{d}x\,. \tag{3.4}$$

From easy direct calculations, we get that if $m, n \in \mathbb{N}$ then

$$\frac{1}{2\pi}\int_{-\pi}^{\pi} e_m(x)\overline{e_n(x)}\mathrm{d}x = \delta_{mn} \tag{3.5}$$

where $\delta_{mn} = 1$ if $m = n$ and it is equal to zero otherwise.
The next theorem is fundamental for all the theory.

Theorem 8. *Let $\sum_{n\in\mathbb{Z}} c_n e_n(x)$ be a 2π-periodic trigonometric series such that*

$$\lim_{m\to\infty} \left\| f - \sum_{k=-m}^{k=m} c_k e_k \right\|_1 = 0 \tag{3.6}$$

where $f \in L^1_{2\pi}(\mathbb{R})$. Then for every $n \in \mathbb{N}$

$$c_n = \frac{1}{2\pi}\int_{-\pi}^{\pi} f(x)\overline{e_n(x)}\mathrm{d}x\,. \tag{3.7}$$

Proof. Let $j \in \mathbb{Z}$ be fixed. Then

$$\begin{aligned}\left\| f\overline{e}_j - \Big(\sum_{k=-m}^{k=m} c_k e_k\Big)\overline{e}_j \right\|_1 &= \frac{1}{2\pi}\int_{-\pi}^{\pi} \left| f(x)\overline{e_j(x)} - \Big(\sum_{k=-m}^{k=m} c_k e_k(x)\Big)\overline{e_j(x)} \right| \mathrm{d}x \\ &= \frac{1}{2\pi}\int_{-\pi}^{\pi} |\overline{e_j(x)}| \left| f(x) - \Big(\sum_{k=-m}^{k=m} c_k e_k(x)\Big) \right| \mathrm{d}x \\ &= \frac{1}{2\pi}\int_{-\pi}^{\pi} \left| f(x) - \Big(\sum_{k=-m}^{k=m} c_k e_k(x)\Big) \right| \mathrm{d}x \\ &= \left\| f - \Big(\sum_{k=-m}^{k=m} c_k e_k\Big) \right\|_1 .\end{aligned}$$

In particular, we can pass the limit under the integral sign and write

$$\lim_{m\to\infty} \frac{1}{2\pi}\int_{-\pi}^{\pi} \Big(\sum_{k=-m}^{k=m} c_k e_k(x)\Big)\overline{e_j(x)}\mathrm{d}x = \int_{-\pi}^{\pi} f(x)\overline{e_j(x)}\mathrm{d}x = c_j(f) .$$

Moreover,

$$\frac{1}{2\pi}\int_{-\pi}^{\pi} \Big(\sum_{k=-m}^{k=m} c_k e_k(x)\Big)\overline{e_j(x)}\mathrm{d}x = \sum_{k=-m}^{k=m} c_k \Big(\frac{1}{2\pi}\int_{-\pi}^{\pi} e_k(x)\overline{e_j(x)}\mathrm{d}x\Big) = \sum_{k=-m}^{k=m} c_k \delta_{kj}$$

which concides with c_j. □

The last theorem gives sense to the following definition.

Definition 4. *Let $f \in L^1_{2\pi}(\mathbb{R})$. We define the Fourier series of f in complex form as*

$$Sf(x) = \sum_{n\in\mathbb{Z}} c_n(f)e_n(x) \quad , \quad x \in \mathbb{R} , \tag{3.8}$$

where for every $n \in \mathbb{Z}$

$$c_n(f) = \frac{1}{2\pi}\int_{-\pi}^{\pi} f(x)\overline{e_n(x)}\mathrm{d}x . \tag{3.9}$$

Moreover, the m-reduction of Sf is the series

$$S_m f(x) = \sum_{k=-m}^{k=m} c_k(f)e_k(x) \quad , \quad x \in \mathbb{R} . \tag{3.10}$$

The question now is if we are able to reconstruct any function $f \in L^1_{2\pi}(\mathbb{R})$ from its Fourier series. This is not always possible, but it is achievable for a large class of functions of common use, in particular for piecewise differentiable functions.

Definition 5. *Let $[a,b]$ be a compact subset of $\mathbb{R}$ and let $l \in \mathbb{Z}_{\geq 0} \cup \{\infty\}$. A function $f : [a,b] \to \mathbb{R}$ is C^l-piecewise differentiable if there exist $t_0 = a < t_1 < ... < b = t_n$ and functions $f_k \in C^l([t_{k-1}, t_k], \mathbb{R})$, $k = 1, ..., m$, such that f_k concides with f on every open interval (t_{k-1}, t_k).*
$f : \mathbb{R} \to \mathbb{R}$ is C^l-piecewise differentiable if so is the restriction of f on every compact subset of $\mathbb{R}$.
If $l = 0$ then f is piecewise continuous.
We say that f is piecewise differentiable if $l \geq 1$.

We observe that piecewise differentiable functions are locally integrable and they always admit right and left limits in every point.
We state the following well-known result.

Theorem 9. *Let $f : \mathbb{R} \to \mathbb{R}$ be 2π-periodic and C^1-piecewise differentiable. Then the Fourier series Sf is pointwise convergent to f where f is continuous. If f is not continuous in $\xi \in \mathbb{R}$, then*

$$\lim_{m\to\infty} S_m f(\xi) = \frac{f(\xi^+) + f(\xi^-)}{2} , \tag{3.11}$$

where $f(\xi^+), f(\xi^-)$ are respectively the right and the left limit of f in ξ.
Moreover, Sf is uniform convergent to f on any compact subinterval of $\mathbb{R}$ which does not contain any leap point c such that $|f(c^+) - f(c^-)| > 0$.

Proof. Omitted, see for example [16]. □

The last theorem about convergence of Fourier series is valid in a more general setting also and can be found in any book about complex analysis and Fourier theory. Nevertheless, the version we stated it is enough for our application issues.

3.2 Coefficients decay rate for functions in $F_k(\mathbb{R})$

We are interested in the behaviour of Fourier coefficients $c_n(f)$ as $n \to \infty$. From the Riemann-Lebesgue lemma (see for example [16]) we know that if $f \in L^1_{2\pi}(\mathbb{R})$ then

$$\lim_{n\to\infty} c_n(f) = 0 . \tag{3.12}$$

There is a strong connection between the smoothness of the function f and the decay rate of the coefficients $c_n(f)$.
We recall the following definition.

Definition 6. *The function f is absolutely continuous on the closed interval $[\alpha, \beta]$ if $\forall \epsilon > 0$ $\exists \delta > 0$ such that for each finite collection of disjoint intervals $(\alpha_j, \beta_j) \subset [\alpha, \beta]$, $j = 1, ..., s$, staisfying $\sum_{j=1}^{s} (\beta_j - \alpha_j) < \delta$ one has $\sum_{j=1}^{s} |f(\beta_j) - f(\alpha_j)| < \epsilon$.*
The function f is locally absolutely continuous on the open set $\Omega \subset \mathbb{R}$ if it is absolutely continuous on each closed interval $[\alpha, \beta] \subset \Omega$.

We introduce also the notion of *weak derivative* for the one-dimensional case, adapted to our situation.

Definition 7. *Let $\Omega \subset \mathbb{R}$ be an open set, $l \in \mathbb{N}$ and $f, g \in L^1_{2\pi}(\mathbb{R})$. The function g is a weak derivative of the function f of order l on Ω (briefly $g = f_w^{(l)}$) if there exists a function h equivalent to f on Ω (i.e. $f = h$ a.e. in Ω) which has a locally absolutely continuous $(l-1)$-th ordinary derivative $h^{(l-1)}$ and such that its ordinary derivative $h^{(l)}$ is equivalent to g in Ω.*

For $k \in \mathbb{Z}_{\geq 0}$, we introduce the following set of functions:

$$F_k(\mathbb{R}) = \{ f \in L^1_{2\pi}(\mathbb{R}) \ : \ \exists f_w^{(k+1)} \notin C(\mathbb{R}) \text{ and it is piecewise differentiable} \} . \tag{3.13}$$

Let $f \in F_k(\mathbb{R})$, using integration by parts we can write

$$\begin{aligned} \frac{1}{2\pi}\int_{-\pi}^{\pi} f(x)e^{-inx}\mathrm{d}x &= \left[\frac{i}{2\pi n} f(x)e^{-inx}\right]_{x=-\pi}^{x=\pi} - \frac{i}{2\pi n}\int_{-\pi}^{\pi} f'(x)e^{-inx}\mathrm{d}x \\ &= -\frac{i}{2\pi n}\int_{-\pi}^{\pi} f'(x)e^{-inx}\mathrm{d}x \end{aligned} \tag{3.14}$$

which gives us the estimate

$$|c_n(f)| \leq \frac{M}{n} , \tag{3.15}$$

where $M = \|f'\|_1$.
We can iterate this process until the step

$$c_n(f) = \left(-\frac{i}{n}\right)^{k+1} \frac{1}{2\pi} \int_{-\pi}^{\pi} f_w^{(k+1)}(x) e^{-inx} \mathrm{d}x \, . \tag{3.16}$$

The function $f_w^{(k+1)}$ is piecewise continuous. Let us suppose that $\xi \in \mathbb{R}$ is the unique leap point of $f_w^{(k+1)}$. We can suppose $\xi \in (-\pi, \pi)$ without loss of generality. Let then f_1, f_2 be the restrictions of the function $f_w^{(k+1)}$ to $(-\pi, \xi)$ and (ξ, π) respectively. We can write

$$\begin{aligned} c_n(f) &= \left(-\frac{i}{n}\right)^{k+1} \frac{1}{2\pi} \left(\int_{-\pi}^{\xi} f_1(x) e^{-inx} \mathrm{d}x + \int_{\xi}^{\pi} f_2(x) e^{-inx} \mathrm{d}x \right) \\ &= \left(-\frac{i}{n}\right)^{k+1} \frac{1}{2\pi} \left(\frac{i}{n} \Big[f_1(x) e^{-inx} \Big]_{x=-\pi}^{x=\xi^-} + \frac{i}{n} \Big[f_2(x) e^{-inx} \Big]_{x=\xi^+}^{x=\pi} - \frac{i}{n} \int_{-\pi}^{\xi} f_1'(x) e^{-inx} \mathrm{d}x + \right. \\ &\left. - \frac{i}{n} \int_{\xi}^{\pi} f_2'(x) e^{-inx} \mathrm{d}x \right) \\ &= \left(-\frac{i}{n}\right)^{k+2} \frac{1}{2\pi} \left(f_2(\xi^+) e^{-in\xi^+} - f_1(\xi^-) e^{-in\xi^-} + \int_{-\pi}^{\xi} f_1'(x) e^{-inx} \mathrm{d}x + \int_{\xi}^{\pi} f_2'(x) e^{-inx} \mathrm{d}x \right) . \end{aligned} \tag{3.17}$$

Therefore we get

$$|c_n(f)| \leq \; M n^{-(k+2)} \, , \tag{3.18}$$

where $M = \frac{1}{2\pi}\big(|f_2(\xi^+)| + |f_1(\xi^-)|\big) + \int_{-\pi}^{\xi} |f_1'(x)| \mathrm{d}x + \int_{\xi}^{\pi} |f_2'(x)| \mathrm{d}x < \infty$.
Since the previous reasoning can be extended to the general case in which $f_w^{(k+1)}$ has a finite number of leap points, we obtain

$$|c_n(f)| \in \mathcal{O}\left(\frac{1}{n^{k+2}}\right) \quad \text{as} \quad n \to \infty \, . \tag{3.19}$$

It is interesting for applications to consider the case in which a function $f \in L^1_{2\pi}(\mathbb{R})$ is not continuous and it is piecewise differentiable. Using the same argument presented for $f_w^{(k+1)}$ in (3.17), we get in this case

$$|c_n(f)| \in \mathcal{O}\left(\frac{1}{n}\right) \quad \text{as} \quad n \to \infty \, . \tag{3.20}$$

Observation 10. *In the definition of the set $F_k(\mathbb{R})$ in* (3.13) *we required $f_w^{(k+1)}$ to be piecewise differentiable. Actually, in order to achieve the final step in* (3.17) *the functions f_1, f_2 can be just absolutely continuous and with piecewise continuous weak derivatives $f_{1,w}', f_{2,w}'$.*

3.3 The Gibbs phenomenon

In the previous section we saw that the decay rate of Fourier coefficients is determined by the smoothness of the function which we are considering. We observed that for piecewise differentiable functions which are discontinuous the decay rate is $\mathcal{O}(1/n)$.
We point out that the step between a decay of order $\mathcal{O}(1/n)$ and a $\mathcal{O}(1/n^2)$-order one is someway crucial. In order to be more precise, we recall a fundamental result for series convergence, that is

$$\sum_{n=0}^{\infty} \frac{1}{n^{\alpha}} < \infty \Longleftrightarrow \alpha > 1 \, . \tag{3.21}$$

Thus, if $f \in F_k(\mathbb{R})$ for some value of $k \geq 1$ then the sum of its Fourier coefficients is convergent, otherwise if we lose the continuity of f then we get the divergence of the considered sum.
This fact is directly involved in the uniform convergence of the partial sum $S_m f$ to f. The reducted Fourier series $S_m f$ converges uniformly to f on a compact subinterval of $\mathbb{R}$ if we are able to put an uniform bound to

$$|f(x) - S_m f(x)| = \left| f(x) - \sum_{k=-m}^{k=m} c_k(f) e_k(x) \right| = \left| \sum_{k=-\infty}^{k=-m-1} c_k(f) e_k(x) + \sum_{k=m+1}^{k=\infty} c_k(f) e_k(x) \right| .$$

We estimate the previous expression writing

$$\left| \sum_{k=-\infty}^{k=-m-1} c_k(f) e_k(x) + \sum_{k=m+1}^{k=\infty} c_k(f) e_k(x) \right| \leq \sum_{k=-\infty}^{k=-m-1} |c_k(f)| + \sum_{k=m+1}^{k=\infty} |c_k(f)| \tag{3.22}$$

and finally

$$\sum_{k=-\infty}^{k=-m-1} |c_k(f)| + \sum_{k=m+1}^{k=\infty} |c_k(f)| \leq \sum_{k=-\infty}^{k=\infty} |c_k(f)| . \tag{3.23}$$

If the Fourier coefficients decay is fast enough, then the right-side member in the inequality (3.23) can be made arbitrary small taking m large enough, obtaining an uniform bound indipendent from x and uniform convergence of the series $S_m f$ to f.
The lost of uniform convergence in presence of one or more leap points causes the manifestation of the *Gibbs phenomenon*.

The Gibbs phenomenon is the particular way in which the reducted Fourier series $S_m f$ of a C^l-piecewise differentiable and discontinuous function f behaves near leap points, presenting high oscillations that do not disappear as m becomes larger. Such oscillations produce an increasing of the maximum of $S_m f$ near jumps, causing a worse approximation of the function f.
At a first sight, this behaviour seems to be in contrast with the pointwise convergence of the series to the considered function. Actually the contrast does not take place, since the region of the overshoot approaches the discontinuity point and it tends to zero in the limit of the partial sum.
For m large, the partial sum $S_m f$ overshoots the jump by approximately the 9% of its length.

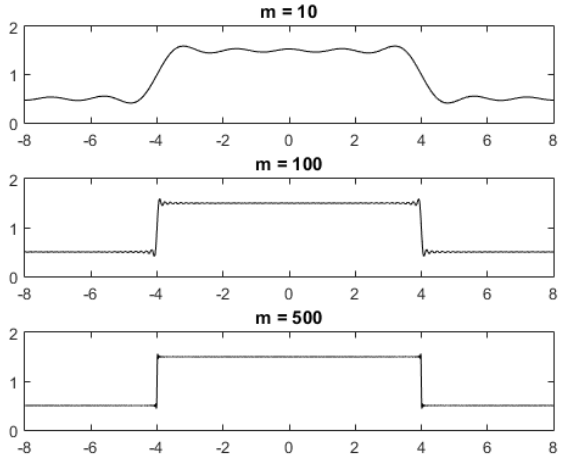

Figure 3.1: Fourier series approximation of a square wave function

3.4 Multi-dimensional Fourier series and coefficients

Let $f : \mathbb{R}^\nu \to \mathbb{R}$ be a real-valued function, $\nu \in \mathbb{N}$, $\nu \geq 2$. We say that f is 2π-periodic if f is 2π-periodic in every variable.
For $1 \leq p \leq \infty$, $\boldsymbol{x} = (x_1, x_2, ..., x_\nu)$, we consider the set

$$L^p_{2\pi}(\mathbb{R}^\nu) = \left\{ f \ : \ f : \mathbb{R}^\nu \to \mathbb{R} \text{ is } 2\pi\text{-periodic and } (2\pi)^{-\nu} \int_{(-\pi,\pi)^\nu} |f(\boldsymbol{x})|^p \mathrm{d}\boldsymbol{x} < \infty \right\}, \quad (3.24)$$

where $\mathrm{d}\boldsymbol{x}$ is the ν-dimensional Lebesgue measure, and the (semi)-norm

$$\|f\|_p := \begin{cases} (2\pi)^{-\nu} \left(\displaystyle\int_{(-\pi,\pi)^\nu} |f(\boldsymbol{x})|^p \mathrm{d}\boldsymbol{x} \right)^{1/p} & \text{if } 1 \leq p < \infty, \\ (2\pi)^{-\nu} \displaystyle\sup_{\boldsymbol{x} \in \mathbb{R}^\nu} |f(\boldsymbol{x})| & \text{if } p = \infty. \end{cases} \quad (3.25)$$

The result of Theorem 8 admits a multi-dimensional generalization, see [19].
Given $\boldsymbol{n} = (n_1, n_2, ..., n_\nu) \in \mathbb{Z}^\nu$, we set $e_{\boldsymbol{n}}(\boldsymbol{x}) = e_{n_1}(x_1) e_{n_2}(x_2) ... e_{n_\nu}(x_\nu)$, with $\overline{e_{\boldsymbol{n}}(\boldsymbol{x})} = \overline{e_{n_1}(x_1)}\, \overline{e_{n_2}(x_2)} ... \overline{e_{n_\nu}(x_\nu)}$.

Definition 8. *Let $f : \mathbb{R}^\nu \to \mathbb{R}$, $f \in L^1_{2\pi}(\mathbb{R}^\nu)$. The multi-dimensional Fourier series of f in complex form is defined as*

$$Sf(\boldsymbol{x}) = \sum_{\boldsymbol{n} \in \mathbb{Z}^\nu} c_{\boldsymbol{n}}(f) e_{\boldsymbol{n}}(\boldsymbol{x}) \quad , \quad \boldsymbol{x} \in \mathbb{R}^\nu \, , \quad (3.26)$$

where for every $\boldsymbol{n} \in \mathbb{Z}^\nu$

$$c_{\boldsymbol{n}}(f) = (2\pi)^{-\nu} \int_{(-\pi,\pi)^\nu} f(\boldsymbol{x}) \overline{e_{\boldsymbol{n}}(\boldsymbol{x})} \mathrm{d}\boldsymbol{x} \, . \quad (3.27)$$

Moreover, if $m \in \mathbb{N}$ the m-reduction of Sf is the series

$$S_m f(\boldsymbol{x}) = \sum_{\substack{\boldsymbol{k} \in \mathbb{Z}^\nu \\ \|\boldsymbol{k}\|_\infty \leq m}} c_{\boldsymbol{k}}(f) e_{\boldsymbol{k}}(\boldsymbol{x}) \quad , \quad \boldsymbol{x} \in \mathbb{R}^\nu \, , \quad (3.28)$$

where $\|\boldsymbol{k}\|_\infty = \|(k_1, k_2, ..., k_\nu)\|_\infty = \sup\{|k_1|, |k_2|, ..., |k_\nu|\}$.

We state a generalization of Theorem 9, which allows us to consider the reducted bivariated Fourier series for approximation issues.

Theorem 11. *Let $1 < p \leq \infty$. If $f \in L^p_{2\pi}(\mathbb{R}^\nu)$ then*

$$\lim_{m \to \infty} S_m f(\boldsymbol{x}) = f(\boldsymbol{x}) \quad (3.29)$$

almost everywhere in $\mathbb{R}^\nu$.

Proof. Omitted, see [19]. □

We want to cover the same path of Section 2.2 and find estimates for Fourier coefficients decay rate considering a sufficient set for our applications.
Let $\boldsymbol{\alpha} = (\alpha_1, \alpha_2, ..., \alpha_\nu) \in \mathbb{Z}^\nu_{\geq 0}$, $\boldsymbol{\alpha} \neq \boldsymbol{0}$. We use the notation

$$D^{\boldsymbol{\alpha}} f \equiv \frac{\partial^{\alpha_1 + \alpha_2 + ... + \alpha_\nu} f}{\partial x_1^{\alpha_1} \partial x_2^{\alpha_2} \partial x_\nu^{\alpha_\nu}} \, . \quad (3.30)$$

We denote $|\boldsymbol{\alpha}| = \alpha_1 + \alpha_2 + ... + \alpha_\nu$. Given an open set $\Omega \subset \mathbb{R}^\nu$, we call $C^\infty_0(\Omega)$ the set of infinitely continuously differentiable functions which have compactly supported in Ω.
We give a more general definition of weak derivative.

Definition 9. *Let $\Omega \subset \mathbb{R}^\nu$ be an open set, $\boldsymbol{\alpha} \in \mathbb{Z}^\nu_{\geq 0}$, $\boldsymbol{\alpha} \neq \mathbf{0}$, and let $f, g \in L^1_{2\pi}(\mathbb{R}^\nu)$. The function g is a weak derivative of the function f of order $\boldsymbol{\alpha}$ on Ω (briefly $g = D^{\boldsymbol{\alpha}}_w f$) if $\forall \phi \in C^\infty_0(\Omega)$ we have*

$$\int_\Omega f(\boldsymbol{x}) D^{\boldsymbol{\alpha}} \phi(\boldsymbol{x}) \mathrm{d}\boldsymbol{x} = (-1)^{|\boldsymbol{\alpha}|} \int_\Omega g(\boldsymbol{x}) \phi(\boldsymbol{x}) \mathrm{d}\boldsymbol{x} \,. \tag{3.31}$$

The previous definition and Definition 7 given for the one-dimensional case are related as one can see in [6].
We consider the set of functions $F_k(\mathbb{R}^\nu)$ defined as:

Definition 10. *Let $k \in \mathbb{Z}_{\geq 0}$. $F_k(\mathbb{R}^\nu)$ is the set of functions $f \in L^2_{2\pi}(\mathbb{R}^\nu)$ such that $f \in C^k(\mathbb{R}^\nu)$ and there exists $D^{\boldsymbol{\alpha}}_w f \notin C(\mathbb{R}^\nu)$ for every $|\boldsymbol{\alpha}| = k+1$.*
Moreover, $D^{\boldsymbol{\alpha}}_w f$ is piecewise differentiable, i.e. there exists a partition $(\Omega_i)_{i=1,\dots,n}$ of $[-\pi, \pi]^\nu$, where Ω_i is a closed set with Lipschitz boundary for every $i = 1, \dots, n$, and differentiable functions $f_i : \Omega_i \to \mathbb{R}$ such that $D^{\boldsymbol{\alpha}}_w f$ coincides with f_i on every open set $\mathring{\Omega}_i$

The Riemann-Lebesgue lemma (see for example [16]) tells us that even for the multivariate case we have

$$\lim_{\boldsymbol{n} \to \infty} c_{\boldsymbol{n}}(f) = 0 \,, \tag{3.32}$$

where with $\boldsymbol{n} \to \infty$ we mean $\max\{n_1, n_2, \dots, n_\nu\} \to \infty$.
We start to discuss the Fourier coefficient decay rate for functions in $F_k(\mathbb{R}^\nu)$. Let then $f \in F_k(\mathbb{R}^\nu)$, integrating by parts we can write

$$\begin{aligned} c_{\boldsymbol{n}}(f) &= (2\pi)^{-\nu} \int_{(-\pi,\pi)^\nu} f(\boldsymbol{x}) \overline{e_{\boldsymbol{n}}(\boldsymbol{x})} \mathrm{d}\boldsymbol{x} \\ &= (2\pi)^{-\nu} \left[\frac{i}{n_i} \int_{\partial(-\pi,\pi)^\nu} f(\boldsymbol{x}) \overline{e_{\boldsymbol{n}}(\boldsymbol{x})} v_{x_i} \mathrm{d}\sigma - \frac{i}{n_1} \int_{(-\pi,\pi)^\nu} \frac{\partial f}{\partial x_i}(\boldsymbol{x}) \overline{e_{\boldsymbol{n}}(\boldsymbol{x})} \mathrm{d}\boldsymbol{x} \right] , \end{aligned} \tag{3.33}$$

where v_{x_i} is the i-component of the outward unit surface normal to $\partial(-\pi, \pi)^\nu$. The surface integral in the last equation is equal to zero, due to the periodicity of the function. Then

$$c_{\boldsymbol{n}}(f) = -(2\pi)^{-\nu} (n_i)^{-1} \int_{(-\pi,\pi)^\nu} \frac{\partial f}{\partial x_i}(\boldsymbol{x}) \overline{e_{\boldsymbol{n}}(\boldsymbol{x})} \mathrm{d}\boldsymbol{x} \tag{3.34}$$

and

$$|c_{\boldsymbol{n}}(f)| \leq \frac{M}{n_i} \,, \tag{3.35}$$

where $M = \| \frac{\partial f}{\partial x_1} \|_1$.
Since by hypothesis $f \in C^k(\mathbb{R}^\nu)$ and admits a weak derivative $D^{\boldsymbol{\alpha}}_w f$ for every $|\boldsymbol{\alpha}| = k+1$, we can iterate the previous integration by parts procedure until the step

$$c_{\boldsymbol{n}}(f) = \left(-\frac{i}{n_i} \right)^{k+1} (2\pi)^{-\nu} \int_{(-\pi,\pi)^\nu} D^{\boldsymbol{\alpha}_\star}_w f(\boldsymbol{x}) \overline{e_{\boldsymbol{n}}(\boldsymbol{x})} \mathrm{d}\boldsymbol{x} \,, \tag{3.36}$$

where $\boldsymbol{\alpha}_\star$ is the ν-dimensional vector with $k+1$ in the i-th component and zeros in the others.
We observe that we can obtain different estimates choosing $i = 1, 2, \dots, \nu$. Every estimate has to be considered as referred to the coefficients decay rate in the i-th direction.

3.4.1 Separated-variables case

Starting from (3.36), we suppose $\nu = 2$ and

$$D_w^{\boldsymbol{\alpha}\star} f(x_1, x_2) = g_1(x_1) g_2(x_2)\,, \tag{3.37}$$

where $g_1 \notin C(\mathbb{R})$ but piecewise differentiable and $g_2 \in F_l(\mathbb{R})$ for some $l \in \mathbb{Z}_{\geq 0}$.
We can easily extend the conclusions of this two-dimensional setting to the general multi-dimensional case.
Using Fubini-Tonelli theorem we can write

$$\begin{aligned}\frac{1}{4\pi^2}\int_{(-\pi,\pi)^2} D_w^{\boldsymbol{\alpha}\star} f(x_1,x_2)\overline{e_{\boldsymbol{n}}(x_1,x_2)}\mathrm{d}x_1\mathrm{d}x_2 &= \frac{1}{4\pi^2}\int_{(-\pi,\pi)^2} g_1(x_1)g_2(x_2)\overline{e_{n_1}(x_1)}\,\overline{e_{n_2}(x_2)}\mathrm{d}x_1\mathrm{d}x_2 \\ &= \frac{1}{2\pi}\int_{-\pi}^{\pi}\left[\frac{1}{2\pi}\int_{-\pi}^{\pi} g_1(x_1)\overline{e_{n_1}(x_1)}\mathrm{d}x_1\right] g_2(x_2)\overline{e_{n_2}(x_2)}\mathrm{d}x_2\,.\end{aligned} \tag{3.38}$$

Hence, we can use the estimates given in the Section 3.2 getting the following two

$$\begin{aligned}&\left|\tfrac{1}{2\pi}\textstyle\int_{-\pi}^{\pi}\left[\tfrac{1}{2\pi}\int_{-\pi}^{\pi} g_1(x_1)\overline{e_{n_1}(x_1)}\mathrm{d}x_1\right] g_2(x_2)\overline{e_{n_2}(x_2)}\mathrm{d}x_2\right| \leq M_1 n_1^{-1}\,, \\ &\left|\tfrac{1}{2\pi}\textstyle\int_{-\pi}^{\pi}\left[\tfrac{1}{2\pi}\int_{-\pi}^{\pi} g_1(x_1)\overline{e_{n_1}(x_1)}\mathrm{d}x_1\right] g_2(x_2)\overline{e_{n_2}(x_2)}\mathrm{d}x_2\right| \leq M_2 n_2^{-(l+2)}\,,\end{aligned} \tag{3.39}$$

for some $0 < M_1, M_2 < \infty$, depending on the direction taken.
Choosing $i = 1$ in (3.36) we conclude

$$|c_{\boldsymbol{n}}(f)| \leq M(n_1)^{-(k+2)}\,, \tag{3.40}$$

taking $i = 2$ we get

$$|c_{\boldsymbol{n}}(f)| \leq M(n_2)^{-(k+l+3)}\,. \tag{3.41}$$

The coefficients decaying in the x_2 direction is then much more faster than in the x_1's one. As a consequence of such a fact, we will observe in Section 3.4.3 that the Gibbs phenomenon could arise in just one direction, the other being regular.
The generalization of the considerations of this subsection to the multi-dimensional case are immediate.

3.4.2 The general case

Let us come back to (3.36). Without loss of generality, we can suppose that the partition described in the Definition 10 is composed of two sets Ω_1 and Ω_2.
Therefore, integrating by parts we can write

$$\begin{aligned}&\textstyle\int_{(-\pi,\pi)^\nu} D_w^{\boldsymbol{\alpha}\star} f(\boldsymbol{x})\overline{e_{\boldsymbol{n}}(\boldsymbol{x})}\mathrm{d}\boldsymbol{x} = \\ &\textstyle\int_{\Omega_1} f_1(\boldsymbol{x})\overline{e_{\boldsymbol{n}}(\boldsymbol{x})}\mathrm{d}\boldsymbol{x} + \int_{\Omega_2} f_2(\boldsymbol{x})\overline{e_{\boldsymbol{n}}(\boldsymbol{x})}\mathrm{d}\boldsymbol{x} = \\ &-\tfrac{i}{n_i}\Big(\textstyle\int_{\Omega_1}\frac{\partial f_1}{\partial x_i}(\boldsymbol{x})\overline{e_{\boldsymbol{n}}(\boldsymbol{x})}\mathrm{d}\boldsymbol{x} + \int_{\Omega_2}\frac{\partial f_2}{\partial x_i}(\boldsymbol{x})\overline{e_{\boldsymbol{n}}(\boldsymbol{x})}\mathrm{d}\boldsymbol{x} + \\ &-\textstyle\int_{\partial\Omega_1} f_1(\boldsymbol{x})\overline{e_{\boldsymbol{n}}(\boldsymbol{x})}v_{x_i}\mathrm{d}\sigma - \int_{\partial\Omega_2} f_2(\boldsymbol{x})\overline{e_{\boldsymbol{n}}(\boldsymbol{x})}v_{x_i}\mathrm{d}\sigma\Big)\,,\end{aligned} \tag{3.42}$$

We observe that by hypothesis the four integrals in the last line of (3.42) are well-defined and finite. Hence finally, putting together the last equation with (3.36) and considering the absolute values as done before we get the "directional" estimate

$$|c_{\boldsymbol{n}}(f)| \in \mathcal{O}(n_i^{-(k+2)}) \quad \text{as} \quad \boldsymbol{n} \to \infty\,. \tag{3.43}$$

Observation 12. *Similarly to what observed for the one-dimensional case in the Observation 10, even in this two-dimensional case one can consider weaker hypothesis on $D^{\boldsymbol{\alpha}}_w f$ in Definition 10. Indeed, it is enough for the functions f_i to admit piecewise continuous weak derivatives .*

Observation 13. *It is well known that Fourier series theory can be applied to approximate integrable functions which could be non-periodic on a more general bounded interval. In order to do this and to preserve the possible continuity of the function, symmetrization and periodic extension are applied both in one-dimensional and multi-dimensional case.*
Therefore, in the next lines we could consider non-periodic functions and there will be no ambiguities in our discussions.

3.4.3 Regularity and Gibbs phenomenon

First, we observe that if a function f is piecewise differentiable according to Definition 10 then we get

$$|c_{\boldsymbol{n}}(f)| \in \mathcal{O}(n_i^{-1}) \quad \text{as} \quad \boldsymbol{n} \to \infty \, . \tag{3.44}$$

We saw in the one-dimensional case that a first order decay rate is slow enough to let the Gibbs phenomenon appear and this happens in the multi-dimensional case also.
As example, we take the function which takes the value 1 inside the centered circle of radius 0.75 and the value 0 outside, displayed in Figure 3.2.

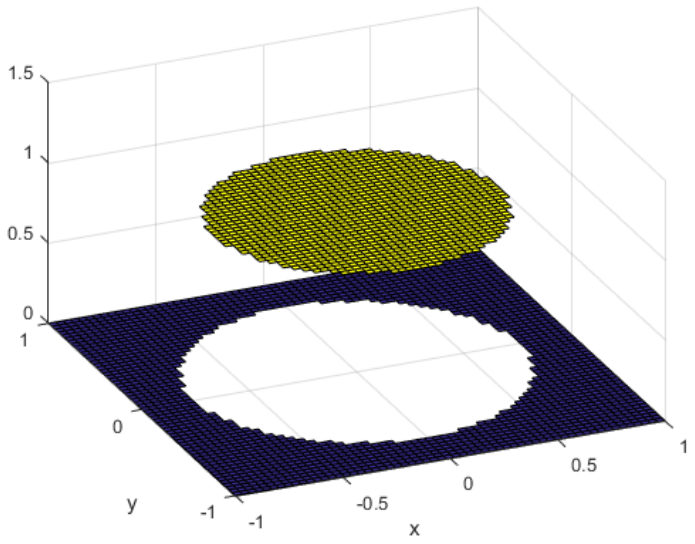

Figure 3.2: *The considered discontinuous function.*

We can see in Figure 3.3 that a Fourier series approximation of this function carries global oscillations, in particular near the discontinuities. More precisely, the Gibbs phenomenon appears if there is at least one direction in which the decaying is too slow.
In order to observe this fact, let us consider the function $f(x, y) = f_1(x) f_2(y)$ where

$$f_1(x) = \begin{cases} x & \text{if } -1/2 \leq x \leq 1/2 \, , \\ 0 & \text{otherwise} \, , \end{cases} \tag{3.45}$$

is discontinuous and $f_2(y) = 10e^{-y^2}$ is very regular. We can see in Figure 3.5 that the oscillations given by the Gibbs phenomenon are directed just in the x-direction, not involving the other one as observed in Section 3.4.1.

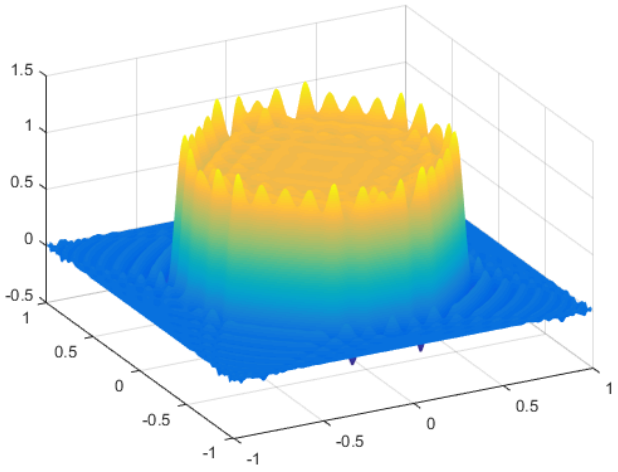

Figure 3.3: Fourier series approximation showing the Gibbs phenomenon.

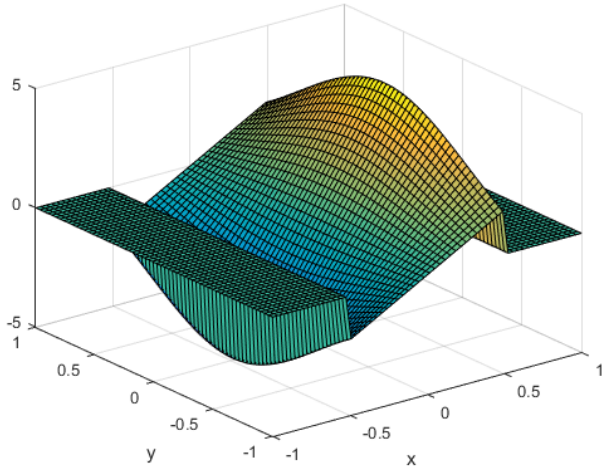

Figure 3.4: Plot of function f.

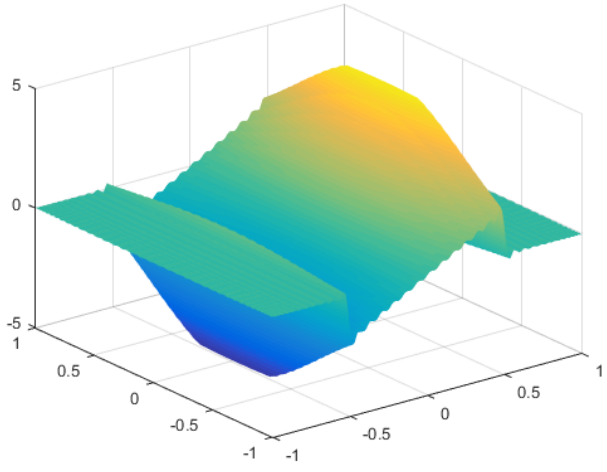

Figure 3.5: Fourier approximation of function f.

3.5 From Chebyshev to Fourier series

In the first chapter we saw that we can express the interpolating polynomial of a function f on Lissajous nodes using a two-dimensional Chebyshev series

$$\mathcal{L}^{\boldsymbol{n}} f(x,y) = \sum_{(j,k)\in\Gamma^{2\boldsymbol{n}}} c_{jk} T_j(x) T_k(y)\,. \tag{3.46}$$

We want to show the connection between Chebyshev and Fourier series. Let $x = \cos(t)$, $y = \cos(s)$. Then

$$\begin{aligned}\mathcal{L}^{\boldsymbol{n}} f(x,y) &= \sum_{(j,k)\in\Gamma^{2\boldsymbol{n}}} c_{jk}\cos(j\arccos(x))\cos(k\arccos(y)) \\ &= \sum_{(j,k)\in\Gamma^{2\boldsymbol{n}}} c_{jk}\cos(jt)\cos(ks) \\ &= \sum_{(j,k)\in\Gamma^{2\boldsymbol{n}}} \frac{c_{jk}}{4}(e_j(t)+\overline{e_j(t)})(e_k(s)+\overline{e_k(s)})\,.\end{aligned} \tag{3.47}$$

We consider the following symmetric extension of the set $\Gamma^{2\boldsymbol{n}}$ defined in (1.6),

$$\Gamma_S^{2\boldsymbol{n}} := \left\{(i,j)\in\mathbb{Z}^2 \;:\; (|i|,|j|)\in\Gamma^{2\boldsymbol{n}}\right\}. \tag{3.48}$$

Hence, we can write

$$\begin{aligned}\mathcal{L}^{\boldsymbol{n}} f(t,s) &= \sum_{(j,k)\in\Gamma^{2\boldsymbol{n}}} \frac{c_{jk}}{4}(e_j(t)+\overline{e_j(t)})(e_k(s)+\overline{e_k(s)})\,. \\ &= \sum_{(j,k)\in\Gamma_S^{2\boldsymbol{n}}} \widetilde{c_{jk}} e_j(t) e_k(s)\,,\end{aligned} \tag{3.49}$$

where

$$\widetilde{c_{jk}} = \begin{cases} c_{jk} & \text{if } (j,k)=(0,0), \\ \dfrac{1}{2}c_{|j||k|} & \text{if } (j,k)\neq(0,0) \text{ but } j=0 \text{ or } k=0, \\ \dfrac{1}{4}c_{|j||k|} & \text{for the others } (j,k)\in\Gamma_S^{2\boldsymbol{n}}. \end{cases} \tag{3.50}$$

It is useful to give to the coefficients a rectangular shape. In order to achieve this, we consider the following set of indices related to $\Gamma^{2\boldsymbol{n}}$,

$$R^{2\boldsymbol{n}} := \left\{(i,j)\in\mathbb{N}_0^2 \;:\; i<2n_1 \text{ and } j\le 2n_2\right\}. \tag{3.51}$$

We observe that $\Gamma^{2\boldsymbol{n}}\subset R^{2\boldsymbol{n}}$.
Considering then the symmetric extension

$$R_S^{2\boldsymbol{n}} := \left\{(i,j)\in\mathbb{Z}^2 \;:\; (|i|,|j|)\in R^{2\boldsymbol{n}}\right\}, \tag{3.52}$$

we get

$$\mathcal{L}^{\boldsymbol{n}} f(t,s) = \sum_{(j,k)\in R_S^{2\boldsymbol{n}}} \widetilde{\widetilde{c_{jk}}} e_j(t) e_k(s)\,, \tag{3.53}$$

where

$$\widetilde{\widetilde{c_{jk}}} = \begin{cases} \widetilde{c_{jk}} & \text{if } (j,k) \in \Gamma_S^{2\boldsymbol{n}}, \\ 0 & \text{if } (j,k) \in R_S^{2\boldsymbol{n}} \setminus \Gamma_S^{2\boldsymbol{n}}. \end{cases} \tag{3.54}$$

Observation 14. *In Theorem 11 we gave a convergence result for series approaching the limit in a square shape. The same result is reached considering more general polygons if the expansion of the chosen polygon involves any direction in the same way. This is a consequence of the Theorem stated by Fefferman in [11].*

Therefore, all the results about spectral filtering of the next chapter are effective for Chebyshev series and for the applications we are interested in also.
The results of this section are also true for the three-dimensional case, since even in this setting the hyperinterpolant is expressed as a Chebyshev series.

Chapter 4

Fourier spectral filters

4.1 Filtering process for solving the Gibbs phenomenon

4.1.1 The one-dimensional case

In the previous chapter we saw that if $f \in L^1_{2\pi}(\mathbb{R})$ is discontinuous but piecewise differentiable then the Fourier coefficients decay rate collapses and Gibbs phenomenon appears. We point out that Gibbs phenomenon does not involve just the behaviour of the reducted Fourier series near the discontinuities, it affects its general behaviour in the whole interval also, providing oscillations and errors. Indeed, the slow decay rate of the coefficients makes the high frequences play a stronger role in the sum.
A possible solution for this problem is to accelerate the decay rate using appropriate functions.

Definition 11. *A real and even function $\sigma(\eta)$ is called a spectral filter of order p if:*

1. $\sigma(0) = 1$, $\sigma^{(l)}(0) = 0$ *for* $1 \leq l \leq p-1$.
2. $\sigma(\eta) = 0$ *for* $|\eta| \geq 1$.
3. $\sigma(\eta) \in C^{p-1}$, $\eta \in (-\infty, \infty)$.

In the Definition 4 in the previous chapter we defined the m-partial Fourier series of a function $f \in L^1_{2\pi}(\mathbb{R})$ as

$$S_m f(x) = \sum_{k=-m}^{k=m} c_k(f) e_k(x) \quad , \quad x \in \mathbb{R}\,. \tag{4.1}$$

We are going to consider the following partial filtered series

$$S^\sigma_m f(x) = \sum_{k=-m}^{k=m} \sigma\left(\frac{k}{m}\right) c_k(f) e_k(x) \quad , \quad x \in \mathbb{R}\,. \tag{4.2}$$

Observation 15. *Given $S^\sigma_m f$, we observe that:*

- *Due to its definition, the filter does not act on low coefficients and it affects mainly the high ones.*
- *It is essential for the filter to be a smooth function. As known, Gibbs phenomenon does not disappear just cutting down the high coefficients, so a step function would be useless as a filter.*
- *The second condition in Definition 11 allows us to write*

$$S^\sigma_m f(x) = \sum_{k=-\infty}^{\infty} \sigma\left(\frac{k}{m}\right) c_k(f) e_k(x) \quad , \quad x \in \mathbb{R}\,. \tag{4.3}$$

We give some well-known examples of filters [12]:

- The Fejér filter (first order)
$$\sigma(\eta) = 1 - \eta \, . \tag{4.4}$$
- The Lanczos or sinc filter (first order)
$$\sigma(\eta) = \frac{\sin(\pi\eta)}{\pi\eta} \, . \tag{4.5}$$
- The *raised cosine* filter (second order)
$$\sigma(\eta) = \frac{1}{2}(1 + \cos(\pi\eta)) \, . \tag{4.6}$$
- The exponential filter of order p (p even)
$$\sigma(\eta) = e^{-\alpha\eta^p} \, . \tag{4.7}$$
In this case, since $\sigma(1) = e^{-\alpha}$ does not respect the formal definition of filter, in applications we set the value of α to the computer's roundoff error.

We state the following theorem, which shows that using a filtering process we can recover precision away from discontinuities in presence of Gibbs phenomenon.

Theorem 16. *Let f be a C^p-piecewise differentiable function with one point of discontinuity ξ. Let σ be a filter of order p and $x \in [-\pi, \pi]$, we denote $d(x) = \min_{k\in\mathbb{Z}} |x - \xi + 2k\pi|$. Let*
$$S_N^\sigma f(x) = \sum_{k\in\mathbb{Z}} \sigma\left(\frac{k}{N}\right) c_k(f) e_k(x) \, . \tag{4.8}$$
Then
$$|f(x) - S_N^\sigma f(x)| \leq CN^{1-p} d(x)^{1-p} K(f) + CN^{1/2-p} \left(\int_{\mathbb{R}} |f(t)^{(p)}|^2 \mathrm{d}t \right)^{1/2} , \tag{4.9}$$
where
$$K(f) = \sum_{l=0}^{p-1} d(x)^l \left(f^{(l)}(\xi^+) - f^{(l)}(\xi^-) \right) \int_{\mathbb{R}} |G_l^{(p-l)}(\eta)| \mathrm{d}\eta \, , \tag{4.10}$$
$$G_l(\eta) = \frac{\sigma(\eta) - 1}{\eta^l} \tag{4.11}$$
and $C > 0$ is a constant.

Proof. The proof is based on some lemmas and results, see [12]. □

4.1.2 A multi-dimensional extension

We want to extend the filtering process introduced in the previous lines.
This could be done in different ways and an intuitive one is to consider a tensor product structure. This pattern is indeed easy to be constructed and applied and, since we know the good properties of one-dimensional filters, we can be sure that the tensor product extension is going to be efficient in our applications.
We recall that for $f \in L^2_{2\pi}(\mathbb{R}^\nu)$, $m \in \mathbb{N}$ we defined the bivariate partial Fourier series as
$$S_m f(\boldsymbol{x}) = \sum_{\substack{\boldsymbol{k}\in\mathbb{Z}^\nu \\ \|\boldsymbol{k}\|_\infty \leq m}} c_{\boldsymbol{k}}(f) e_{\boldsymbol{k}}(\boldsymbol{x}) \quad , \quad \boldsymbol{x} \in \mathbb{R}^\nu \, , \tag{4.12}$$

where $\|\boldsymbol{k}\|_\infty = \|(k_1, k_2, ..., k_\nu)\|_\infty = \sup\{|k_1|, |k_2|, ..., |k_\nu|\}$. As in the last subsection, we consider from now on multivariate piecewise differentiable functions.
Let σ be a spectral filter according to the Definition 11. Fixed a number $N \in \mathbb{N}$, we can consider the vector of length $2N+1$

$$\sigma_k = \sigma\left(\frac{k}{N}\right) \quad , \quad -N \leq k \leq N \tag{4.13}$$

and write

$$S_N^\sigma f(x) = \sum_{k\in\mathbb{Z}} \sigma_k c_k(f) e_k(x) \ . \tag{4.14}$$

We can construct a tensor product pattern

$$\boldsymbol{\sigma_k} = \sigma_{k_1}\sigma_{k_2}...\sigma_{k_\nu} \quad , \quad -N \leq k_1, k_2, ..., k_\nu \leq N \ . \tag{4.15}$$

We can then consider the filtered series

$$S_N^\sigma f(\boldsymbol{x}) = \sum_{\boldsymbol{k}\in\mathbb{Z}^\nu} \boldsymbol{\sigma_k} c_{\boldsymbol{k}}(f) e_{\boldsymbol{k}}(\boldsymbol{x}) \ . \tag{4.16}$$

Observation 17. *The choice of the function $\boldsymbol{\sigma}(\eta_1, \eta_2, ..., \eta_\nu) = \sigma(\eta_1)\sigma(\eta_2)...\sigma(\eta_\nu)$ is well justified. Indeed, it is easy to see that if σ is a filter of order p then:*

1. $\boldsymbol{\sigma}(\mathbf{0}) = 1$, $(D^{\boldsymbol{\alpha}}\boldsymbol{\sigma})(\mathbf{0}) = 0$ *for* $1 \leq |\boldsymbol{\alpha}| \leq p-1$.
2. $\boldsymbol{\sigma}(\eta_1, \eta_2, ..., \eta_\nu) = 0$ *for* $\|(\eta_1, \eta_2, ..., \eta_\nu)\|_\infty \geq 1$.
3. $\boldsymbol{\sigma}(\eta_1, \eta_2, ..., \eta_\nu) \in C^{p-1}$.

It follows that the function $\boldsymbol{\sigma}$ acts on high frequences in a regular way as σ in the univariated case.

Observation 18. *We defined $\boldsymbol{\sigma}$ using a unique one-dimensional filter. Actually, one could consider a more general definition*

$$\boldsymbol{\sigma} = \sigma_1 \cdot \sigma_2 \cdot ... \cdot \sigma_\nu \tag{4.17}$$

where $\sigma_1, \sigma_2, ..., \sigma_\nu$ are different filters which can be of different orders. Such a definition could be interesting in the case we know the function which we are handling a priori. For example, we could decide to apply a strong filter in a direction and a weak one in the other, or if we know that the Gibbs phenomenon appears in only one direction (see Section 3.4.3), let us say x_1-direction, we can set $\sigma_2 \equiv 1$ deciding to not act on the regular direction.
In fact, in applications we are not given the possibility to know the function which we are dealing with. Therefore, we prefer a more "neutral" approach.

4.2 Adaptive filtering process

4.2.1 Introduction

Spectral filters act on the Fourier coefficients and do not consider the physical position of the discontinuities.
It is known that the operation of such filters is equivalent to mollification in the physical space. Indeed, defining the mollifier

$$\Phi^\sigma(y) \coloneqq \frac{1}{2\pi} \sum_{k\in\mathbb{Z}} \sigma_k e_k(y) \tag{4.18}$$

we can write

$$S_N^\sigma f(x) \equiv f * \Phi^\sigma(y) = \frac{1}{2\pi} \int_{-\pi}^{\pi} \Phi^\sigma(y) f(x-y) \mathrm{d}y \ . \tag{4.19}$$

In order to gain more adaptivity, we slightly modify the filter vector introduced in (4.13), considering

$$\sigma_k = \sigma\left(\frac{|k|}{N}\right) \quad , \quad -N \leq k \leq N \; . \tag{4.20}$$

With the filter vector defined in this way, we have more freedom in choosing the filter function.
We take then the following function as filter

$$\sigma^p(x) = \begin{cases} \exp\left(\dfrac{x^p}{x^2-1}\right) & |x| < 1 \; , \\ 0 & |x| \geq 1 \; , \end{cases} \tag{4.21}$$

observing that due to the new definition given in (4.21) we are allowed to let $p \in \mathbb{R}$, $p > 0$. This is a fundamental step for our discussion, since the parameter $p = p(x, N)$ is the key for adaptivity.
In the next subsection we consider a two-dimensional tensor product setting, referring to the one-dimensional case discussion in [17].

4.2.2 Tensor product adaptive filtering

Let $\boldsymbol{x} = (x_1, x_2) \in \mathbb{R}^2$ and let us consider the bivariate real function $f(\boldsymbol{x})$, which is piecewise analytic (and not just differentiable) according to Definiton 10 and to the discussion of previous chapter. For $\boldsymbol{y} = (y_1, y_2) \in \mathbb{R}^2$, we take

$$\Phi^\sigma(\boldsymbol{y}) \coloneqq \frac{1}{4\pi^2} \sum_{\boldsymbol{k} \in \mathbb{Z}^2} \boldsymbol{\sigma_k} e_{\boldsymbol{k}}(\boldsymbol{y}) \; , \tag{4.22}$$

where

$$\boldsymbol{\sigma_k} = \sigma_{k_1}^{p_1} \sigma_{k_2}^{p_2} \; , \tag{4.23}$$

in the sense given by (4.20) and (4.21).

Let $\boldsymbol{\xi} = (\xi_1, \xi_2)$ be the nearest point of discontinuity with respect to $\boldsymbol{x}$ in the euclidean norm.
For $i = 1, 2$, we call $d_i(x_i) = |x_i - \xi_i|$.
We claim the following result, proved in the following lines of this section.

Theorem 19. *Let $f : \mathbb{R}^2 \to \mathbb{R}$ be a piecewise analytic function. Then, defining*

$$\boldsymbol{p} = (p_1, p_2) = ((N\eta_1^* d_1(x_1))^{1/2}, (N\eta_2^* d_2(x_2))^{1/2}) \; , \tag{4.24}$$

we get the asymptotic exponential decaying of the error $|f - S_N^\sigma f|$ away from the points of discontinuity of f, where $S_N^\sigma f = f * \Phi^\sigma$ and in (4.18) we use the parameters p_1, p_2 defined in (4.24).

We define the two cut-off functions

$$\rho_i(x_i) = \begin{cases} 1 & \text{if } |x_i| \leq 1/2 \; , \\ 0 & \text{if } |x_i| \geq 1 \; , \end{cases} \tag{4.25}$$

with $\rho_1, \rho_2 \in C_0^\infty$.
We also define the auxiliary function

$$\chi(\boldsymbol{y}) = \chi_{\boldsymbol{x}}(\boldsymbol{y}) = \chi_1(y_1)\chi_2(y_2) = \rho_1(y_1/d_1(x_1))\rho_2(y_2/d_2(x_2)) \; . \tag{4.26}$$

We can split the error $f - S_N^\sigma f = f - f * \Phi^\sigma$ in

$$\begin{aligned} f(\boldsymbol{x}) - f * \Phi^\sigma(\boldsymbol{x}) &= \int_{(-\pi,\pi)^2} \Phi^\sigma(\boldsymbol{y})[f(\boldsymbol{x}) - f(\boldsymbol{x}-\boldsymbol{y})][1-\chi(\boldsymbol{y})]\mathrm{d}\boldsymbol{y} + \\ &+ \int_{(-\pi,\pi)^2} \Phi^\sigma(\boldsymbol{y})[f(\boldsymbol{x}) - f(\boldsymbol{x}-\boldsymbol{y})]\chi(\boldsymbol{y})\mathrm{d}\boldsymbol{y} \\ &:= \mathcal{I}_1 + \mathcal{I}_2 \ , \end{aligned} \tag{4.27}$$

We observe that the $\boldsymbol{y}$-function $f(\boldsymbol{x}) - f(\boldsymbol{x}-\boldsymbol{y})$ is smooth if $|y_1| \leq d_1(x_1)$ and $|y_2| \leq d_2(x_2)$. We consider now the two-dimensional filter function

$$\boldsymbol{\sigma}(\boldsymbol{x}) = \sigma^{p_1}(x_1)\sigma^{p_2}(x_2) \tag{4.28}$$

and the Fourier transform

$$\begin{aligned} \boldsymbol{\sigma}(\boldsymbol{x}) &= \frac{1}{4\pi^2}\int_{\mathbb{R}^2} \phi^\sigma(\boldsymbol{y}) e^{-i\boldsymbol{x}\cdot\boldsymbol{y}}\mathrm{d}\boldsymbol{y} \\ &= \frac{1}{4\pi^2}\int_{\mathbb{R}^2} \phi_1^\sigma(y_1)e^{-ix_1y_1}\phi_2^\sigma(y_2)e^{-ix_2y_2}\mathrm{d}y_1\mathrm{d}y_2 \ . \end{aligned} \tag{4.29}$$

The tensor product structure allows us to sample two univariated Fourier transforms separately and to write

$$\begin{aligned} \boldsymbol{\sigma}_{\boldsymbol{k}} &= \sigma^{p_1}\left(\frac{|k_1|}{N}\right)\sigma^{p_2}\left(\frac{|k_2|}{N}\right) \\ &= \frac{N^2}{4\pi^2}\int_{\mathbb{R}^2} \phi_1^\sigma(Ny_1)e^{-iNy_1(|k_1|/N)}\phi_2^\sigma(Ny_2)e^{-iNy_2(|k_2|/N)}\mathrm{d}y_1\mathrm{d}y_2 \\ &= \frac{N^2}{4\pi^2}\sum_{\boldsymbol{n}\in\mathbb{Z}^2}\int_{[-\pi,\pi]^2} \phi_1^\sigma(N(y_1+2\pi n_1))\phi_2^\sigma(N(y_2+2\pi n_2))e^{-i|\boldsymbol{k}|\cdot\boldsymbol{y}}\mathrm{d}\boldsymbol{y} \\ &= \frac{N^2}{4\pi^2}\int_{[-\pi,\pi]^2}\sum_{\boldsymbol{n}\in\mathbb{Z}^2} \phi_1^\sigma(N(y_1+2\pi n_1))\phi_2^\sigma(N(y_2+2\pi n_2))e^{-i|\boldsymbol{k}|\cdot\boldsymbol{y}}\mathrm{d}\boldsymbol{y} \ , \end{aligned} \tag{4.30}$$

where $|\boldsymbol{k}| = (|k_1|, |k_2|)$. Observing then that

$$\boldsymbol{\sigma}_{\boldsymbol{k}} = \int_{\mathbb{R}^2} \Phi^\sigma(\boldsymbol{y})e^{-i|\boldsymbol{k}|\cdot\boldsymbol{y}}\mathrm{d}\boldsymbol{y} \ , \tag{4.31}$$

we get finally

$$\Phi^\sigma(\boldsymbol{y}) \equiv \frac{N^2}{4\pi^2}\sum_{\boldsymbol{n}\in\mathbb{Z}^2} \phi_1^\sigma(N(y_1+2\pi n_1))\phi_2^\sigma(N(y_2+2\pi n_2)) \ . \tag{4.32}$$

We estimate the absolute value writing

$$\begin{aligned} |\Phi^\sigma(\boldsymbol{y})| &\leq \frac{N^2}{4\pi^2}\sum_{\boldsymbol{n}\in\mathbb{Z}^2} |\phi_1^\sigma(N(y_1+2\pi n_1))\phi_2^\sigma(N(y_2+2\pi n_2))| \\ &= \frac{N^2}{4\pi^2}\sum_{n_1\in\mathbb{Z}} |\phi_1^\sigma(N(y_1+2\pi n_1))| \sum_{n_2\in\mathbb{Z}} |\phi_2^\sigma(N(y_2+2\pi n_2))| \\ &\leq CN^2\|\sigma^{p_1}\|_{C^{p_1}}\|\sigma^{p_2}\|_{C^{p_2}}(N|y_1|)^{-p_1}(N|y_2|)^{-p_2} \ , \end{aligned} \tag{4.33}$$

for $\boldsymbol{y} \in (-\pi,\pi)^2$, any p_1, p_2 and $C > 0$ a constant.
We state the following result.

Lemma 2. *Let σ^p be as defined in* (4.21). *Then there exist constants $M_\sigma, \eta_\sigma > 0$ indipendent from p such that*

$$\|\sigma^p\|_{C^p} \leq M_\sigma(p!)^2\eta_\sigma^{-p} \ . \tag{4.34}$$

Proof. See [17] Lemma 2.1. □

Observation 20. *Since $p > 0$ can be a positive real and non integer number, we mean*

$$\|f\|_{C^p} = \max_{k \le p} \|f^{(k)}\|_{L^\infty} , \quad k \in \mathbb{N} , \tag{4.35}$$

$$p! = \Gamma(p+1) . \tag{4.36}$$

In view of the previous lemma, we get

$$|\Phi^\sigma(\boldsymbol{y})| \le CN^2 M_{\sigma_1} M_{\sigma_2} (p_1!)^2 (p_2!)^2 (N\eta_{\sigma_1}|y_1|)^{-p_1} (N\eta_{\sigma_2}|y_2|)^{-p_2} . \tag{4.37}$$

We choose then

$$p_1 = p_{1,\min} = (N\eta_{\sigma_1}|y_1|)^{1/2} , \; p_2 = p_{2,\min} = (N\eta_{\sigma_2}|y_2|)^{1/2} . \tag{4.38}$$

With this choice of adaptive p_1, p_2 the localized mollifier $\Phi^\sigma(\boldsymbol{y})$ admits an exponential decay

$$|\Phi^\sigma(\boldsymbol{y})| \le C_{\boldsymbol{\sigma}} (1 + N|y_1|) e^{-(N\eta_{\sigma_1}|y_1|)^{1/2}} (1 + N|y_2|) e^{-(N\eta_{\sigma_2}|y_2|)^{1/2}} . \tag{4.39}$$

In particular, since $\mathcal{I}_1$ is supported at $|y_1| \ge \frac{d_1(x_1)}{2}$ and $|y_2| \ge \frac{d_2(x_2)}{2}$, if we let N be larger enough we obtain asymptotically

$$|\mathcal{I}_1| \le C_{\boldsymbol{\sigma},f} (1 + Nd_1(x_1)) e^{-(N\eta_{\sigma_1} d_1(x_1))^{1/2}} (1 + Nd_2(x_2)) e^{-(N\eta_{\sigma_2} d_2(x_2))^{1/2}} , \tag{4.40}$$

where the constant $C_{\boldsymbol{\sigma},f}$ depends now also on the function f.

We estimate now the second integral $\mathcal{I}_2 = \int_{(-\pi,\pi)^2} \Phi^\sigma(\boldsymbol{y})[f(\boldsymbol{x}) - f(\boldsymbol{x}-\boldsymbol{y})]\chi(\boldsymbol{y})\mathrm{d}\boldsymbol{y}$.
Let $g(\boldsymbol{y})$ be defined as

$$g(\boldsymbol{y}) = g_{\boldsymbol{x}}(\boldsymbol{y}) = [f(\boldsymbol{x}) - f(\boldsymbol{x}-\boldsymbol{y})]\chi(\boldsymbol{y}) . \tag{4.41}$$

For the Plancherel's Theorem we can write

$$\mathcal{I}_2 = \int_{(-\pi,\pi)^2} \Phi^\sigma(\boldsymbol{y}) g(\boldsymbol{y}) \mathrm{d}\boldsymbol{y} \equiv \sum_{\substack{|k_1| \le N \\ |k_2| \le N}} \boldsymbol{\sigma_k} \hat{g}(\boldsymbol{k}) , \tag{4.42}$$

where $\hat{g}(\boldsymbol{k}) = \hat{g}(k_1, k_2)$ are the Fourier coefficients of the function g.
First we work on such coefficients. We can estimate the smooth functions χ_1, χ_2 at the same regularity of $\sigma^{p_1}, \sigma^{p_2}$, i.e. for $i = 1, 2$

$$\|\chi_i\|_{C^{p_i}} \le M_{\rho_i} (p_i!)^2 (\eta_{\rho_i} d_i(x_i))^{-p_i} , \tag{4.43}$$

writing then for $\boldsymbol{p} = (p_1, p_2)$,

$$\|\chi\|_{C^{\boldsymbol{p}}} = \|\chi_1\|_{C^{p_1}} \|\chi_2\|_{C^{p_2}} , \tag{4.44}$$

meaning

$$\|\chi\|_{C^{\boldsymbol{p}}} := \max_{\substack{k_1 \le p_1 \\ k_2 \le p_2}} \|D^{\boldsymbol{k}} \chi\|_{L^\infty} , \tag{4.45}$$

where $\boldsymbol{k} = (k_1, k_2) \in \mathbb{N}^2$.
Using the analyticity of the function f we get then

$$\|g\|_{C^{\boldsymbol{p}}} \le M_f \|\chi\|_{C^{\boldsymbol{p}}} = M_f \|\chi_1\|_{C^{p_1}} \|\chi_2\|_{C^{p_2}} . \tag{4.46}$$

We can finally estimate the Fourier coefficients

$$\begin{aligned} |\hat{g}(\boldsymbol{k})| &\le C \|g\|_{C^{\boldsymbol{p}}} |k_1|^{-p_1} |k_2|^{-p_2} \\ &\le C_{f,\rho} (p_1!)^2 (\eta_{\rho_1} d_1(x_1)|k_1|)^{-p_1} (p_2!)^2 (\eta_{\rho_2} d_2(x_2)|k_2|)^{-p_2} , \end{aligned} \tag{4.47}$$

with $C_{f,\rho} = CM_f M_{\rho_1} M_{\rho_2} > 0$ is a constant.
We are ready to estimate the integral $\mathcal{I}_2$. In order to do this, we split the sum in (4.42) in

$$\mathcal{I}_2 \coloneqq \mathcal{S}_1 + \mathcal{S}_2 + \mathcal{S}_3 + \mathcal{S}_4 \ , \tag{4.48}$$

with

$$\begin{aligned} \mathcal{S}_1 &\coloneqq \textstyle\sum_{\substack{|k_1|\leq N \\ |k_2|\leq N}} (\sigma_{k_1}^{p_1} - 1)(\sigma_{k_2}^{p_2} - 1)\hat{g}(\boldsymbol{k}) \ , \\ \mathcal{S}_2 &\coloneqq \textstyle\sum_{\substack{|k_1|\leq N \\ |k_2|\leq N}} (\sigma_{k_1}^{p_1} - 1)\hat{g}(\boldsymbol{k}) \ , \\ \mathcal{S}_3 &\coloneqq \textstyle\sum_{\substack{|k_1|\leq N \\ |k_2|\leq N}} (\sigma_{k_2}^{p_2} - 1)\hat{g}(\boldsymbol{k}) \ , \\ \mathcal{S}_4 &\coloneqq -\textstyle\sum_{\substack{|k_1|> N \\ |k_2|> N}} \hat{g}(\boldsymbol{k}) \ . \end{aligned} \tag{4.49}$$

We are going to estimate these sums separately.
Since $|\sigma_{k_1}^{p_1} - 1|, |\sigma_{k_2}^{p_2} - 1| \leq 1$, we can then write

$$|\mathcal{S}_1| \leq |\mathcal{S}_2| \ , \ |\mathcal{S}_1| \leq |\mathcal{S}_3| \tag{4.50}$$

and focus then on the other sums.
Let us consider $\mathcal{S}_2$, we split it in $\mathcal{S}_2 \coloneqq \mathcal{S}_{21} + \mathcal{S}_{22}$ defined as

$$\begin{aligned} \mathcal{S}_{21} &\coloneqq \textstyle\sum_{\substack{|k_1|\leq N/2 \\ |k_2|\leq N}} (\sigma_{k_1}^{p_1} - 1)\hat{g}(\boldsymbol{k}) \ , \\ \mathcal{S}_{22} &\coloneqq \textstyle\sum_{\substack{N/2\leq|k_1|\leq N \\ |k_2|\leq N}} (\sigma_{k_1}^{p_1} - 1)\hat{g}(\boldsymbol{k}) \ . \end{aligned} \tag{4.51}$$

We start with $\mathcal{S}_{21}$. Using the Taylor expansion and the result in (4.47) we get

$$\begin{aligned} |\mathcal{S}_{21}| &\leq \sum_{\substack{|k_1|\leq N/2 \\ |k_2|\leq N}} |\sigma_{k_1}^{p_1} - 1||\hat{g}(\boldsymbol{k})| \\ &\leq \sum_{\substack{|k_1|\leq N/2 \\ |k_2|\leq N}} \frac{1}{p_1!}\|\sigma^{p_1}\|_{C^{p_1}(-\frac{1}{2},\frac{1}{2})} \left(\frac{|k_1|}{N}\right)^{p_1} C_{f,\rho} \frac{(p_1!)^2}{(\eta_{\rho_1} d_1(x_1)|k_1|)^{p_1}} \frac{(p_2!)^2}{(\eta_{\rho_2} d_2(x_2)|k_2|)^{p_2}} \\ &= C_{f,\rho} \sum_{\substack{|k_1|\leq N/2 \\ |k_2|\leq N}} \frac{1}{p_1!}\|\sigma^{p_1}\|_{C^{p_1}(-\frac{1}{2},\frac{1}{2})} \frac{(p_1!)^2}{(\eta_{\rho_1} d_1(x_1)N)^{p_1}} \frac{(p_2!)^2}{(\eta_{\rho_2} d_2(x_2)|k_2|)^{p_2}} \ . \end{aligned} \tag{4.52}$$

With appropriated constants, we can estimate

$$\|\sigma^{p_1}\|_{C^{p_1}(-\frac{1}{2},\frac{1}{2})} \leq C_{\sigma_1} p_1! \eta_{\sigma_1}^{-p_1} \ . \tag{4.53}$$

Using such a result we have

$$\begin{aligned} |\mathcal{S}_{21}| &\leq C_{f,\rho} \sum_{\substack{|k_1|\leq N/2 \\ |k_2|\leq N}} \frac{1}{p_1!}\|\sigma^{p_1}\|_{C^{p_1}(-\frac{1}{2},\frac{1}{2})} \frac{(p_1!)^2}{(\eta_{\rho_1} d_1(x_1)N)^{p_1}} \frac{(p_2!)^2}{(\eta_{\rho_2} d_2(x_2)|k_2|)^{p_2}} \\ &\leq C_{f,\rho} C_{\sigma_1} \sum_{\substack{|k_1|\leq N/2 \\ |k_2|\leq N}} \frac{(p_1!)^2}{(\eta_{\rho_1}\eta_{\sigma_1} d_1(x_1)N)^{p_1}} \frac{(p_2!)^2}{(\eta_{\rho_2} d_2(x_2)|k_2|)^{p_2}} \\ &\leq C_{f,\rho} C_{\sigma_1} \sum_{|k_1|\leq N/2} \frac{(p_1!)^2}{(\eta_{\rho_1}\eta_{\sigma_1} d_1(x_1)N)^{p_1}} \sum_{|k_2|\leq N} \frac{(p_2!)^2}{(\eta_{\rho_2} d_2(x_2)|k_2|)^{p_2}} \\ &\leq C_{f,\rho} C_{\sigma_1} N \frac{(p_1!)^2}{(\eta_{\rho_1}\eta_{\sigma_1} d_1(x_1)N)^{p_1}} \sum_{|k_2|\leq N} \frac{(p_2!)^2}{(\eta_{\rho_2} d_2(x_2)|k_2|)^{p_2}} \\ &\leq C_{f,\rho,\sigma_1} B_{d_2,p_2^*} N \frac{(p_1!)^2}{(\eta_{\rho_1,\sigma_1} d_1(x_1)N)^{p_1}} \ , \end{aligned} \tag{4.54}$$

where $C_{f,\rho,\sigma_1} = C_{f,\rho}C_{\sigma_1}$, $\eta_{\rho_1,\sigma_1} = \eta_{\rho_1}\eta_{\sigma_1}$ and B_{d_2,p_2^*} is such that

$$\sum_{|k_2|\leq N} \frac{(p_2!)^2}{(\eta_{\rho_2} d_2(x_2)|k_2|)^{p_2}} \leq B_{d_2,p_2^*} \ , \tag{4.55}$$

dependent on $d_2(x_2)$ and

$$p_2 = p_2^* \coloneqq \max\{p_{2,\min}, 2\} \ , \tag{4.56}$$

with $p_{2,\min}$ defined in (4.38) (with a different constant η). The reason for this choice is that we will consider such a $p_{2,\min}$ with a possible different η as adaptive parameter for $\mathcal{I}_2$, but we have to be sure about the convergence of the series in (4.55). Nevertheless, we observe that as N becomes larger the series is convergent for $p_2 = p_{2,\min}$ by definition of this parameter.
We consider now $\mathcal{S}_{22}$. Since $|\sigma_{k_1}^{p_1} - 1| \leq 1$, here we have

$$\begin{aligned}
|\mathcal{S}_{22}| &\leq \sum_{\substack{N/2\leq|k_1|\leq N\\ |k_2|\leq N}} |\sigma_{k_1}^{p_1} - 1||\hat{g}(\boldsymbol{k}| \\
&\leq \sum_{\substack{N/2\leq|k_1|\leq N\\ |k_2|\leq N}} |\hat{g}(\boldsymbol{k}| \\
&\leq \sum_{\substack{N/2\leq|k_1|\leq N\\ |k_2|\leq N}} C_{f,\rho} \frac{(p_1!)^2}{(\eta_{\rho_1} d_1(x_1)|k_1|)^{p_1}} \frac{(p_2!)^2}{(\eta_{\rho_2} d_2(x_2)|k_2|)^{p_2}} \\
&= C_{f,\rho} \sum_{N/2\leq|k_1|\leq N} \frac{(p_1!)^2}{(\eta_{\rho_1} d_1(x_1)|k_1|)^{p_1}} \sum_{|k_2|\leq N} \frac{(p_2!)^2}{(\eta_{\rho_2} d_2(x_2)|k_2|)^{p_2}} \\
&\leq C_{f,\rho} B_{d_2,p_2^*} N \frac{(p_1!)^2}{(\eta_{\rho_1} d_1(x_1)N)^{p_1}} \ ,
\end{aligned} \tag{4.57}$$

with a little abuse of notation $\eta_{\rho_1} = \eta_{\rho_1}/2$ and the other constants as before.
We got

$$\begin{aligned}
|\mathcal{S}_2| &\leq |\mathcal{S}_{21}| + |\mathcal{S}_{22}| \\
&\leq C_{f,\rho,\sigma_1} B_{d_2,p_2^*} N \frac{(p_1!)^2}{(\eta_{\rho_1,\sigma_1} d_1(x_1)N)^{p_1}} + C_{f,\rho} B_{d_2,p_2^*} N \frac{(p_1!)^2}{(\eta_{\rho_1} d_1(x_1)N)^{p_1}} \\
&\leq C_{s_2} N \frac{(p_1!)^2}{(\eta_{s_2} d_1(x_1)N)^{p_1}} \ ,
\end{aligned} \tag{4.58}$$

where $\eta_{s_2} = \min\{\eta_{\rho_1,\sigma_1}, \eta_{\rho_1}\}$ and $C_{s_2} = C_{f,\rho,\sigma_1} B_{d_2,p_2^*} + C_{f,\rho} B_{d_2,p_2^*}$.
Concerning $\mathcal{S}_3$, the situation is totally symmetric to $\mathcal{S}_2$. Splitting it into two series we eventually get the estimate

$$|\mathcal{S}_3| \leq C_{s_3} N \frac{(p_2!)^2}{(\eta_{s_3} d_2(x_2)N)^{p_2}} \ , \tag{4.59}$$

with constants similarly to before $\eta_{s_3} = \min\{\eta_{\rho_2,\sigma_2}, \eta_{\rho_2}\}$ and $C_{s_3} = C_{f,\rho,\sigma_2} B_{d_1,p_1^*} + C_{f,\rho} B_{d_1,p_1^*}$
The final step deals with $\mathcal{S}_4$.

$$\begin{aligned}
|\mathcal{S}_4| &\leq \sum_{\substack{|k_1|>N\\ |k_2|>N}} |\hat{g}(\boldsymbol{k})| \\
&\leq C_{f,\rho} \sum_{|k_1|>N} \frac{(p_1!)^2}{(\eta_{\rho_1} d_1(x_1)|k_1|)^{p_1}} \sum_{|k_2|>N} \frac{(p_2!)^2}{(\eta_{\rho_2} d_2(x_2)|k_2|)^{p_2}}
\end{aligned} \tag{4.60}$$

We use the following general fact

$$\sum_{k>n} \frac{1}{k^p} < \int_n^\infty \frac{1}{x^p} \mathrm{d}x = \frac{1}{p-1} \frac{1}{n^{p-1}} \ . \tag{4.61}$$

Hence,

$$|\mathcal{S}_4| \leq C_{f,\rho} N \frac{1}{p_1 - 1} \frac{(p_1!)^2}{(\eta_{\rho_1} d_1(x_1)|k_1|)^{p_1}} N \frac{1}{p_2 - 1} \frac{(p_2!)^2}{(\eta_{\rho_2} d_2(x_2)|k_2|)^{p_2}} \ . \tag{4.62}$$

One could be worried about the two terms $(p_1 - 1)^{-1}, (p_2 - 1)^{-1}$. In fact, as N becomes larger $p_1, p_2 > 1$, so since we are interested in the asymptotically behaviour of the estimate in the next lines we will simply write $C_{s_4} = C_{f,\rho}(p_1 - 1)^{-1}(p_2 - 1)^{-1}$.
In the end, we have then asymptotically

$$\begin{aligned}
|\mathcal{I}_2| &\leq |\mathcal{S}_1| + |\mathcal{S}_2| + |\mathcal{S}_3| + |\mathcal{S}_4| \\
&\leq 2|\mathcal{S}_2| + |\mathcal{S}_3| + |\mathcal{S}_4| \\
&\leq 2C_{s_2} N \frac{(p_1!)^2}{(\eta_{s_2} d_1(x_1) N)^{p_1}} + C_{s_3} N \frac{(p_2!)^2}{(\eta_{s_3} d_2(x_2) N)^{p_2}} + C_{s_4} N^2 \frac{(p_1!)^2}{(\eta_{\rho_1} d_1(x_1)|k_1|)^{p_1}} \frac{(p_2!)^2}{(\eta_{\rho_2} d_2(x_2)|k_2|)^{p_2}} \ .
\end{aligned}$$

Choosing then

$$p_1 = p_{1,\min} = (N\eta_1 d_1(x_1))^{1/2} \ , \ p_2 = p_{2,\min} = (N\eta_2 d_2(x_2))^{1/2} \ , \tag{4.63}$$

with $\eta_1 = \min\{\eta_{\rho_1}, \eta_{s_2}\}$ and $\eta_2 = \min\{\eta_{\rho_2}, \eta_{s_3}\}$, we get

$$|\mathcal{I}_2| \leq 2C_{s_2} N e^{-(N\eta_1 d_1(x_1))^{1/2}} + C_{s_3} N e^{-(N\eta_2 d_2(x_2))^{1/2}} + C_{s_4} N^2 e^{-(N\eta_1 d_1(x_1))^{1/2} - (N\eta_2 d_2(x_2))^{1/2}} \ . \tag{4.64}$$

Coming back to the very beginning of this section,

$$\begin{aligned}
|f - S_N^\sigma f| &\leq |\mathcal{I}_1| + |\mathcal{I}_2| \\
&\leq C_{\boldsymbol{\sigma},f}(1 + Nd_1(x_1))e^{-(N\eta_{\sigma_1} d_1(x_1))^{1/2}}(1 + Nd_2(x_2))e^{-(N\eta_{\sigma_2} d_2(x_2))^{1/2}} + \\
&+ 2C_{s_2} N e^{-(N\eta_1 d_1(x_1))^{1/2}} + C_{s_3} N e^{-(N\eta_2 d_2(x_2))^{1/2}} + C_{s_4} N^2 e^{-(N\eta_1 d_1(x_1))^{1/2} - (N\eta_2 d_2(x_2))^{1/2}} \\
&\leq 2C_{s_2} N e^{-(N\eta_1^* d_1(x_1))^{1/2}} + C_{s_3} N e^{-(N\eta_2^* d_2(x_2))^{1/2}} + \\
&+ [C_{\boldsymbol{\sigma},f}(1 + Nd_1(x_1))(1 + Nd_2(x_2)) + C_{s_4} N^2] e^{-(N\eta_1^* d_1(x_1))^{1/2} - (N\eta_2^* d_2(x_2))^{1/2}} \ ,
\end{aligned} \tag{4.65}$$

where $\eta_1^* = \min\{\eta_{\sigma_1}, \eta_1\}$, $\eta_2^* = \min\{\eta_{\sigma_2}, \eta_2\}$.
We have obtained then asymptotic exponential accuracy recovery away from the discontinuities with the adaptive

$$\boldsymbol{p} = ((N\eta_1^* d_1(x_1))^{1/2}, (N\eta_2^* d_2(x_2))^{1/2}) \ . \tag{4.66}$$

Observation 21. *In this section we required the analyticity of f away from its discontinuities. In f is not such smooth, we lose the exponential accuracy obtaining a polynomial decay rate.*

Observation 22. *The tensor product structure allows us to extend the result to a multidimensional setting. The adaptive parameter in this general case is*

$$\boldsymbol{p} = ((N\eta_1^* d_1(x_1))^{1/2}, (N\eta_2^* d_2(x_2))^{1/2}, ..., (N\eta_\nu^* d_\nu(x_\nu))^{1/2}) \ . \tag{4.67}$$

Chapter 5

Numerical tests

5.1 Introduction to the problem

Let $f : \mathbb{R}^\nu \to \mathbb{R}$, $f \in F_k(\mathbb{R}^\nu)$ as in Definition 10 and $\nu = 2, 3$.
We consider the problem of reconstructing the function f from a set of samples, using the theorical instruments about interpolation and filtering introduced in the previous chapters and considering f as the underlying function of a two or three-dimensional image.
First of all, we discuss how we can evaluate the final reconstruction $\tilde{f}$ which we will get in the end of the process. The parameters described in this section are valid in the three-dimensional case also.

- In applications we mainly deal with discontinuous functions, that is the case in which the Gibbs phenomenon appears.
  Thus, we do not consider the behaviour of the error in infinity norm $\|f - \tilde{f}\|_\infty$ to evaluate our results, since as known we can not expect to gain more and more precision in the points where the function f is discontinuous, and so there is no hope to make the error go down increasing the number of sample points.

- In order to measure the quality of a reconstructed image, a common used parameter is the PSNR (Peak-Signal-to Noise-Ratio).
  If $F, \tilde{F}$ are the two $n \times n$ matrices representing the images obtained evaluating respectively $f, \tilde{f}$ on a suitable mesh grid, the PSNR parameter is defined as

$$PSNR(F, \tilde{F}) = 10 \cdot \log_{10} \frac{(\max_F)^2}{MSE(F, \tilde{F})} , \tag{5.1}$$

  where $\max_F$ is the value of the maximum element (pixel) of F and

$$MSE(F, \tilde{F}) = \frac{1}{n^2} \sum_{i=1}^{n} \sum_{j=0}^{n} (F(i, j) - \tilde{F}(i, j))^2 \tag{5.2}$$

  is the mean squared error.
  We observe that such a parameter is strictly connected to the L^2-norm error $\|f - \tilde{f}\|_{L^2}$.
  For this reason, the PSNR is not a good parameter for our applications.
  Indeed, the filtering process makes the Gibbs phenomenon disappear but it also causes the loss of the optimal properties of the initial Fourier-like interpolant in minimizing the L^2-error (see [16]). Thus, the final reconstruction $\tilde{f}$ it's not optimal with respect to the PSNR parameter.

- A good parameter that can be considered is the SSIM (Structural Similarity Index). This parameter has been introduced to evaluate the quality of a reconstruction according to human visual perception and it is nowadays one of the most used parameter in imaging science [18].

Considering two $k \times k$ submatrices X, Y of $F, \tilde{F}$ respectively, the parameter is defined as

$$SSIM(X,Y) = \frac{(2\mu_x\mu_y + c_1)(2\sigma_{xy} + c_2)}{(\mu_x^2 + \mu_y^2 + c_1)(\sigma_x^2 + \sigma_y^2 + c_2)} , \tag{5.3}$$

where μ_x, μ_y are the average values of X and Y, σ_x, σ_y are the variances, σ_{xy} is the covariance between the two matrices and c_1, c_2 are parameters defined as

$$c_1 = (k_1 L)^2 \qquad c_2 = (k_2 L)^2 , \tag{5.4}$$

where L is the dynamic range of the pixel-values and $k_1 = 0.01, k_2 = 0.03$ by default. The parameter $SSIM(F, \tilde{F})$, which is a value between -1 and 1, is computed as the mean of the parameters given by different submatrices.
We refer to this parameter to evaluate our results, but as we will see the human sight perception will play an important role too.

5.2 Two-dimensional experiments

The setting of our experiments in Matlab is:

- The domain is the square $[-1, 1]^2$.
- The evaluation matrix is a 201×201 matrix. The step of the grid is indeed $s = 0.01$.
- A modified version of the *Chebfun* 5.3.0 package, which is avaiable in the inclosed CD.

We describe the steps of our procedure, considering as example the function $f : [-1, 1]^2 \to \mathbb{R}$ defined as

$$f(x,y) = \begin{cases} 1 & x^2 + y^2 \leq (0.6)^2 , \\ 0 & \text{otherwise} . \end{cases} \tag{5.5}$$

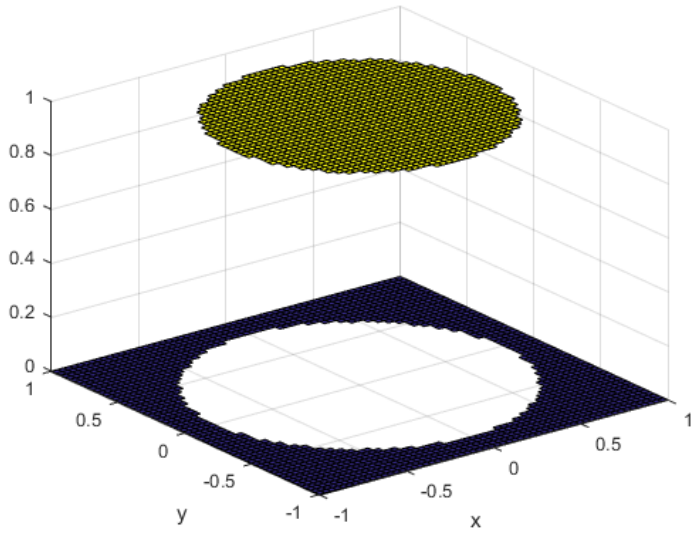

Figure 5.1: Function f.

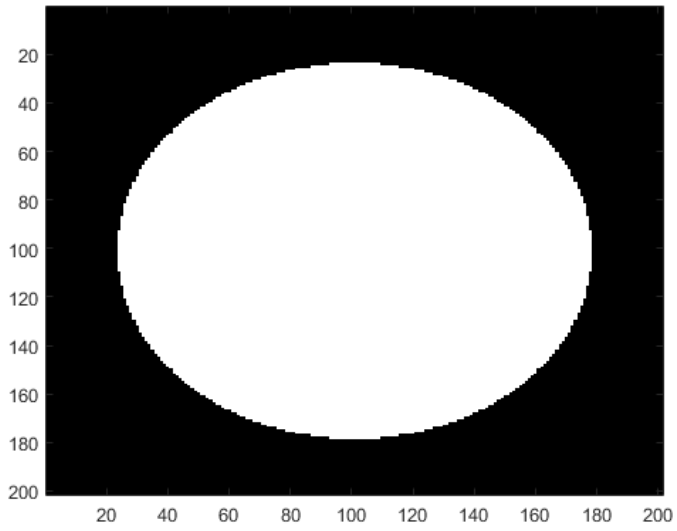

Figure 5.2: Function f as a gray scale image.

5.2.1 Lissajous sampling

We want to reconstruct the function f sampling on Lissajous nodes. The *Chebfun* package is suitable for our purposes, since it already contains an algorithm which performs the global polynomial interpolation on Padua points in an optimized way. We can then slightly modify the package, obtaining a fast and efficient way to interpolate on Lissajous nodes.
First, we find the Lissajous nodes and the relative weights given by a chosen curve $\gamma_2^{(32,33)}$.

```
pars=[32,33,2];            % [n1,n2,flag]
x=lissapts([pars(1),pars(2)],pars(3));
```

The function *lissapts.m* included in the package is defined in the following way.

```
function [xy,idx,w] = lissapts(n,e,range)

% (C) Francesco Marchetti 23.03.2016
%
% Note: lissapts.m is a variation of LSpts.m by Wolfgang Erb
%
% USAGE of
% [xy,idx,w] = lissapts(n,e,range)
%
% Computes Lissa (LS) points with parameter n1, n2 (relatively prime)
% and e for a given range.
% If range is not given then range = [-1, 1, -1, 1].
% If n is a natural number then n = [n,n+1].
%
% ------------------------------------------------------------------
% INPUT:
%
% n             : vector of parameters of the Lissajous curve.
% e             : e = 1 (degenerate), e = 2 (non-degenerate).
% range         : [x.start,x.end,y.start,y.end] range of the x-
%                 and y-coordinates.
%
```

```
% OUTPUT:
%
% xy            : 2-columns array of x,y coordinates of the LS nodes.
% idx           : logical matrix which denotes the entries of the Chebyshev
%                 tensor product grid that form XY.
% w             : 1-column array of weights of the LS nodes.
%
```

We can then write

```
fx=f(x(:,1),x(:,2));
f_lissa=chebfun2(fx,[-1 1 -1 1],'lissa',pars);
```

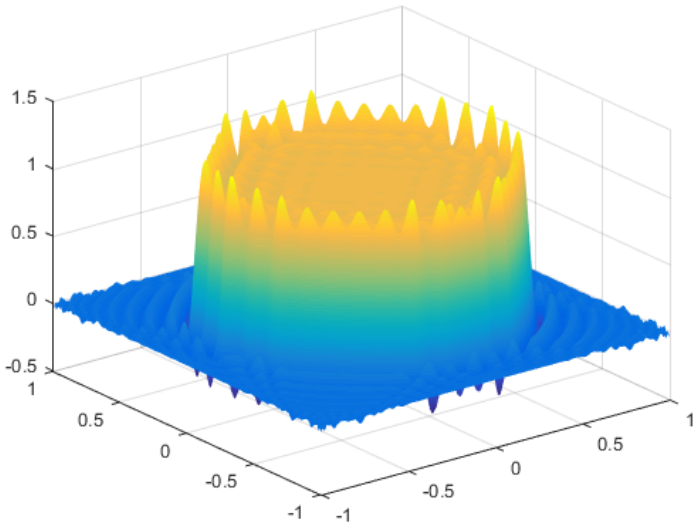

Figure 5.3: Plot of f_lissa. The Gibbs phenomenon is clearly visible.

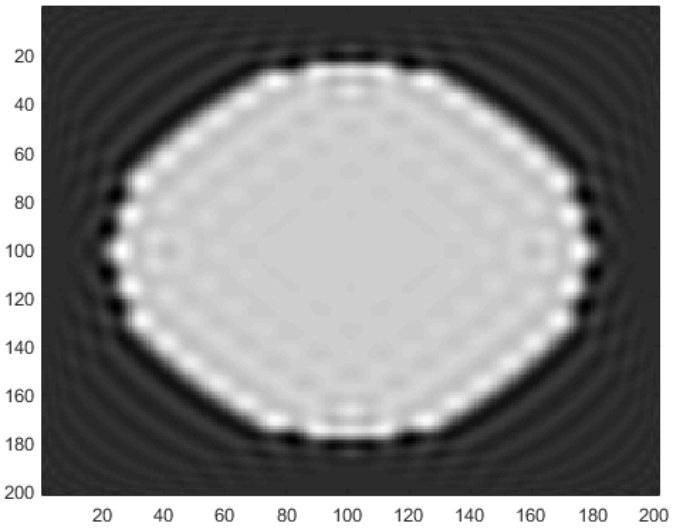

Figure 5.4: f_lissa as a gray scale image

Late versions of Matlab provide a default function to calculate the SSIM parameter. We have

$$SSIM(f, f\_lissa) = 0.5122\ . \tag{5.6}$$

5.2.2 Spectral filtering

Using

```
C=chebcoeffs2(f_lissa);       % Fourier coefficients
C(abs(C)<1e-10)=0;       % Set to 0 if too small
```

we get the spectral coefficients of f_lissa in a matrix C.
We recall the definitions of some filters.

- The Fejér filter (first order)
$$\sigma(\eta) = 1 - \eta\ . \tag{5.7}$$
- The sinc filter (first order)
$$\sigma(\eta) = \frac{\sin(\pi\eta)}{\pi\eta}\ . \tag{5.8}$$
- The *raised cosine* filter (second order)
$$\sigma(\eta) = \frac{1}{2}(1 + \cos(\pi\eta))\ . \tag{5.9}$$
- The exponential filter of order p (p even)
$$\sigma(\eta) = e^{-\alpha\eta^p}\ , \tag{5.10}$$
where α is the computer's roundoff error.

Taking as example the raised cosine filter, we write

```
eta1=[0:(pars(3)*pars(1))].*(1/(pars(3)*pars(1)));
eta2=[0:(pars(3)*pars(2))].*(1/(pars(3)*pars(2)));
filt1=1/2.*(ones(1,length(eta1))+cos(pi.*eta1));
filt2=1/2.*(ones(1,length(eta2))+cos(pi.*eta2));
F1=filt2.'*filt1;
P_filt=C.*F1;             % Application of the filter
f_filt=chebfun2(P_filt,[-1,1,-1,1],'coeffs');
```

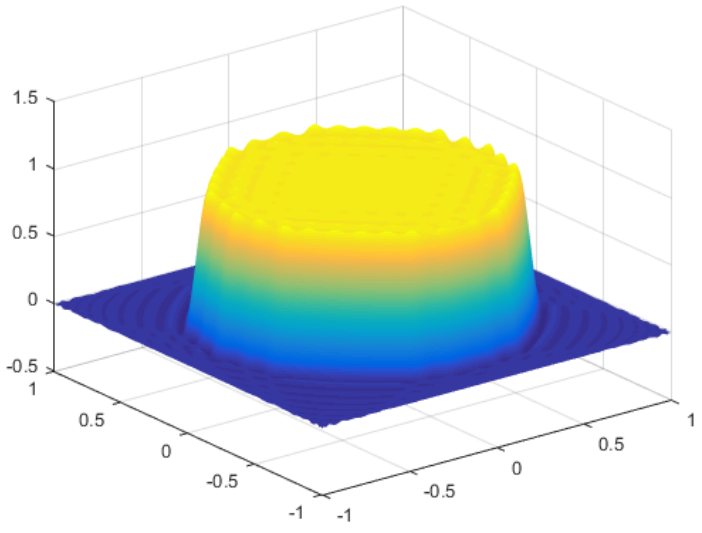

Figure 5.5: Plot of f_filt. We managed to dimish the Gibbs phenomenon.

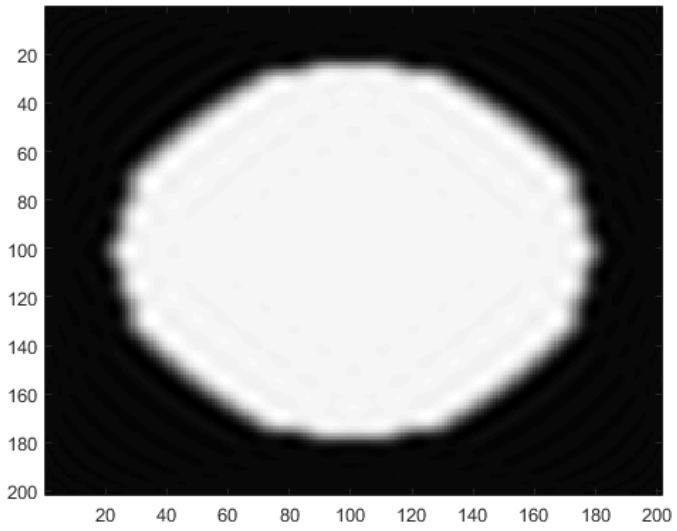

Figure 5.6: f_filt as a gray scale image

We have

$$SSIM(f, f\_filt) = 0.8232\ . \tag{5.11}$$

5.2.3 Edges detection and distance matrix

As described in the previous chapters, we are going to apply an adaptive filter to recover more precision (Section 4.2.2). In order to do it, we need to know where are the discontinuities, where is the nearest point of discontinuity related to each non-discontinuous point and what is the distance between them.
The edge detection can be performed by the default Matlab function *edge*, in particular we use the Canny edge-detector.
We observe that in the polynomial reconstruction there are no real discontinuities. Indeed, the edge-detector find the large variation zones of the gradient and it claims that an underlying discontinuity of the original function is hidden there.
We apply the algorithm to the filtered matrix f_filt, since the massive perturbations in f_lissa could be wrongly detected as discontinuities.

```
s=0.01;
t=-1:s:1;            % Mesh in the square
[X,Y]=meshgrid(t);
f_filt_mesh=feval(f_filt,X,Y);
peaks=edge(p_filt_mesh,'Canny',[],3);    % '3' is a chosen parameter
peaks=double(peaks);                      % peaks is a logical matrix
```

5.2.4 Adaptive filter application

We can efficiently find for each point its closest discontinuity point with respect to the Euclidan distance using the function *ipdm.m* (Inter-Point Distance Matrix)[1] , avaiable in the inclosed CD.

```
function d = ipdm(data1,varargin)
% ipdm: Inter-Point Distance Matrix
% usage: d = ipdm(data1)
% usage: d = ipdm(data1,data2)
```

[1] http://it.mathworks.com/matlabcentral/fileexchange/18937-ipdm–inter-point-distance-matrix

```
% usage: d = ipdm(data1,prop,value)
% usage: d = ipdm(data1,data2,prop,value)
%
% [...]
%
% Author: John D'Errico
% e-mail: woodchips@rochester.rr.com
% Release: 1.0
% Release date: 2/26/08
```

Let then $\boldsymbol{\xi} = (\xi_1, \xi_2)$ be the closest discontinuity point related to the point $\boldsymbol{x} = (x_1, x_2)$. We can find the two distances

$$d_1 = d_1(x_1) = |x_1 - \xi_1| \quad , \quad d_2 = d_2(x_2) = |x_2 - \xi_2| \, . \tag{5.12}$$

We consider then as suggested by the theory

$$p_1 = (\eta_1^\star N_1 d_1)^{1/2} \quad , \quad p_2 = (\eta_2^\star N_2 d_2)^{1/2} \, , \tag{5.13}$$

where N_1, N_2 are natural numbers which depend on the degree parameters of the Lissajous curve which we are considering.
We are ready then to perform the adaptive filtering process.
A complete script including all the previous passages and a numerical implementation of the adaptive filter is avaiable in the CD. We point out that in applications we use a unique

$$\eta = \eta_1^* = \eta_2^* \tag{5.14}$$

in the final expression (4.24).

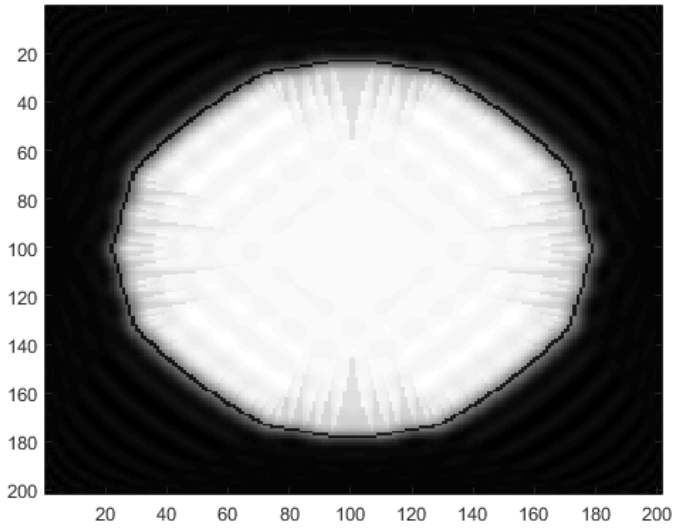

Figure 5.7: Final result after adaptive filtering.

Let f_apt be the final result in Figure 5.7. We get

$$SSIM(f, f\_apt) = 0.6592 \, . \tag{5.15}$$

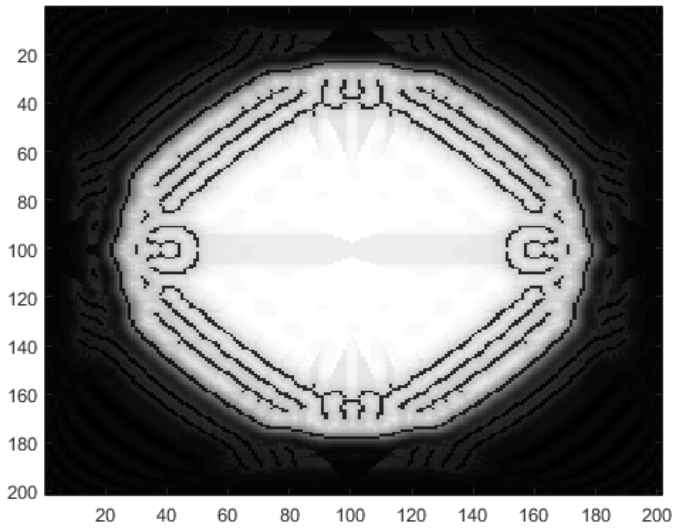

Figure 5.8: As example, this would be the result if we applied the edge-detector to f_lissa.

We can observe that f_apt is affected by a striped distortion, given by the tensor-product structure of the adaptive filter.
In order to improve the final result and to avoid the appearance of such a distortion, we can modify the definition of the adaptive parameters trying to improve our result.
We point out that what follows in the section is conjectured from sperimentation and observations and it is not supported by the theory as before.
We look for a unique parameter $p = p_1 = p_2$ which depends on the euclidean distance

$$d(\boldsymbol{x}) = \|\boldsymbol{x} - \boldsymbol{\xi}\| = \sqrt{d_1^2 + d_2^2}\,. \tag{5.16}$$

Then, we define first

$$N = \sqrt{N_1^2 + N_2^2}\,, \tag{5.17}$$

and we slightly modify the initial parameters in

$$p_1 = (\eta N d_1)^{1/2} \quad , \quad p_2 = (\eta N d_2)^{1/2}\,. \tag{5.18}$$

We can define then

$$p = \sqrt{p_1^4 + p_2^4} = \eta N d(\boldsymbol{x}) \tag{5.19}$$

In Figure 5.9 we see the new result $f^\star\_apt$, which is no more affected by the considered distortion. Moreover,

$$SSIM(f, f^\star\_apt) = 0.6120\,. \tag{5.20}$$

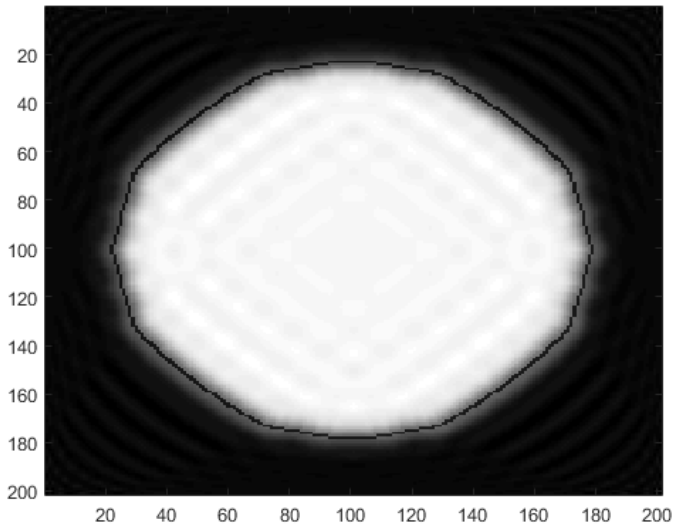

Figure 5.9: The result $f^\star\_apt$.

5.2.5 Non-linear adaptive parameter

In the filtering process we have to deal with two different situations:

- Using a strong filter we get a robust reduction of the Gibbs phenomenon all over the image, but we also cause a large smoothing effect near the edges of the object represented by the function.
- Using a weak filter we almost preserve the function near the discontinuities, but we can not greatly reduce the Gibbs phenomenon.

Our aim is to find a balance between these two aspects, therefore we can make a step forward.
The parameter p depends linearly on $d(\boldsymbol{x})$. We conjecture what follows.

Conjecture 23. *Let us consider the function $\Phi : [0, +\infty) \to [0, +\infty)$ with the following properties:*

- $\Phi(0) = 0$.
- Φ *is a regular and increasing function in* $[0, +\infty)$.
- Φ *has a saturation property, that is there exists* $\epsilon > 0$ *such that*

$$\Phi(x) \geq x \tag{5.21}$$

for $x \in [0, \epsilon]$.

We claim that there exists at least one function with the previous properties, possibly dependent on the setting of the sperimentations, such that using the adaptive parameter

$$p = \eta N \Phi(d(\boldsymbol{x})) \tag{5.22}$$

we can improve the final result of the process in terms of resolution of Gibbs phenomenon and image reconstruction.

A possible family of functions which have the described properties and which we consider for our experiments is

$$\Phi_\beta(x) = x^\beta \,, \tag{5.23}$$

where $0 < \beta < 1$. Then we can define a new parameter

$$p_\beta = \eta N(d(\boldsymbol{x}))^\beta \tag{5.24}$$

The new parameter p_β is more sensitive and has a larger variation in small distances with respect to the linear one. On the other side, p_β has a saturation effect as the distance increases.

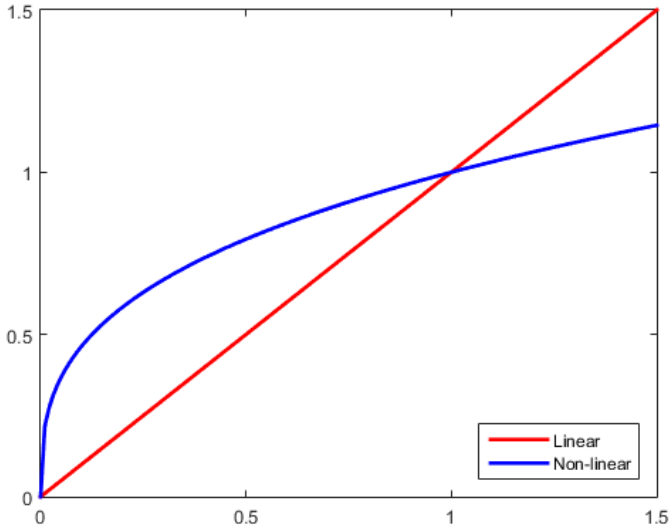

Figure 5.10: As example, $\Phi_\beta(x) = x$ (linear) and $\Phi_\beta(x) = x^{1/3}$ (non-linear).

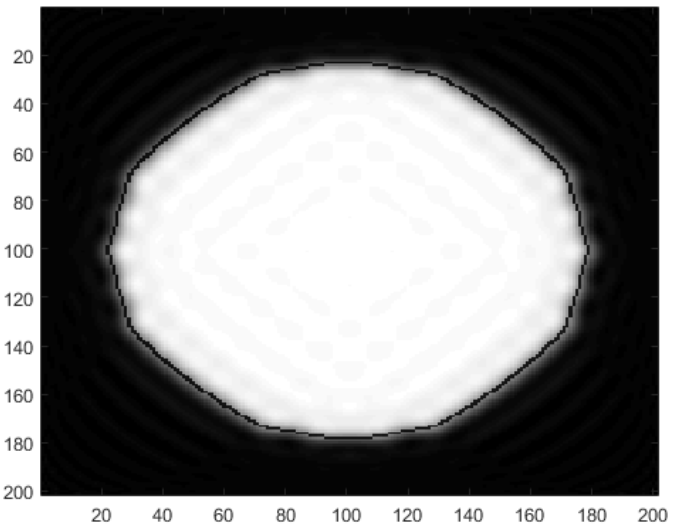

Figure 5.11: Final reconstruction $f^{1/4}\_apt$ using p_β with $\beta = 1/4$.

$$SSIM(f, f^{1/4}\_apt) = 0.7073 \,. \tag{5.25}$$

At this point one could wonder about what is a good choice for the parameter β and how much we can let it become close to zero. Of course the choice depends on the step of the grid which is used in sperimentations, since a large step is not sensitive to small values of the parameter and so it would make no sense to set β too small, and can be made through a computational search.
In our setting with the step $s = 0.01$, a good choice is for example $\beta = 1/4$.
A complete code related to the considerations of this subsection in avaiable in the CD.

In the next applications we will use then $p_{1/4}$ as adaptive parameter.
The SSIM value after the first filtering process is higher than the value related to the final reconstruction. As we said in the introduction of the chapter, the SSIM parameter is good to evaluate our results, but for example it can not appreciate so deeply the edges definition, which is the best quality of the adaptive filtering process.
Therefore, in applications one would prefer the final result, despite the values of the parameters.

5.2.6 More numerical results

We consider the following two functions defined in $[-1, 1]^2$.

$$f_1(x,y) = \begin{cases} 2 & |x| \le 0.5\ ,\ |y| \le 0.5\ , \\ 1 & -0.8 \le x \le -0.65\ ,\ |y| \le 0.8\ , \\ 0.5 & 0.65 \le x \le 0.8\ ,\ |y| \le 0.2\ , \\ 0 & \text{otherwise}\ . \end{cases}$$

$$f_2(x,y) = \begin{cases} 2 & (x+0.4)^2 + (y+0.4)^2 \le 0.4^2\ , \\ 1.5 & (x-0.5)^2 + (y-0.5)^2 \le 0.3^2\ , \\ 1 & (x-0.5)^2 + (y+0.5)^2 \le 0.2^2\ , \\ 0.5 & (x+0.5)^2 + (y-0.5)^2 \le 0.1^2\ , \\ e^{-(x^2+y^2)} & \text{otherwise}\ . \end{cases} \tag{5.26}$$

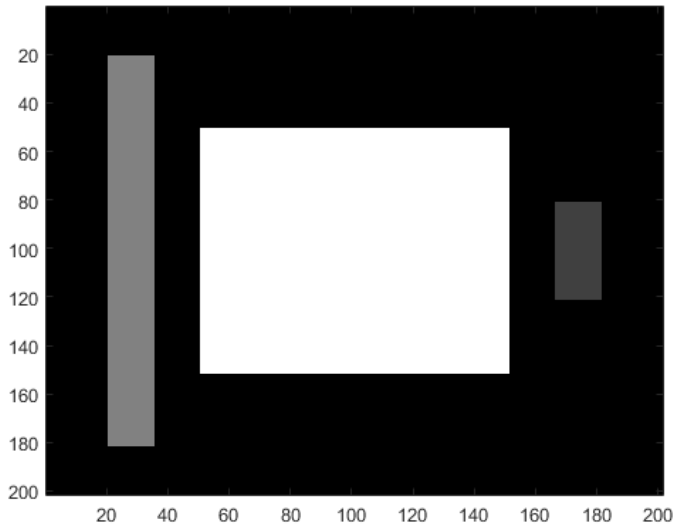

Figure 5.12: Function f_1.

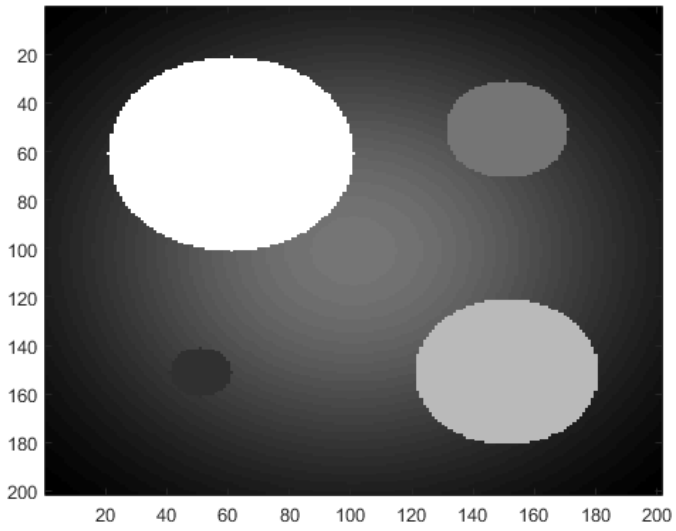

Figure 5.13: Function f_2.

We want to observe the behaviour of the SSIM parameter between these functions and the reconstructions which are obtained as the degree $(n, n+1)$ of the Lissajous curve becomes larger.
At first, we investigate the behaviour of the parameter in the application of the first spectral filter.
Let us start with f_1.

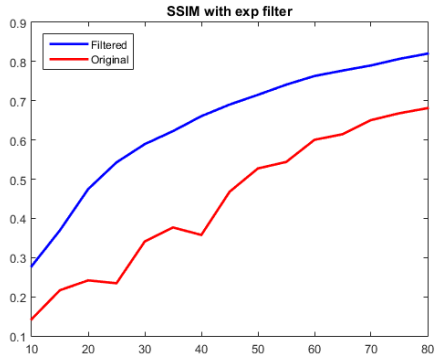

(a) Using the exponential filter with $p = 4$.

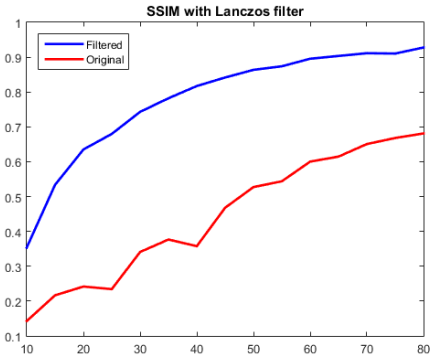

(b) Using the sinc filter.

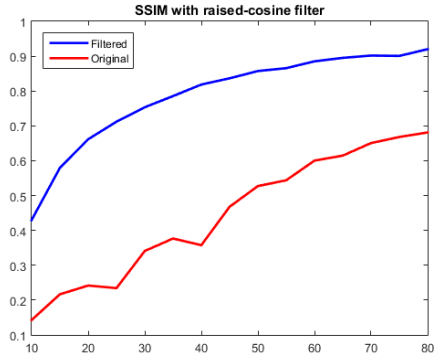

(c) Using the raised-cosine filter.

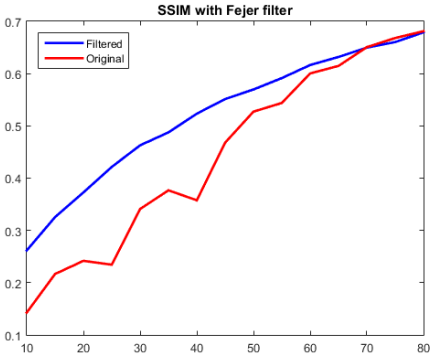

(d) Using the Fejer filter.

Figure 5.14: Different results for each different filter for f_1 .

We observe that the Fejer filter is not so effective for very high degrees.

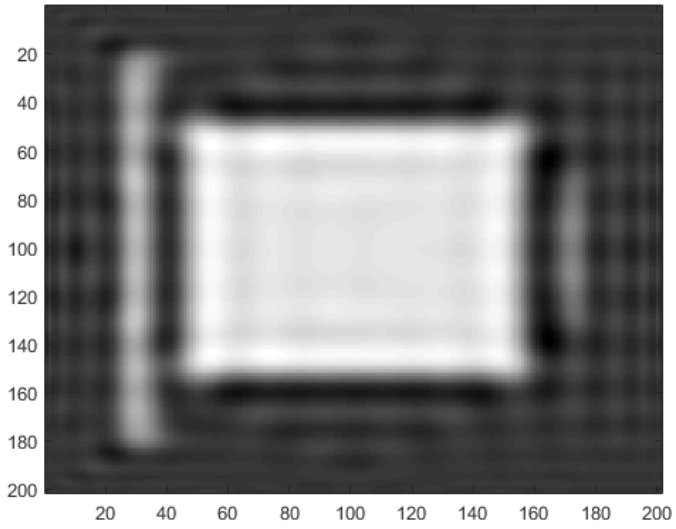

Figure 5.15: For $n = 15$, the first reconstruction from Lissajous sampling.

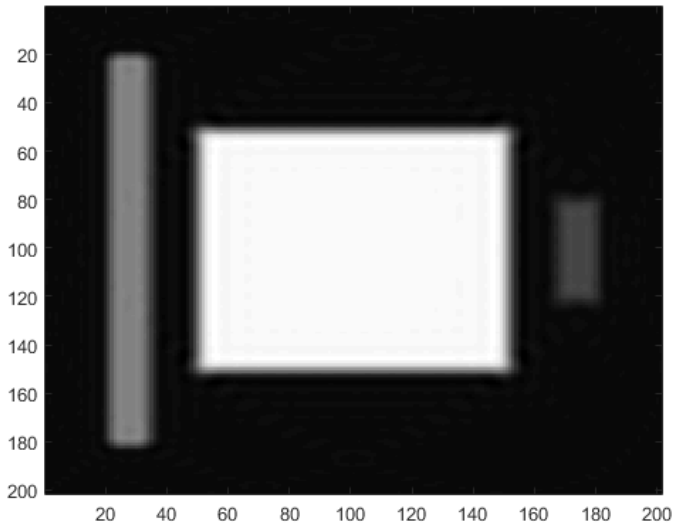

Figure 5.16: Result after sinc filter application for $n = 40$.

For f_2 we get the following.

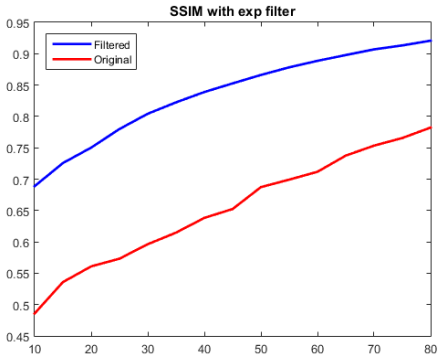

(a) Using the exponential filter with $p = 4$.

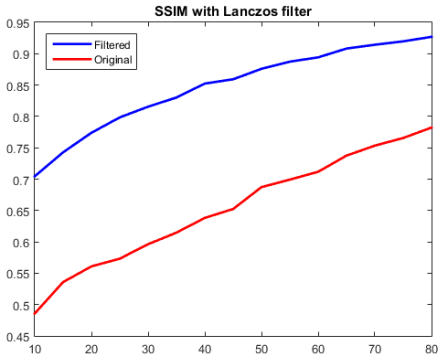

(b) Using the sinc filter.

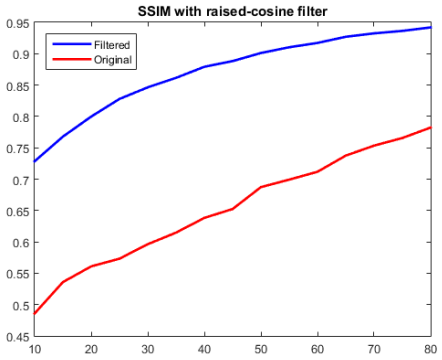

(c) Using the raised-cosine filter.

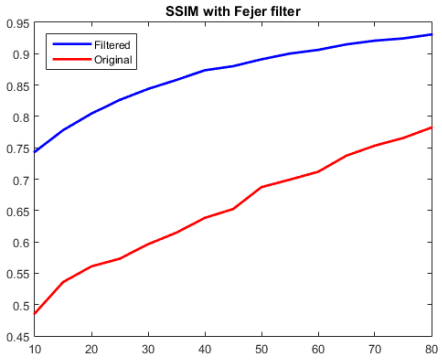

(d) Using the Fejer filter.

Figure 5.17: Different results for each different filter for f_2 .

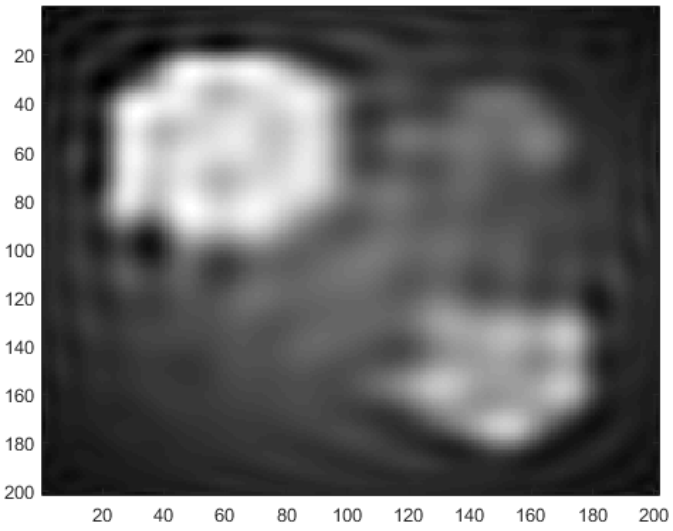

Figure 5.18: For $n = 15$, the first reconstruction from Lissajous sampling.

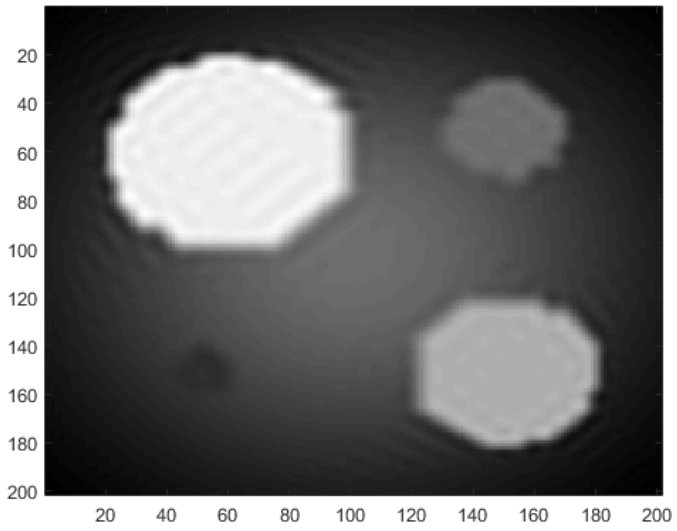

Figure 5.19: Result after sinc filter application for $n = 40$.

We can also analyze the behaviour of the SSIM parameter after the application of the adaptive filter. We observe that in this case the first filtering process is important just in order to apply the edge-detector in an efficient way.
Therefore, without loss of generality we decided to use the sinc filter among the others. Moreover, in the following applications we use the same parameters in the edge-detector and in the adaptive filter for both the functions and for all the degrees. We point out that for obvious reasons the parameter η should not depend on the different choices of the underlying function, while could be slightly modified for different degrees N related to the considered Lissajous curve.
More information about the setting of the parameters can be found in the inclosed CD.

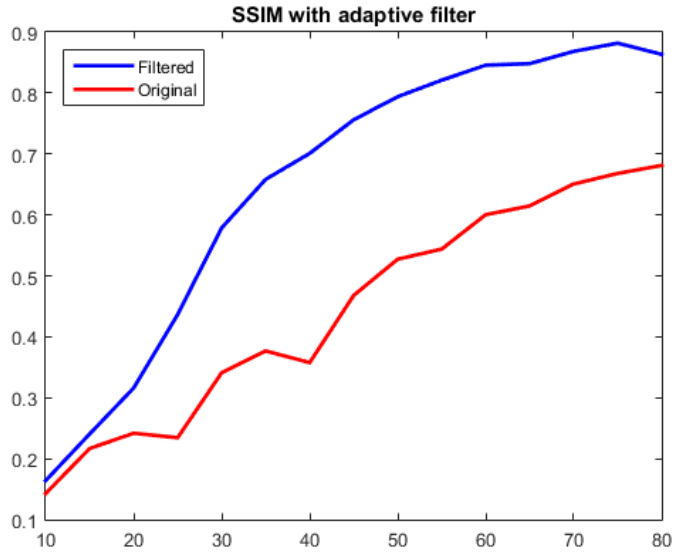

Figure 5.20: SSIM behaviour after adaptive filtering process for f_1.

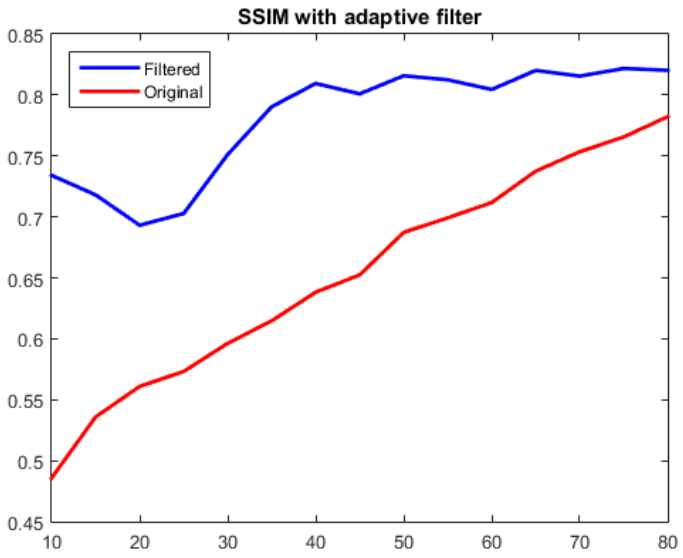

Figure 5.21: SSIM behaviour after adaptive filtering process for f_2.

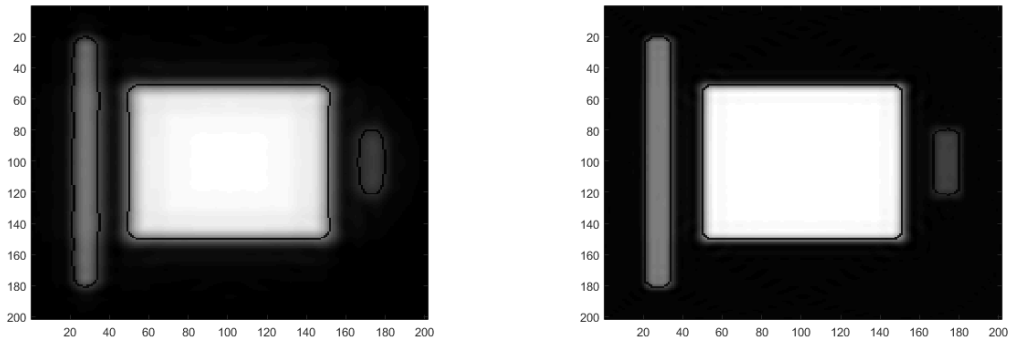

(a) $n = 25$. (b) $n = 40$.

Figure 5.22: Two results for f_1.

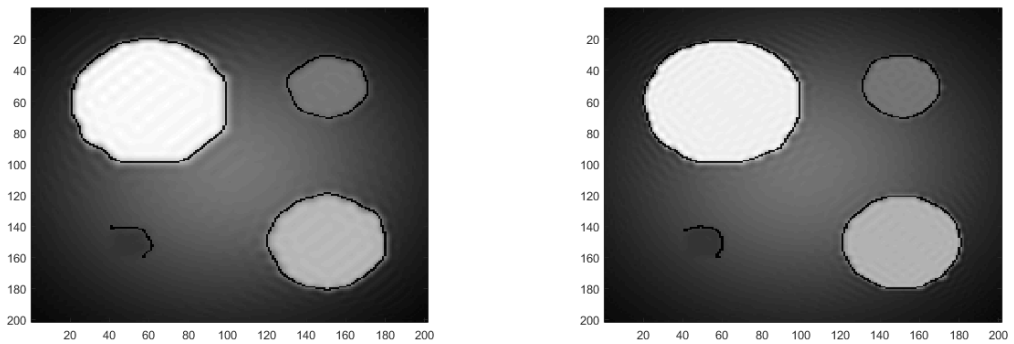

(a) $n = 45$. (b) $n = 65$.

Figure 5.23: Two results for f_2.

5.3 MPI applications

We can apply all the previous procedures to improve the image which we get from a MPI scanner. The setting will be the following.

- The domain is the square $[-1,1]^2$.
- The evaluation matrix is a 201×201 matrix. The step of the grid is indeed $s = 0.01$.
- A modified version of the *Chebfun* 5.3.0 package, which is avaiable in the inclosed CD.
- Two 201×201 matrices containing the two phantoms which we consider.
- The sampling process is a simulated procedure, representing the mode of operation of a real MPI scanner placed at the University of Lübeck. For technical reasons, the scanner needs to perform the sampling on a non-degenerate Lissajous curve of maximum degree $(32, 33)$. Thus, the curve $\gamma_2^{(32,33)}$ is the only curve which is considered in this section.

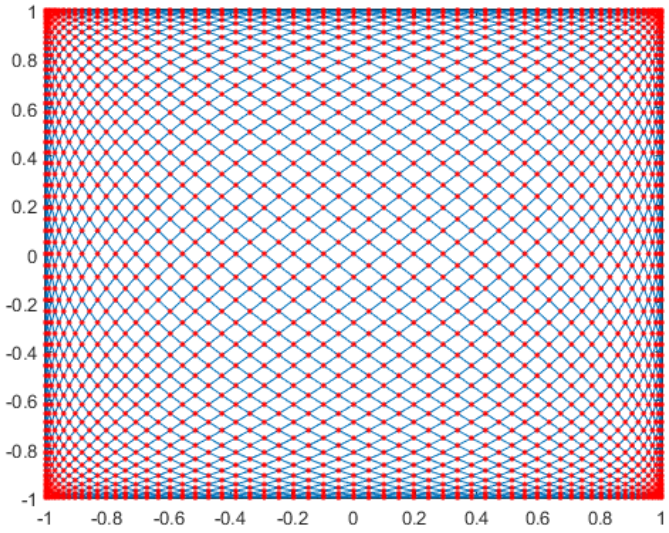

Figure 5.24: The Lissajous curve $\gamma_2^{(32,33)}$ and nodes.

We call A and B the two phantoms which we consider. They are displayed in the following figures.

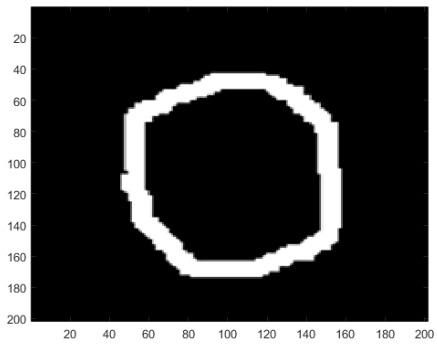

(a) The phantom A.

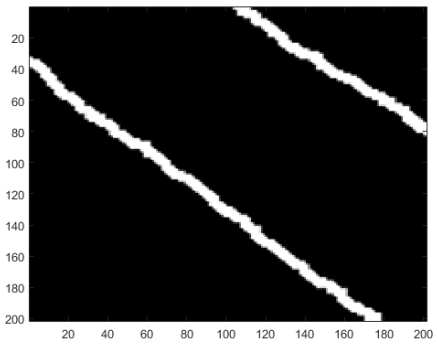

(b) The phantom B.

The polynomial interpolation on the Lissajous nodes given by $\gamma_2^{(32,33)}$ brings the two following images.

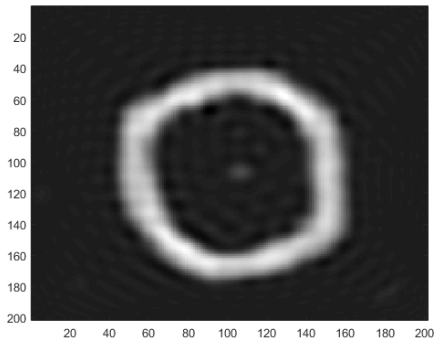

(a) The phantom A reconstructed from Lissajous sampling. $SSIM = 0.665$.

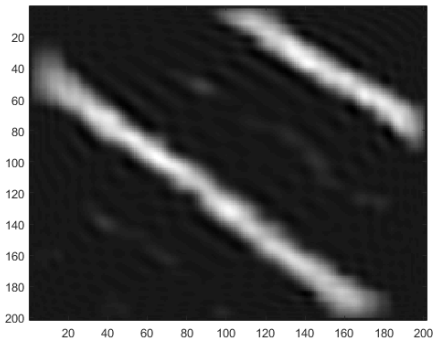

(b) The phantom B reconstructed from Lissajous sampling. $SSIM = 0.616$.

Starting with A and then taking B, we can follow the path of the previous section and we experiment first with the classical filter functions which we have introduced and then with the presented adaptive filter.

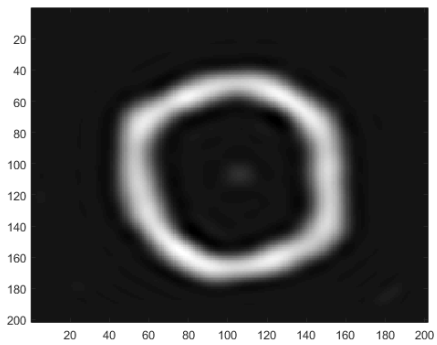

(a) Using the exponential filter with $p = 6$. $SSIM = 0.698$.

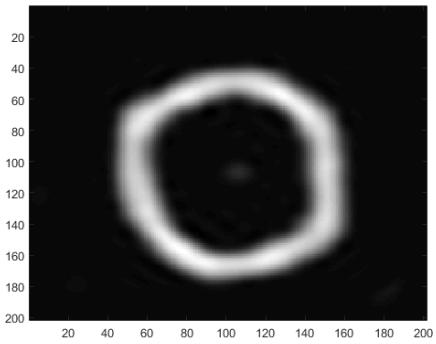

(b) Using the sinc filter. $SSIM = 0.736$.

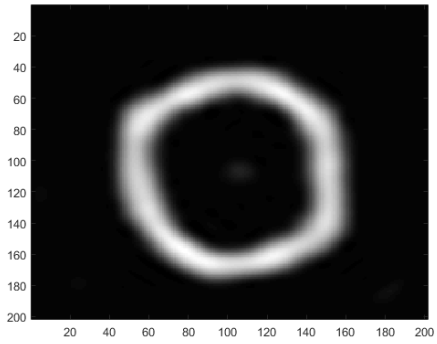

(c) Using the raised-cosine filter. $SSIM = 0.738$.

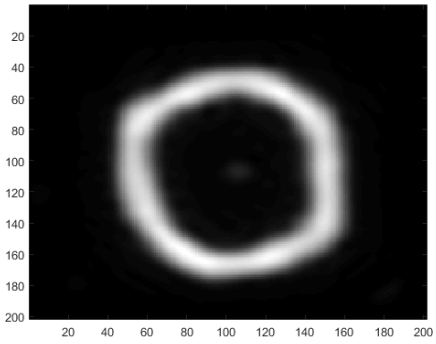

(d) Using the Fejer filter. $SSIM = 0.539$.

Figure 5.27: Different results for A.

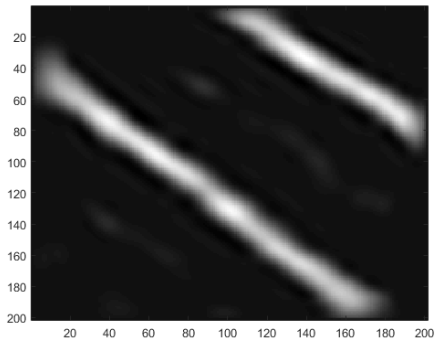

(a) Using the exponential filter with $p = 6$. $SSIM = 0.649$.

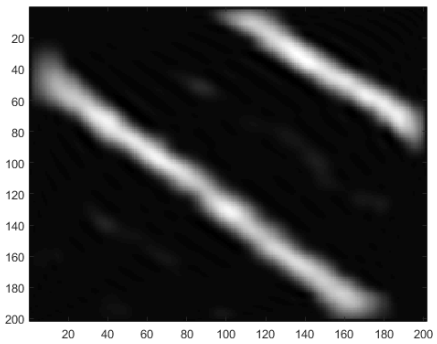

(b) Using the sinc filter. $SSIM = 0.674$.

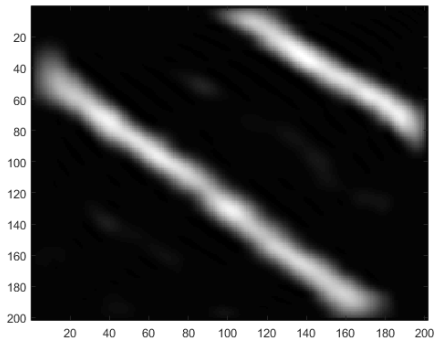

(c) Using the raised-cosine filter. $SSIM = 0.673$.

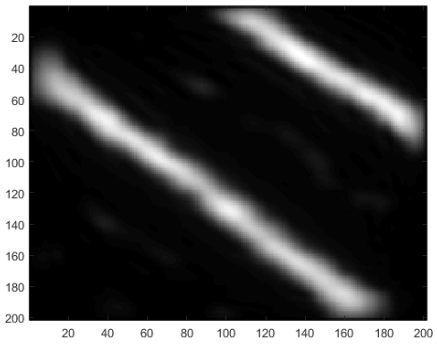

(d) Using the Fejer filter. $SSIM = 0.496$.

Figure 5.28: Different results for B.

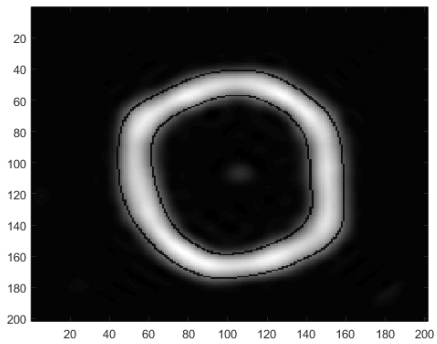

(a) Final reconstruction of A after adaptive filtering process. $SSIM = 0.701$.

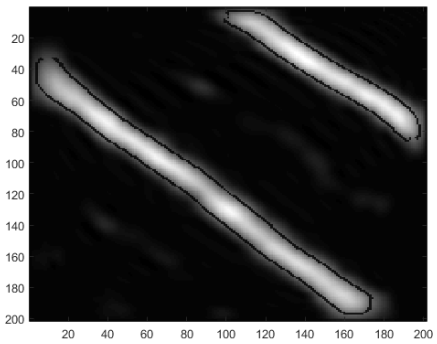

(b) Final reconstruction of B after adaptive filtering process. $SSIM = 0.649$.

A complete script with all the passages of this reconstruction is included in the inclosed CD.

We observe that the image related to the phantom B is more perturbated than the one related to A, due to the position of the phantom which is not completely "included" in $(-1, 1)^2$ and it goes up to the boundary, causing a loss of quality in the reconstruction. In these cases, one has to pay more attention in choosing the parameters in the algorithm, avoiding the wrong detection of non-existing edges.

In practice this is not a big problem, since the scanner can move its field of view, solving then the positioning problem.

5.4 Three-dimensional experiments

In this section we perform some experiments in the three-dimensional case, referring to Chapter 2. Our setting is:

- The domain is the cube $[-1, 1]^3$.
- The evaluation matrix is a $21 \times 21 \times 21$ matrix. The step of the grid is indeed $s = 0.1$.
- The *Chebfun* package, which is avaiable in the inclosed CD and in the official website (not necessarily the modified version).

We follow the same steps of the two-dimensional case. What slightly changes is the way we do it.

1. In order to reconstruct a test function from the samples and to apply the spectral filtering process we use the function *hyperlissa_pro.m* (avaiable in the inclosed CD), which is a modification of *hyperlissa.m*[2].

```
function [hypval,cfs]=hyperlissa_pro(deg,pts,f3,flag,filter);

% Francesco Marchetti, September 2016

% This function is a modification of hyperlissa.m from Stefano De Marchi
% and Marco Vianello
%
% It computes the hyperinterpolation polynomial of a trivariate function
% at a rank-1 Chebyshev lattice on a Lissajous curve of the cube, applying
% if desired a spectral filter

% NOTE: to be used in connection with the Chebfun package
% http://www.chebfun.org

% input:
% deg: hyperinterpolation degree
% pts: 3-column array of evaluation points
% f3: Trivariate function handle
% flag: 0 no-filter, 1 use filter
% filter: natural number to choose the type of filter

% output:
% hypval: 1-column array of values of the hyperinterpolation polynomial
% at the points pts
% cfs: hyperinterpolation coefficients
```

2. The edge-detection is performed using the default *edge.m* Matlab function combined with the function *canny.m*[3]. As observable in the example script in the CD, we use the function *edge.m* on the different two-dimensional slices of the 3D matrix representing the image in order to find suitable tresholds for the edge detection, then we pass the found treshold to *canny.m* to find the edges in the matrix. The tresholds setting is already included in *canny.m*, but the results are often not satisfying.

[2] http://www.math.unipd.it/ marcov/CAAsoft.html
[3] https://it.mathworks.com/matlabcentral/fileexchange/45459-canny-edge-detection-in-2-d-and-3-d

```
function [e, thresh] = canny(im, varargin)
%CANNY is an implementation of the Canny edge detector
%   E = CANNY(IM) takes a 2-D grey-level image or a 3-D array representing
%   a volume and returns a 2-D or 3-D logical edge map using centred
%   differences and non-maximum suppression. No smoothing or thresholding
%   is done when only one argument is given.
%
%   [...]
%
%   E = CANNY(IM, SIGMA, THRESH) also carries out hysteresis thresholding.
%   THRESH has the same functionality as the threshold argument of EDGE.
%   (Name-value pairs may be used instead of the THRESH argument for more
%   control.)
%
%    [...]
```

We use the function *ipdm.m* as before in order to find the distances between points and related closest discontinuities.

3. The adaptive filtering is performed in the same way with respect to the two-dimensional case, through tensor product extension and then considering a modified adaptive parameter.
   Since in the three-dimensional setting we consider a step of the grid which is 10 times larger with respect to the one chosen in the two-dimensional case, the adaptive filter can not express all its good properties about adaptivity and definition of the edges. Moreover, due to computational issues we experiment just in the case with $m = 10$ as degree of the three-dimensional Lissajous curve, and we use $\beta = 4$ in the adaptive parameter without knowing if it is optimal for this setting.

5.4.1 Numerics

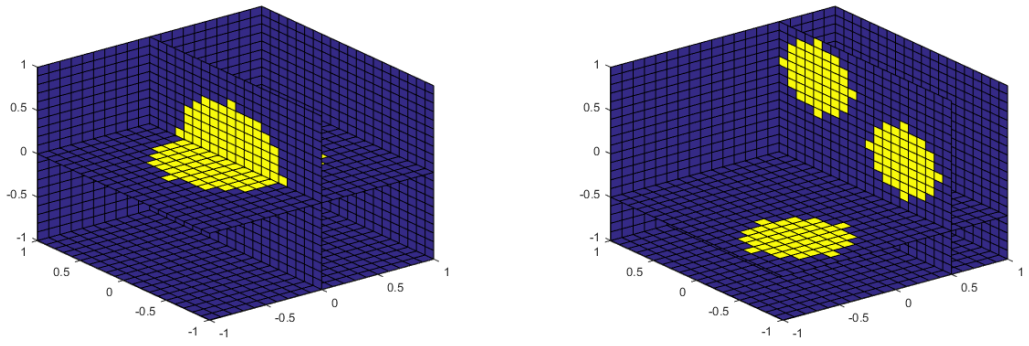

(a) The function f_1. (b) The function f_2.

Figure 5.30: A representation for the two functions.

We consider the functions f_1, f_2 from $[-1, 1]^3$ to $\mathbb{R}$ defined as

$$f_1(x, y, z) = \begin{cases} 1 & x^2 + y^2 + z^2 \leq (0.6)^2 \ , \\ 0 & \text{otherwise} \ . \end{cases} \tag{5.27}$$

$$f_2(x,y,z) = \begin{cases} 1 & (x+0.5)^2 + (y+0.5)^2 + (z+0.5)^2 \leq (0.4)^2 \ , \\ 1 & (x-0.5)^2 + (y-0.5)^2 + (z-0.5)^2 \leq (0.4)^2 \ , \\ 1 & (x+0.5)^2 + (y-0.5)^2 + z^2 \leq (0.4)^2 \ , \\ 1 & (x-0.5)^2 + (y+0.5)^2 + z^2 \leq (0.4)^2 \ , \\ 0 & \text{otherwise} \ . \end{cases} \tag{5.28}$$

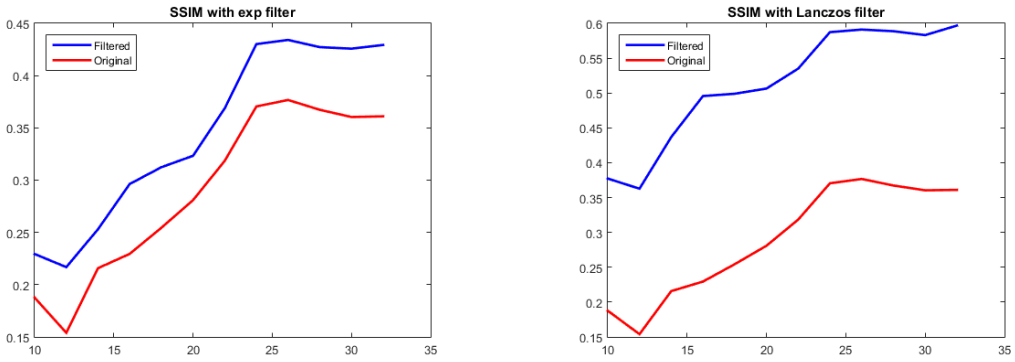

Figure 5.31: Different results for f_1 with exponential and Lanczos filters.

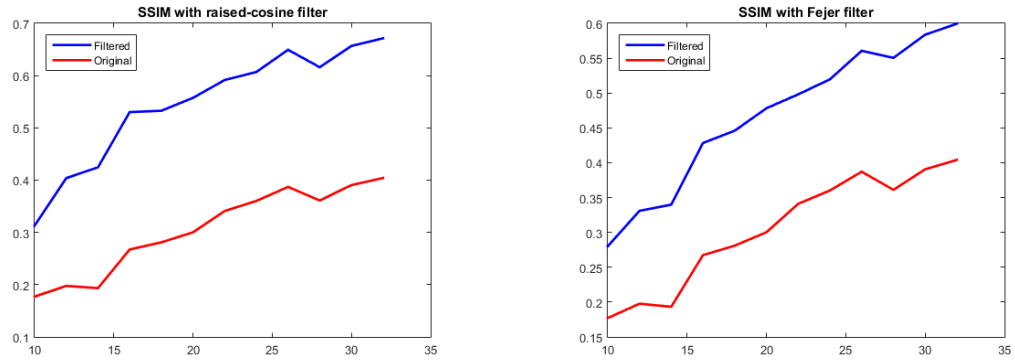

Figure 5.32: Different results for f_2 with raised cosine and Fejer filters.

We can perform the adaptive filtering process, obtaining the following results. We recall that we used the degree $m = 10$.

Table 5.1 SSIM values

Functions	f_1	f_2
Lissajous reconstruction	0.1876	0.1771
After adaptive filtering	0.3285	0.2200

We observe an improvement of the SSIM value in both cases.

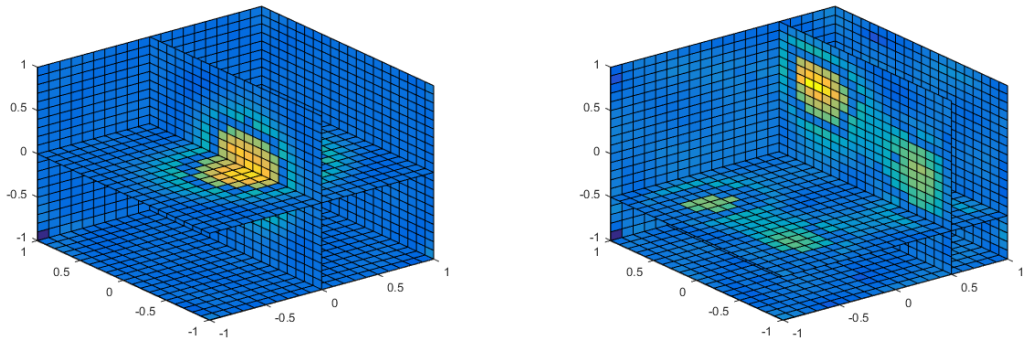

(a) The reconstructed function f_1.

(b) The reconstructed function f_2.

Figure 5.33: The reconstruction of the two functions using the adaptive filter.

Chapter 6

Conclusions

This work arises from a collaboration between the University of Padua and the University of Lübeck and it started during an Erasmus placement exchange program of the autor in Germany.

1. The Lissajous sampling is a stable and effective way to reconstruct a function without using a very large number of sample points and it is a suitable procedure for MPI applications. However, in the reconstruction of discontinuous functions it is inevitable to face the Gibbs phenomenon.

2. Classic Fourier spectral filtering methods are efficient in dimishing the distortions given by the Gibbs phenomenon, but they also provide a general smoothing in the image and they cause a loss of definition.
   In our setting, these spectral methods are useful to improve the image before the application of the edge-detector. In order to get an acceptable result, we have to focus on the resolution of strong warps given by the Gibbs phenomenon, since otherwise they could be interpreted as edges by the detector.
   Therefore, one should prefer a proper strong filter, even if some precision is lost near the existing edges in the figure. We performed the application of such filters, obtaining good results.

3. The adaptive parameter suggested by the theory related to the adaptive filter is affected by some distortions given by the consideration of separated one-dimensional distances in a tensor product setting.
   In order to improve the final result, we conjectured a different parameter, first linearly dependent from the euclidean distance between points and related closest discontinuities. After that, we presented the idea of considering a non-linearly dependence from the distance in the parameter. This has brought an improvement in the general quality of the final reconstructed image, hence this conjecture could be investigated in the theory in order to find a related theorical background.

4. The three-dimensional case is much more expensive in terms of computational costs with respect to the two-dimensional case. Therefore, we experimented with a larger step in the grid and we could not manage to perform deep tests as in the previous case. Thus, the results obtained could be enriched and improved considering a setting which guarantees more accuracy.

Bibliography

[1] Ahlborg M., Dencker P., Erb W. and Kaethner C. Bivariate Lagrange interpolation at the node points of non-degenerate Lissajous nodes. *Numerische Mathematik* (2015).

[2] Bogle M.G.V., Hearst J.E., Jones V.F.R. and Stoilov L. Lissajous knots. *J. Knot Theory Ramifications 3* (1994), 121–140.

[3] Bos M., De Marchi S. and Vianello M. Trivariate polynomial approximation on Lissajous curves. *IMA J. Num. Anal.* (2016).

[4] Bos M., De Marchi S. and Vianello M. Polynomial approximation on Lissajous curves in the d-cube. *Submitted* (2016) online.

[5] Bos L., Caliari M., De Marchi S., Vianello M. and Xu Y. Bivariate Lagrange interpolation at the Padua points: the generating curve approach. *J. Approx. Theory 143* (2006), 15–25.

[6] Burenkov V.I. Sobolev spaces on domains(1998).

[7] Caliari M„ De Marchi S. and Vianello M. Bivariate polynomial interpolation on the square at new nodal sets. *Appl. Math. Comput. 165(2)* (2005), 261–274

[8] De Marchi S. Lectures on multivariate polynomial interpolation. *http://www.math.unipd.it/∼ demarchi/*.

[9] Dencker P., and Erb W. Multivariate polynomial interpolation on Lissajous-Chebyshev nodes. *arXiv:1511.04564 [math.NA]* (2015).

[10] Erb W., Kaethner C., Dencker P., and Ahlborg M. A survey on bivariate Lagrange interpolation on Lissajous nodes. *Dolomites Res. Notes Approx. 8* (2015), 23–36.

[11] C. Fefferman On the convergence of multiple Fourier series. *Bull. AMS 5* (1971).

[12] Gottlieb D. and Shu C. On the Gibbs phenomenon and its resolution. *Society for Industrial and Applied Mathematics* (1997), 644–668.

[13] Kaethner C., Erb W., Ahlborg M., Szwargulski P., Knopp T. and Buzug T. M. Non-Equispaced System Matrix Acquisition for Magnetic Particle Imaging based on Lissajous Node Points. *IEEE Trans. Med. Imag.* (2016), in press.

[14] Knopp T. and Buzug T. M. Magnetic Particle Imaging. *Springer* (2012).

[15] Navarra A., Stern W.F. and Miyakoda K. Reduction of the Gibbs oscillations in spectral model simulations. *Journal of Climate Vol. 7* (1994).

[16] Rudin W. Real and complex analysis(1966).

[17] Tadmor E. and Tanner J. Adaptive filters for piecewise smooth spectral data. *IMA J. Num. Anal.* (2005), 635–647.

[18] Wang Z., Bovik A.C., Sheikh H.R. and Simoncelli E.P. Image Qualifty Assessment: From Error Visibility to Structural Similarity. *IEEE Trans. Med. Imag. Vol.13 Issue 4* (2004), 600–612.

[19] Weisz F. Summability of multi-dimensional trigonometric Fourier series. *Surveys in Approximation Theory* (2012), 1–179.

[20] Chebfun official website: *http://www.chebfun.org*